Siberian Snakes in high-energy accelerators



2005 J. Phys. G: Nucl. Part. Phys. 31 R151

(http://iopscience.iop.org/0954-3899/31/9/R01)

INSTITUTE OF PHYSICS PUBLISHING JOURNAL OF PHYSICS G: NUCLEAR AND PARTICLE PHYSICS

J. Phys. G: Nucl. Part. Phys. **31** (2005) R151–R209 doi:10.1088/0954-3899/31/9/R01

**TOPICAL REVIEW**

# Siberian Snakes in high-energy accelerators

**S R Mane**[1], **Yu M Shatunov**[2] **and K Yokoya**[3]

[1] Convergent Computing Inc, PO Box 561, Shoreham, NY 11786, USA
[2] Budker Institute of Nuclear Physics, Novosibirsk 630090, Russia
[3] National Laboratory for High-Energy Physics (KEK), 1-1 Oho, Tsukuba, Ibaraki 305-0801, Japan

E-mail: srmane@optonline.net and kaoru.yokoya@kek.jp

Received 22 March 2005
Published 1 August 2005
Online at stacks.iop.org/JPhysG/31/R151

**Abstract**

We review modern techniques to accelerate spin-polarized beams to high energy and to preserve their polarization in storage rings. Crucial to the success of such work is the use of so-called Siberian Snakes. We explain these devices and the reason for their necessity. Closely related to Snakes is the concept of 'spin rotators'. The designs and merits of several types of Snakes and spin rotators are examined. Theoretical work with Snakes and spin rotators, and experimental results from several storage rings, are reviewed, including the so-called Snake resonances.

(Some figures in this article are in colour only in the electronic version)

## 1. Introduction

There is an increasing interest in the availability of spin-polarized beams at high-energy and nuclear physics facilities. For example, Jefferson Lab has operated exclusively with polarized electrons since 1999. The designs of most new facilities include provision for polarized beams. The recent successes at BNL (Brookhaven National Laboratory) to accelerate, store and collide counterrotating polarized proton beams at high energy, by using so-called 'Siberian Snakes', 'spin rotators' and 'partial Snakes', mark the successful culmination of three decades of both theoretical ideas and experimental work in the field. (Note. As of the date of the writing of this review, RHIC has accelerated polarized proton beams to 100 GeV. All of the material on RHIC in this review will discuss only 100 GeV beams. However, the top design energy of RHIC is 250 GeV and RHIC will undoubtedly accelerate polarized proton beams to a higher energy in the future.) Anyone looking at the underlying physics will appreciate that the need for polarized relativistic particle beams is likely to remain the case for a long time, and thus that new generations of physicists—both accelerator builders and the research users—will

  

need to understand these phenomena. Presently there is no one place for a student/researcher to obtain the pertinent information.

This is one of two reviews whose aim is to provide a broad, but also detailed, survey of the dynamics of spin-polarized beams in high-energy particle accelerators. The companion review (Mane, Shatunov and Yokoya 2005) will be denoted by MSY2 below; the present review being MSY1. MSY2 will treat a broad set of topics, e.g. important historical works, precision tests of the Standard Model using polarized beams, including the recently completed E821 muon storage ring experiment at BNL to measure the muon anomalous magnetic moment (and also a proposed experiment to measure the muon *electric* dipole moment), fundamental theory and experimental work on a large variety of depolarizing spin resonances, case studies of work with polarized beams at various laboratories, etc.

This review will cover a more specific topic of important current interest, namely the storage of spin polarized beams in storage rings using Siberian Snakes and spin rotators. Both the underlying theory and the recent experimental work will be reviewed. We shall deliberately *not* explain what a Siberian Snake is here; you must read the article to find out!

Although we shall touch on various topics of particle physics below, our focus is on accelerator physics, not particle physics. An excellent modern text is *Spin in Particle Physics* by Leader (2001), which, as the title states, describes many of the important roles spin-polarized beams have played, and continue to play, in high-energy physics.

Typically, a polarized beam is injected into a synchrotron and accelerated to high energy. This requires one to overcome the so-called depolarizing spin resonances which are encountered during the acceleration process. The above terms will be explained below. However, the number of resonances to be crossed becomes prohibitively large for very high energy rings such as RHIC, the Relativistic Heavy Ion Collider at BNL. The elegant idea of Siberian Snakes (Derbenev and Kondratenko 1976) avoids all such depolarizing resonances, at least in principle. RHIC is the world's first (and to date only) high-energy polarized proton collider.

The proton beams are vertically polarized in the RHIC arcs. However, *longitudinal* polarization is desired at the interaction points. To achieve this, pairs of so-called 'spin rotators' are installed around the interaction points of the two principal RHIC experiments (STAR and PHENIX). The rotators rotate the polarization from the vertical to the horizontal plane, and back to the vertical.

In practice, Siberian Snakes do not eliminate all of the depolarizing spin resonances. So-called Snake resonances, which are depolarizing resonances in rings equipped with Snakes, have been observed, first at the IUCF Cooler ring (Phelps *et al* 1997), and later at RHIC (Ranjbar *et al* 2003). The existence of Snake resonances was predicted theoretically many years earlier by Lee and Tepikian (1986). Given the complexity of modern accelerators, most theoretical analyses of the spin dynamics in storage rings naturally employ computer programs and/or perturbation theory. However, much insight can also be gained by solving simplified models of accelerators. Recently, an exact analytical solution was obtained for the spin dynamics for an idealized model of a ring with Snakes (Mane 2003a). Snake resonances will be reviewed below.

Most of the above statements tacitly assumed that a polarized beam is injected into a ring and accelerated to high energy. For ultrarelativistic electron and positron beams, Sokolov and Ternov (1964) calculated the spin motion in a homogenous magnetic field and showed that the particles 'self-polarize' via the emission of spin-flip synchrotron radiation. Radiative polarization will be reviewed in detail in MSY2. The polarization builds up from zero to an asymptotic equilibrium value. However, the time constant for the polarization buildup is strongly energy dependent (going inversely as the fifth power of the energy), and can be

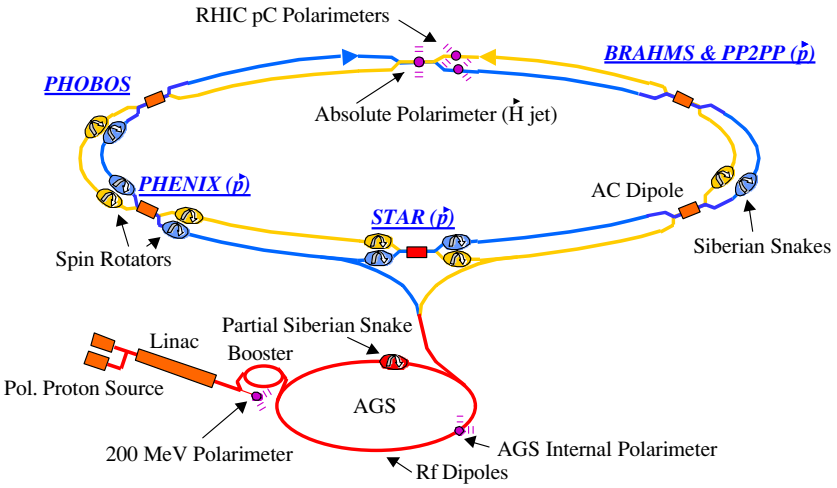


**Figure 1.** Schematic layout of BNL complex for polarized proton operations. Courtesy of W W MacKay (private communication) and BNL.

unacceptably long for low or medium energy electron storage rings. The storage rings AmPS (Amsterdam Pulse Stretcher) and the SHR (South Hall Ring) at MIT-Bates both inject beams from a polarized electron source and employ a Siberian Snake to preserve the polarization of the stored beam. (AmPS was decomissioned in 1998.)

Figure 1 is a schematic view of the BNL complex showing RHIC and its injector chain. The structure of the complex is a cascaded chain of accelerators, fairly typical for modern laboratories, and will serve as a useful example to explain some important concepts. A polarized proton source produces a spin-polarized beam which is injected into a linear accelerator (linac), from which the beam is then transferred to a Booster synchrotron. The particles are then transferred to the AGS (Alternating Gradient Synchrotron), and then to RHIC. As is evident, there are many steps involved in the delivery of the final polarized beam, namely a polarized particle source, acceleration and preservation of the polarization in lower energy booster synchrotrons, transfer of a polarized beam from one ring to the next, polarimetry, etc. These issues will be treated in greater detail in the companion review MSY2. Note that RHIC consists of a pair of intersecting rings. Each ring is equipped with a pair of Siberian Snakes, making a total of four in all. Each RHIC ring also has two pairs of spin rotators (for the experiments STAR and PHENIX) making a total of eight spin rotators. Alekseev *et al* (2003) give a detailed review of the RHIC polarized proton collider.

Schematic layouts of the AmPS and SHR are shown in figures 2 and 3, respectively. These rings are each equipped with a single Siberian Snake. There are important differences in the operation of a ring with only a single Snake or a pair of Snakes (such as RHIC). These differences, and the merits of both modes of operation, will be explained below. For example, RHIC is a collider, whereas AmPS and SHR circulate a single polarized beam, which collides with an internal (gas jet) target.

AmPS ran from 1992 through 1998, and operated with a Snake and polarized beam from roughly 1995. The first results from AmPS using a longitudinally polarized electron beam and an internal polarized target were reported by Poolman *et al* (2000). Polarized electrons were injected at 442 MeV (653 MeV), and a partial (full) Siberian Snake was employed to preserve the polarization. The longitudinal polarization at the interaction point and the polarization lifetime of the stored electrons were determined with laser Compton backscattering.

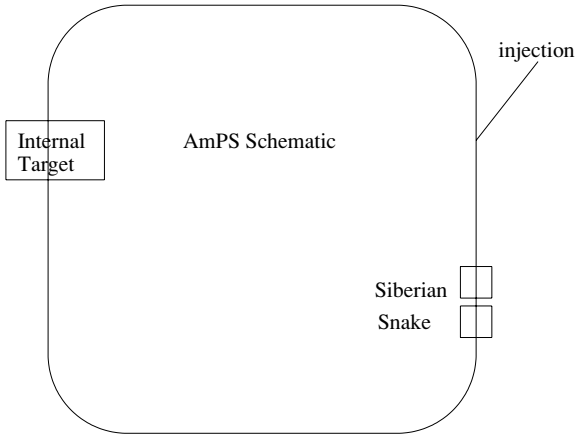


**Figure 2.** Schematic layout of AMPS.

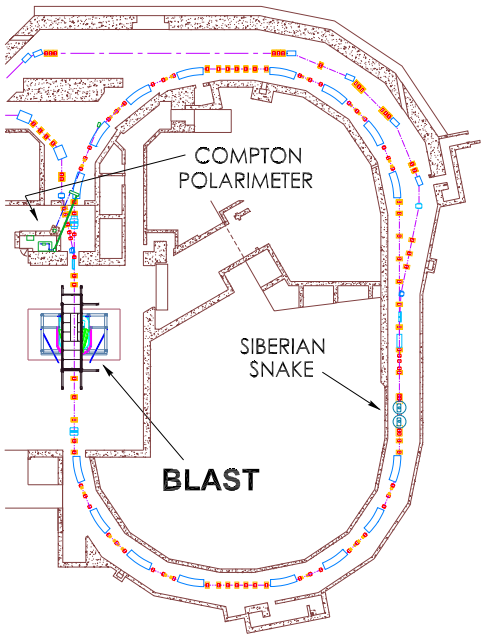


**Figure 3.** Schematic layout of the SHR at MIT-Bates. Courtesy of MIT-Bates Linear Accelerator Center.

Spin observables were measured over a large phase space, for electrodisintegration of polarized $^3$He.

SHR is also equipped with an internal target at the BLAST detector (Bates Large Acceptance Spectrometer Toroid), as shown in figure 3. Both the ring and the detector are new, and the data are still preliminary. A recent status report on the experiment is by Hasell (2004) for the BLAST Collaboration.

Historically, the first storage ring to be equipped with a full-strength Siberian Snake was the IUCF Cooler ring. It operated from 1987 to 2003 (with a Snake from 1989 onwards) and

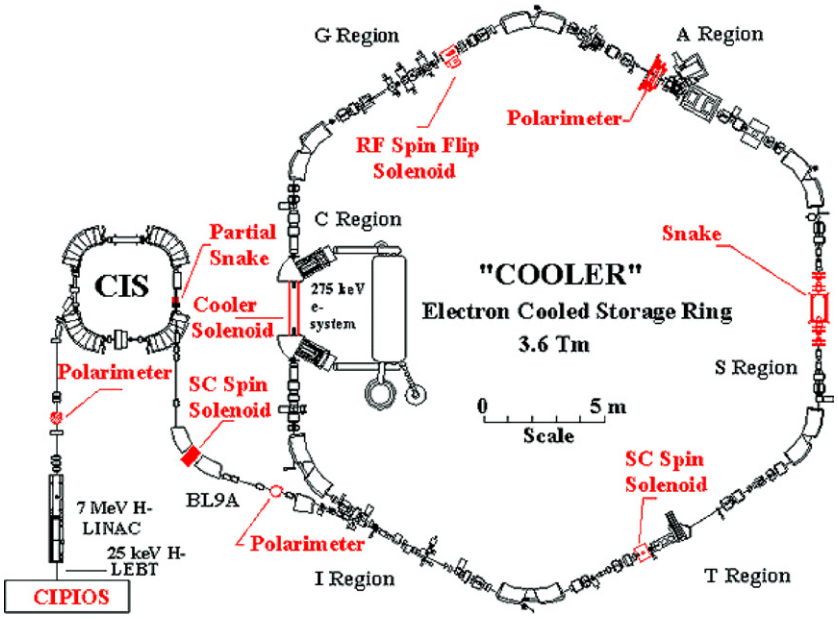


**Figure 4.** Schematic of the IUCF CIS/Cooler layout. Courtesy of D L Friesel (private communication) and IUCF.

stored polarized protons and deuterons. A schematic of the IUCF Cooler complex is shown in figure 4. The Snake in this ring was unusual in that it was actually used for a number of accelerator physics experiments, as a proof-of-principle of the Siberian Snake concept. Many important beam physics discoveries pertaining to Snakes were made at this machine, e.g. the first demonstration that a Snake does avoid the depolarization from a resonance driving term (Goodwin *et al* 1990), the (inadvertent) discovery of 'type 3' Siberian Snakes (Pollock 1991) and the first observation of a Snake resonance (Phelps *et al* 1997), to name just a few.

To date, the IUCF Cooler, AmPS, SHR and RHIC are the only four rings to be equipped with full-strength Siberian Snakes. There are also so-called partial Siberian Snakes, which are also useful devices, but they will not be discussed here (see MSY2 for details of partial Snakes).

The structure of this review is as follows. There is regrettably no standard coordinate system and notational convention for the particle motion in an accelerator, and so we explain our position in section 2. We then briefly review the equation of motion of spin precession in an accelerator, and the depolarizing spin resonances, in section 3. This will explain the need for new ideas to accelerate polarized beams to high energy. The notion of Siberian Snakes will then be introduced in section 4, and how they are able to avoid the depolarizing resonances. Spin rotators are similar in concept to the Siberian Snakes, and will also be reviewed in the same section. Section 5 is by far the longest, and examines the designs of several types of Snakes and spin rotators, and the relative merits of the various ideas. Section 6 presents a somewhat unusual topic, namely that the circuit of a spin around a ring equipped with Siberian Snakes is actually an example of a geometric quantum phase, more popularly known as a 'Berry phase' (Berry 1984). Section 7 reviews theoretical and analytical work on Snake resonances. The exact analytical solution referred to above will be displayed here. Section 8 concludes.

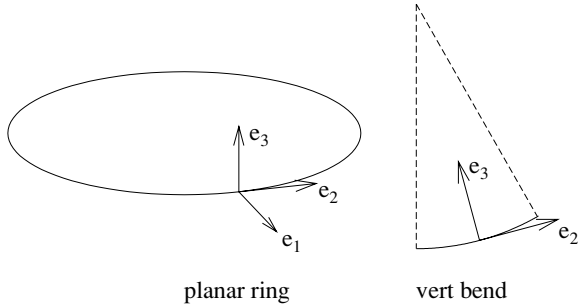


**Figure 5.** Sketch of the coordinate basis for a planar ring and a vertical bend.

A note on units: we employ cgs units in the equations in this review, the same as in the classic text by Jackson (1998). We also do *not* set $\hbar$ and $c$ to unity.

## 2. Coordinate systems and conventions

The particle motion in accelerators is usually referenced to a *design orbit*. We take as the independent variable the arc-length $s$ along the design orbit, or more usually the generalized azimuth $\theta = 2\pi s/C$, where $C$ is the machine circumference. We also define the mean radius $R = C/(2\pi)$, so $\theta = s/R$. The coordinate basis vectors are $\{\boldsymbol{e}_1, \boldsymbol{e}_2, \boldsymbol{e}_3\}$, a right-handed orthonormal triad, where $\boldsymbol{e}_1$ points radially outwards, $\boldsymbol{e}_2$ points longitudinally and $\boldsymbol{e}_3$ points vertically up. The positive sense of circulation is counterclockwise around the ring circumference. For definiteness, we shall assume that in any one magnet the design orbit bends either in the horizontal plane or in the vertical plane, but not both simultaneously. A positive vertical bend rotates counterclockwise around $\boldsymbol{e}_1$. A sketch of the coordinate basis is shown in figure 5.

It should be noted that, unfortunately, there are a wide variety of coordinate bases and notations in the literature. There is no standard notation in the field. Some authors use $(x, y, z)$ or $(x, y, s)$, where $x$ is radial, $y$ is vertical and $z$ or $s$ is longitudinal and increases clockwise around the circumference. Other authors use the basis $(x, s, z)$, so that '$z$' refers to the vertical (here '$s$' increases in the counterclockwise sense). We chose the notation $(\boldsymbol{e}_1, \boldsymbol{e}_2, \boldsymbol{e}_3)$ partly to avoid choosing between the above notations, and also because we want the orbital revolution frequency to be positive. However, because of the wide scope of our review, we include formulae by many authors, and it is too difficult (and prone to errors) to transcribe every formula to an $(\boldsymbol{e}_1, \boldsymbol{e}_2, \boldsymbol{e}_3)$ basis. Furthermore, to do so would break contact with the original literature. When reproducing formulae from the literature, e.g. (57), we explain the basis used (which is $(x, y, s)$ in the case of (57)) when we display the formula. The reader is *strongly* advised to *always* consult the original literature to obtain the definitive formulae, and to verify the notations and coordinate conventions used. In general, we use the notation '$x$' for the radial motion, '$y$' for the vertical motion and either '$z$' or '$s$' for the longitudinal motion.

## 3. Basic equations

### *3.1. Orbital motion*

Our primary interest is in the spin precessions, so we present only the most cursory description of the particle orbital motion. The particle charge and mass are denoted by $e$ and $m$,

respectively, and the prescribed external electric and magnetic fields of the accelerator are denoted by $\boldsymbol{E}$ and $\boldsymbol{B}$, respectively. At relativistic energies the effect of the spin on the orbital motion (via the Stern–Gerlach force) is negligble, and so the orbital motion satisfies the Lorentz equation

$$\frac{\mathrm{d}\boldsymbol{p}}{\mathrm{d}t} = e(\boldsymbol{E} + \boldsymbol{\beta} \times \boldsymbol{B}). \tag{1}$$

Here $\boldsymbol{p}$ is the particle momentum and $\boldsymbol{\beta} = \boldsymbol{v}/c$ is its dimensionless velocity. As stated in the introduction, we employ cgs units, so $\boldsymbol{E}$ and $\boldsymbol{B}$ have the same dimensions. In practice the particles execute transverse and longitudinal oscillations around the design orbit. The transverse orbital oscillations are called (horizontal and vertical) *betatron oscillations*. The longitudinal oscillations are called *synchrotron oscillations* and are more subtle to visualize. The particles in an accelerator have not only a spread of coordinates but also a spread of energies. Hence they circulate around the ring circumference with different frequencies, leading to a longitudinal separation between the particles (or time of arrival at a given point around the ring). The longitudinal oscillations are therefore (energy, time-of-arrival) oscillations.

Most accelerators are built from a fairly standard set of magnets. The design orbit in almost all accelerators lies in the horizontal plane. Dipole magnets are used to guide the particles along the design orbit. Quadrupole magnets are used to focus the transverse particle motion to keep the the orbital oscillations bounded. (The dipole magnets also provide some focussing.) Higher order multipole magnets (e.g. sextupoles) are used to control various higher-order aberrations in the orbital motion. In addition to magnets, radio-frequency (rf) cavities contain longitudinal electric fields which are used to (i) provide longitudinal focussing, (ii) increase the particle energy during acceleration and (iii) replenish the energy loss due to synchrotron radiation in electron and positron rings. In the gaps between the magnets (drift spaces), the particle motion is a straight line. Additionally, in colliding beam rings, solenoids are frequently employed in the particle detectors. Other magnets such as skew quadrupoles, etc are also used. The precise operation of such devices need not concern us. A good text on the orbital motion in accelerators is by Edwards and Syphers (1993). Note however that they do not discuss spin.

Due to unavoidable tolerances of manufacture and alignment, the actual closed orbit in an accelerator differs from the true design orbit. We refer to it as the *imperfect closed orbit*, or speak of 'closed orbit imperfections'. Figure 6 shows a sketch of the design orbit and imperfect closed orbit, and also a (horizontal) betatron oscillation.

At the simplest level (which will generally be adequate for our purposes below), the orbital oscillations can be modelled as pseudo-harmonic oscillations. Furthermore, we have tacitly assumed that the horizontal and vertical betatron oscillations are decoupled. In practice, there can be coupling of the two 'normal modes' of the transverse oscillations to both the horizontal and the vertical planes, but for our purposes it will be adequate to neglect coupling. We generally write $x$ to denote the horizontal motion and $y$ to denote the vertical motion. It is also usual practice to refer not to the energy but to the relative energy offset $\Delta E/E_0$, where $E_0$ is the energy of the reference particle.

Let the revolution frequency of the reference particle be denoted by $\omega_0$, and the oscillation frequency of the horizontal betatron oscillations be denoted by $\omega_x$. A key parameter in accelerator physics is the *tune*, which is defined as the dimensionless ratio $Q_x \equiv \omega_x/\omega_0$ for the horizontal betatron oscillations. The tune is the number of betatron oscillations a particle completes in one circumference around the ring (see figure 6). There is correspondingly a vertical betatron tune $Q_y$ and a synchrotron tune $Q_s$. In general the tunes are *not* integers, so, unlike the closed orbit, the orbital oscillations do *not* repeat after one circumference.

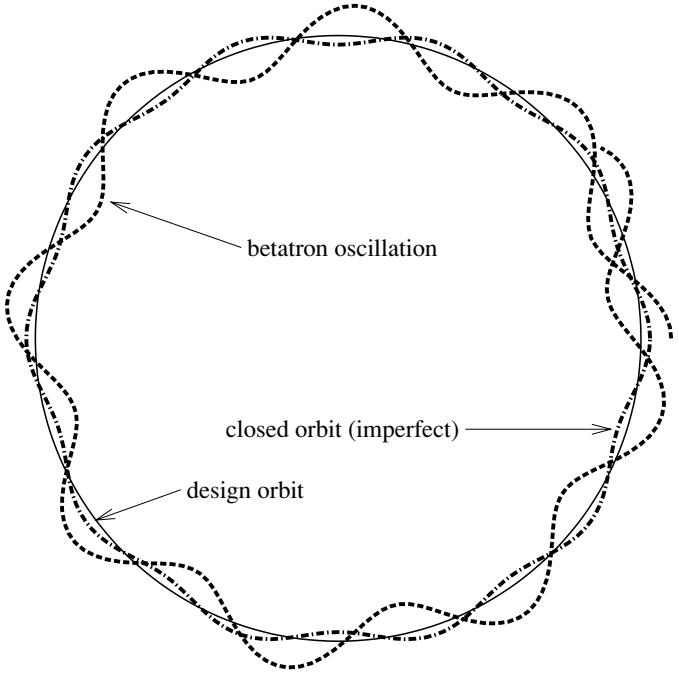


**Figure 6.** Sketch of the design orbit, imperfect closed orbit and a horizontal betatron oscillation in a synchrotron. The amplitudes of the imperfections and oscillations are highly exaggerated.

In fact, the values of the tunes are usually irrational, because the orbital oscillations can develop resonances, leading to unbounded amplitude growth and beam loss, if the orbital tune values are equal to (low-order) rational numbers. In general $Q_{x,y} \gg 1$ while $Q_s \ll 1$.

### *3.2. Spin precession equation*

For our purposes it is satisfactory to employ a classical spin model. The limitations of such a model will be discussed in MSY2. Because a particle on an off-axis trajectory sees fields whose values depend on the orbital trajectory, the spin precession depends on the particle orbit. It is essential to understand this fact. The spin of a particle is denoted by $\boldsymbol{s}$, a unit vector (not to be confused with the scalar $s$ for arc-length). The polarization of the whole beam is denoted by $\boldsymbol{P}$. Other variables have their usual meanings, e.g. $\boldsymbol{p}$ for the particle momentum and $E$ for the energy. As stated above the dimensionless velocity is $\boldsymbol{\beta} = \boldsymbol{v}/c$. We denote the Lorentz factor by $\gamma = 1/\sqrt{1-\beta^2}$. The anomalous part of the particle $g$-factor is given by the *magnetic moment anomaly* $a = \frac{1}{2}(g-2)$. For protons it is more common to write $G = \frac{1}{2}(g-2)$. The spin precession equation is

$$\frac{\mathrm{d}\boldsymbol{s}}{\mathrm{d}t} = \boldsymbol{\Omega} \times \boldsymbol{s}. \tag{2}$$

Here $\boldsymbol{\Omega}$ is the spin precession vector. When $\boldsymbol{\Omega}$ is specified in terms of the accelerator fields $\boldsymbol{E}$ and $\boldsymbol{B}$, (2) is called the Thomas-BMT equation (Thomas 1927, Bargmann *et al* 1959). The expression for $\boldsymbol{\Omega}$ is

$$\boldsymbol{\Omega} = -\frac{e}{mc}\left[\left(a+\frac{1}{\gamma}\right)\boldsymbol{B}_{\perp} + \frac{a+1}{\gamma}\boldsymbol{B}_{\parallel} - \left(a+\frac{1}{\gamma+1}\right)\boldsymbol{\beta}\times\boldsymbol{E}\right]. \tag{3}$$

The magnetic field has been decomposed into components parallel and perpendicular to the particle velocity:

$$\boldsymbol{B}_{\parallel} = \frac{\boldsymbol{B}\cdot\boldsymbol{v}}{v^2}\boldsymbol{v}, \qquad \boldsymbol{B}_{\perp} = \boldsymbol{B} - \boldsymbol{B}_{\parallel}. \tag{4}$$

An equivalent expression, which does not decompose the fields into components, is

$$\boldsymbol{\Omega} = -\frac{e}{mc}\left[\left(a+\frac{1}{\gamma}\right)\boldsymbol{B} - \frac{a\gamma}{\gamma+1}\boldsymbol{\beta}\cdot\boldsymbol{B}\boldsymbol{\beta} - \left(a+\frac{1}{\gamma+1}\right)\boldsymbol{\beta}\times\boldsymbol{E}\right]. \tag{5}$$

The above expressions include both the coupling of the particle magnetic dipole moment to the external fields and the Thomas precession.

Note that the independent variable in (2) is the time $t$. In accelerator physics we employ the arc-length $s$ as the independent variable. A common practice, which we shall employ below, is to use the generalized azimuth $\theta = s/R$ as the independent variable. (See the definitions at the beginning of section 2. Note that $\theta$ is not in general the bend angle in a dipole.) In terms of $\theta$, the spin precession equation of motion is

$$\frac{\mathrm{d}\boldsymbol{s}}{\mathrm{d}\theta} = \boldsymbol{W}\times\boldsymbol{s}. \tag{6}$$

We employ the notation $\boldsymbol{W}$ to distinguish it from $\boldsymbol{\Omega}$. We shall present the expression for $\boldsymbol{W}$ momentarily. It is also common to parametrize a spin via a spinor $\Psi$, where $\boldsymbol{s} = \Psi^{\dagger}\boldsymbol{\sigma}\Psi$, where $\boldsymbol{\sigma}$ is a vector of Pauli matrices. The equation of motion in spinor form is

$$\frac{\mathrm{d}\Psi}{\mathrm{d}\theta} = -\frac{\mathrm{i}}{2}\boldsymbol{W}\cdot\boldsymbol{\sigma}\Psi. \tag{7}$$

This is formally equivalent to a Schrödinger equation, although one must note that the orbital motion (and also the spin) are being modelled classically. Both the vector and spinor representations will be used below.

For simplicity consider the case where the design orbit bends in the horizontal plane, with a radius of curvature $\rho$. The expression for the spin precession vector is

$$\boldsymbol{W} = -\frac{eR}{pc}\left(1+\frac{x}{\rho}\right)\left[(a\gamma+1)\boldsymbol{B}_{\perp} + (a+1)\boldsymbol{B}_{\parallel} - \left(a\gamma+\frac{\gamma}{\gamma+1}\right)\boldsymbol{\beta}\times\boldsymbol{E}\right] - \frac{R}{\rho}\boldsymbol{e}_3. \tag{8}$$

Analogous expressions can be written if the design orbit bends vertically. The term in $\rho$ vanishes in beamline elements where the design orbit does not curve. The above expressions have important implications:

- The anomalous part of the magnetic moment couples differently to the electric and magnetic fields than do the other terms. For example, when traversing a magnet, the orbit and spin rotate through different angles. This is a fact of the utmost significance, and underlies almost all of the spin manipulations in the field of spin dynamics in accelerators.
- From (8), we see that the ratio of the effect on the spin precession due to transverse and longitudinal magnetic fields (of equal magnitude) is $(a\gamma+1)/(a+1)$. Hence transverse magnetic fields usually have a greater effect on the spin precession than do longitudinal magnetic fields. For example at RHIC, $G\gamma \simeq 46.5$ at injection and $G\gamma > 100$ at the top energy. For lower energy rings, $G\gamma \simeq 2$ at the IUCF Cooler and $a\gamma \simeq 1$–2 at AmPS and SHR.
- The influence of electric fields on the spin is generally negligible in high energy accelerators. In the rf cavities the electric field is longitudinal and so to leading order $\boldsymbol{\beta}\times\boldsymbol{E} = 0$ anyway. We shall mostly ignore electric fields below.

**Table 1.** Mass $m$, magnetic moment anomaly $a = \frac{1}{2}(g-2)$ and the energy spacing between imperfection resonances, given by $\Delta E = mc^2/a$.

| Particle | Mass (MeV) | Anomaly | $\Delta E$ (MeV) |
|---|---|---|---|
| Electron | 0.510 9989 | $1.159\,652\,1859 \times 10^{-3}$ | 440.65 |
| Proton | 938.272 | 1.792 847 351 | 523.34 |

### *3.3. Spin tune and depolarizing resonances*

Let us solve the spin precession equation for the important case of motion in a uniform vertical magnetic field $\boldsymbol{B} = B\boldsymbol{e}_3$. The design orbit is a circle and so $R = \rho$. In addition $eB\rho = -pc$ (the minus sign is because of our coordinate system). Then

$$\boldsymbol{W} = -\frac{eBR}{pc}(a\gamma + 1)\boldsymbol{e}_3 - \boldsymbol{e}_3 = a\gamma\boldsymbol{e}_3. \tag{9}$$

Hence the spin precesses around the vertical with a dimensionless frequency $a\gamma$. The ratio of the spin precession frequency to the orbital revolution frequency is called the *spin tune*, denoted by $\nu$ or $\nu_{\text{spin}}$. Hence for a planar ring the value of the spin tune is

$$\nu_{\text{spin}} = a\gamma. \tag{10}$$

Equation (10) is one of the most important in the entire subject of spin dynamics in accelerators. It is valid in general for planar rings, not just the simplified model treated above. Since most rings are planar by design, the spin tune is *proportional to the particle energy*. Note also that this proportionality is entirely because $g \neq 2$ for real particles. Obviously real rings are not exactly planar and there are small systematic errors; a detailed examination of such systematic errors will be given in MSY2.

As already noted, the spins undergo additional precessions driven by the magnetic fields seen on the off-axis particle orbits. Such perturbations include both fields due to the closed orbit imperfections and the betatron and synchrotron oscillations. Under suitable circumstances, these spin precessions can sum coherently causing a particle spin to tilt far from the vertical. Furthermore, and this is significant, the spins of different particles will, in general, tilt through different angles, leading to a decoherence of the spins. This leads to the depolarization of the beam. The condition for such *depolarizing spin resonances* to occur is given by

$$\nu_{\text{spin}} = m + m_x Q_x + m_y Q_y + m_s Q_s. \tag{11}$$

Here $m$ and $m_{x,y,s}$ are integers, including zero. Hence a depolarizing resonance occurs when the spin tune equals an integer plus an integer linear combination of the orbital tunes.

At the simplest level, ignoring the orbital tunes, (11) implies that a resonance occurs whenever the spin tune equals an integer. Hence for a planar ring, where the spin tune is proportional to the energy, resonances occur at regular energy steps as a polarized beam is accelerated to high energy. The energy interval between the resonances is approximately 523 MeV for protons and 440 MeV for electrons, as listed in table 1. In addition to these resonances (called 'imperfection resonances' because they are usually driven by the spin precessions on the imperfect closed orbit) there are additional depolarizing resonances involving the orbital tunes. The most important of these are of first order in the vertical betatron tune

$$\nu_{\text{spin}} = m \pm Q_y. \tag{12}$$

Such resonances are called 'intrinsic resonances' because the vertical betatron resonances are intrinsic to the machine and exist even in a perfectly aligned ring.

The depolarization from the resonances has to be corrected or avoided. For the imperfection resonances, which by definition are due to the closed orbit imperfections, a widely used technique is to employ corrector dipoles to cancel the offending Fourier harmonics of the imperfect closed orbit. An idea to circumvent the intrinsic resonances is to trigger pulsed quadrupoles to 'jump' the resonances by rapidly changing the value of the vertical betatron tune $Q_y$, so that the resonance condition in (12) is never satisfied. These 'resonance correction' and 'resonance jumping' techniques have been employed at a large number of synchrotrons, and will be reviewed in MSY2. However, they are tedious to implement. One correction or jump has to be applied per resonance, and the correction is never perfect. There are additional complications if two resonances overlap, for example. The fact that a polarized beam crosses depolarizing resonances at regular energy steps, approximately two per GeV increase of beam energy, plus additional intrinsic resonances, is the fundamental reason why it is impractical to accelerate spin-polarized beams to very high energies using resonance correction or jumping. Beyond a few GeV, there are simply too many resonances to cross. Alternative ideas are required to circumvent the resonances. This is where Siberian Snakes enter.

## 4. Siberian Snakes and spin rotators I

### *4.1. General remarks*

A Siberian Snake is theoretically defined as a device which rotates a particle spin through 180° around an axis in the horizontal plane, while leaving the orbital motion unaffected. There are no 'generic' Snakes with spin rotation axes oriented at arbitrary angles out of the median plane. Mathematically, a Siberian Snake is frequently modelled as a $\delta$-function point object which rotates a spin through 180° but is an identity map for the orbital motion. We shall make extensive use of the $\delta$-function model later in this review.

Siberian Snakes can exist because the orbit and spin rotate through different angles when traversing a magnetic (or electric) field. One constructs a Snake by employing a sequence of magnets with noncommuting rotations such that the overall spin rotation adds up to 180° while the orbital rotation adds up to zero.

Why are such devices so named? First, the basic idea was proposed by Derbenev and Kondratenko (1976) (in more detail by Derbenev *et al* (1978)), who were then at the Institute of Nuclear Physics at Novosibirsk in Siberia. Their idea was immediately popular, although it would be several years before a real Snake would actually be built. Because the orbit excursions twist or wriggle like a snake inside the combination of magnets, and in honor of the fact that the inventors of the idea came from Siberia, Ernest Courant, a major theorist on spin dynamics in accelerators, named the idea a Siberian Snake (Courant and Ratner 1978), an appellation which has stuck.

### *4.2. Solenoid Snake*

A practical implementation of a Siberian Snake, neglecting the complications of the betatron and synchrotron oscillations, is a solenoid. To leading order, the particle velocity is parallel to the solenoid field and so the Lorentz force vanishes: $\boldsymbol{v} \times \boldsymbol{B}_{\rm sol} = 0$. The spin rotation axis is along the solenoid axis. The spin rotation angle is

$$\psi_{\rm sol} = -(1+a)\frac{e}{pc}\int \boldsymbol{B}_{\rm sol}\cdot \mathrm{d}\boldsymbol{\ell}. \tag{13}$$

One adjusts the parameters so that $\psi_{\rm sol} = 180^\circ$. Since the solenoid length is fixed, one sees that the value of the magnetic field must scale with the momentum: we require $|\boldsymbol{B}_{\rm sol}| \propto \beta\gamma$:

$$\int \boldsymbol{B}_{\rm sol} \cdot {\rm d}\ell[{\rm Tm}] \simeq \frac{10.479}{1+a}\, p\ ({\rm GeV}/c). \tag{14}$$

This makes solenoids practical as implementations of Siberian Snakes basically only at low energies. At AmPS (Luijckx *et al* 1997) and SHR (Zwart *et al* 2001) the Snake consists of two solenoids in series. Both Snakes were designed and built by the same team from BINP (Shatunov 1993). The designs are basically the same; only the maximum energy is different (900 MeV at AmPS and 1 GeV at SHR). The solenoid length at AmPs is 1.624 m, so the requisite magnetic field is

$$B_{\rm sol}({\rm T}) = 6.45E\ ({\rm GeV}). \tag{15}$$

Superconducting solenoids are required to attain fields of this magnitude. Also, two pairs of skew quadrupoles and a pair of quadrupoles are required to match the orbital motion to the beam optics of the ring. The overall combination can be considered a 'Siberian Snake system'. The design will be studied in more detail in section 5.

Equation (13) also reveals a practical limitation of real Snakes, as opposed to the theoretical ideal: the spin rotation angle $\psi_{\rm sol}$ is inversely proportional to the particle's longitudinal momentum. Hence the spins of particles with a positive momentum offset will rotate through a smaller angle than will those with a negative momentum offset. Essentially, this is a chromatic aberration for the spin, analogous to the more familiar notion of chromatic aberration for the orbital motion. Such higher-order effects will be studied in more detail in MSY2.

### *4.3. Transverse magnetic fields*

As we have noted, transverse magnetic fields are more effective for rotating a spin at high energies, and so the Snakes at RHIC employ transverse magnetic fields. The RHIC Snake design is more complicated, employing helical magnetic fields, i.e. the field direction rotates along the length of the Snake. The designs of several types of Snakes will be reviewed in section 5. For motion in transverse fields, and $G\gamma \gg 1$,

$$\boldsymbol{W} = -\frac{e}{pc}(G\gamma+1)\boldsymbol{B}_\perp \simeq -\frac{eG}{mc^2}\frac{\boldsymbol{B}_\perp}{\beta}. \tag{16}$$

This means that, at high energies, the magnitude of a transverse magnetic field needs only to scale like $\beta$, to maintain a fixed spin rotation angle. Hence Snake designs composed of transverse magnetic fields can operate to arbitrarily high energies, without requiring unreasonably strong magnetic fields. Indeed, if the value of $\beta$ does not vary too greatly from injection to the top energy, the magnetic fields in the Snake can simply be held fixed. This practice is adopted at RHIC. The resulting Snakes will of course then not be 'perfect' 180° spin rotators, although they will nearly be so. Unlike solenoids, Snakes made from transverse magnetic fields can also be configured to have spin rotation axes oriented at any angle in the horizontal plane.

The converse consequence is that we shall necessarily require more than one magnet, and the design orbit will be nonplanar. The orbital bending angle decreases with energy:

$$\theta_{\rm bend} = \frac{e}{pc} B_\perp L_{\rm bend}, \tag{17}$$

where $L_{\rm bend}$ is the length of the magnet. We have seen that for $G\gamma \gg 1$, we would like $B_\perp$ to scale like $\beta$. Hence in this case

$$\theta_{\rm bend} \propto \frac{\beta}{\beta\gamma} \propto \frac{1}{\gamma}. \tag{18}$$

Hence the orbital excursions scale like $1/\gamma$. This is good at high energy. At *low* energy, however, e.g. at injection into the accelerator, the orbital excursions may be large. This can and does place a limitation on the construction of practical designs of Snakes with transverse magnetic fields. Note that a solenoidal Snake has no such orbit excursion issues: the design orbit is a straight line along the solenoid axis, at any energy.

For Snakes built using transverse fields the magnet bore must therefore be large enough to accommodate the beam excursions, or else the magnets must be displaced from a straight line axis, which complicates the design. The former is the case for the RHIC Snakes and spin rotators, which have a maximum orbit excursion at injection of 32 mm (Snake) and 24 mm (spin rotator) (Syphers *et al* 1997). The latter is the case for the HERA spin rotators: the maximum horizontal excursion varies from $-11$ cm to 8 cm for an operating energy of 27–35 GeV, and the maximum vertical excursion varies between 20 and 22 cm in the same energy range (Buon and Steffen 1986). This is too large to be contained in the bore of a magnet, so the magnets must be repositioned for different operating energies, and then locked into position.

### *4.4. Partial Snakes*

It was also realized by the Novosibirsk group that the spin rotation angle need not be exactly 180°. A 'partial Snake' will also work (Derbenev *et al* 1977b), where by 'partial' we mean that the spin rotation angle is less than 180°. Roser (1989) later independently realized the same idea. It is conventional to refer to a partial Snake in terms of a percentage, namely a '5%' partial Snake is one whose spin rotation angle is $0.05 \times 180°$, i.e. 9°.

To do justice to partial Snakes it is necessary to discuss the Froissart–Stora formula (Froissart and Stora 1960). The above formula, and the use of partial Snakes, will be reviewed in detail in MSY2. However for self-containedness we present a *very* brief summary of partial Snakes. The first experiments with a partial Snake were performed at the VEPP-2M ring (Derbenev *et al* 1977b), using a stored polarized electron beam. This was a 5% partial Snake, and the energy range through which the beam could be accelerated was fairly small. The CMD-2 detector at VEPP-2M has a 1 T solenoidal field, and two compensating solenoids with 3.5 T. In the initial experiment, a room-temperature air core solenoid was installed in the ring. After the first experiment, the partial Snake technique was subsequently employed many times to avoid depolarization from the $a\gamma = 1$ ($E = 440$ MeV) imperfection resonance. In that later work, to arrange the partial Snake option the compensating solenoids of the CMD-2 detector were detuned for the resonance crossing and then returned back. Partial Snakes have also proven themselves extremely useful to aid in the acceleration of polarized proton beams at the AGS (Huang *et al* 1994, 2003). A solenoid was employed as a partial Snake from 1993 to 2003. This was a 5% partial Snake. In 2004 a transverse-field partial Snake (approximately a 7% partial Snake) was installed and operated at the AGS. The design employed a variable-pitch helical magnetic field. (The helical-field design for Siberian Snakes will be reviewed in section 5.) A superconducting helical-field partial Snake (with a strength of approximately 20%) is under construction for use at the AGS in the near future.

### *4.5. Snake spin rotation matrices*

If the spin rotation axis of a Snake is at an angle $\xi$ relative to the radial direction $\boldsymbol{e}_1$, the overall spin rotation can be decomposed into a 180° rotation around the radial axis $\boldsymbol{e}_1$ followed by a rotation through an angle $2\xi$ around the vertical axis $\boldsymbol{e}_3$:

$$\begin{aligned} M_{\text{Snake}} &= \mathrm{e}^{-\mathrm{i}\pi\boldsymbol{\sigma}\cdot(\boldsymbol{e}_1\cos\xi+\boldsymbol{e}_2\sin\xi)/2} \\ &= -\mathrm{i}(\sigma_1\cos\xi+\sigma_2\sin\xi) = \mathrm{e}^{-\mathrm{i}\xi\sigma_3}(-\mathrm{i}\sigma_1) = (-\mathrm{i}\sigma_1)\,\mathrm{e}^{\mathrm{i}\xi\sigma_3}. \end{aligned} \tag{19}$$

The last line shows that we can also rotate clockwise through $2\xi$ around the vertical, and then by $180^\circ$ around the radial axis. We can call $\xi$ the 'Snake axis angle', although this is not standard terminology. For a partial Snake, with a spin rotation angle $\lambda_s\pi$, the spin rotation matrix is

$$M_{\text{partial}} = \mathrm{e}^{-\mathrm{i}\lambda_s\pi\boldsymbol{\sigma}\cdot(\boldsymbol{e}_1\cos\xi+\boldsymbol{e}_2\sin\xi)/2} = \cos\frac{\lambda_s\pi}{2} - \mathrm{i}\sin\frac{\lambda_s\pi}{2}\,\mathrm{e}^{-\mathrm{i}\xi\sigma_3}\sigma_1. \tag{20}$$

For a partial Snake, one tacitly assumes $0 \leqslant \lambda_s \leqslant 1$.

### *4.6. Ring with one Siberian Snake*

Consider the spin motion on the design orbit for a planar ring with one full-strength Siberan Snake localized at one point in the ring. The Snake spin rotation axis lies in the horizontal plane, at an angle $\xi$ relative to the radial direction $\boldsymbol{e}_1$. We model the Snake by a point rotator, with the spin rotation matrix given in (19). Let us define $\nu_0 = a\gamma$. The one-turn spin rotation matrix on the design orbit of a planar ring is

$$M_{\text{planar}} = \mathrm{e}^{-\mathrm{i}\pi\nu_0\sigma_3}, \tag{21}$$

which is a rotation through $2\pi\nu_0$ around the vertical $\boldsymbol{e}_3$. To analyse the contribution of a Snake to the spin motion, it is also convenient to calculate the one-turn spin rotation matrix. For reasons soon to become clear, we select the origin to be at the point *diametrically opposite* to the Snake. The spin rotation angle in an arc is $\pi\nu_0$. Then

$$\begin{aligned} M_{\text{Snake}} &= \mathrm{e}^{-\mathrm{i}\xi\sigma_3}(-\mathrm{i}\sigma_1) \\ M_{\text{arc}} &= \mathrm{e}^{-\frac{\mathrm{i}}{2}\pi\nu_0\sigma_3} \\ M_{\text{ring}} &= M_{\text{arc}}M_{\text{Snake}}M_{\text{arc}} = \mathrm{e}^{-\frac{\mathrm{i}}{2}\pi\nu_0\sigma_3}\,\mathrm{e}^{-\mathrm{i}\xi\sigma_3}(-\mathrm{i}\sigma_1)\,\mathrm{e}^{-\frac{\mathrm{i}}{2}\pi\nu_0\sigma_3} = \mathrm{e}^{-\mathrm{i}\xi\sigma_3}(-\mathrm{i}\sigma_1). \end{aligned} \tag{22}$$

It is just the spin rotation matrix of the Snake! The spin rotations in the arcs cancel out. The spin tune (on the closed orbit) can be obtained by noting that the spin rotation angle after one circumference is $2\pi\nu_{\text{c.o.}}$. Hence we parametrize the one-turn spin rotation matrix via

$$M_{\text{ring}} \equiv \mathrm{e}^{-\mathrm{i}\pi\nu_{\text{c.o.}}\boldsymbol{\sigma}\cdot\boldsymbol{n}_0}, \tag{23}$$

where $\boldsymbol{n}_0$ is a unit vector (the spin rotation axis). We deduce that the value of the spin tune is simply

$$\nu_{\text{c.o.}} = \tfrac{1}{2}. \tag{24}$$

*Very* significantly, the spin tune is *independent* of the beam energy. Hence, during acceleration, the spin tune will *never* cross any imperfection or intrinsic depolarizing resonances! The finding by Derbenev and Kondratenko that the spins would encounter no resonances during acceleration, up to arbitrarily high energies, was enthusiastically received in the field. The use of Siberian Snakes immediately raised the possibility of a simple scheme to accelerate polarized beams to high energy.

The spin rotation axis, at the origin, is parallel to the spin rotation axis of the Snake, namely

$$\boldsymbol{n}_0 = \boldsymbol{e}_1\cos\xi + \boldsymbol{e}_2\sin\xi, \tag{25}$$

and is also independent of the beam energy. The vector $\boldsymbol{n}_0$ is the direction of the stable long-term polarization. At other points in the ring the direction of $\boldsymbol{n}_0$ depends on both $\theta$ and the beam energy. A sketch of the orientation of the stable long-term polarization around the ring circumference, for a racetrack accelerator with a solenoidal Snake (longitudinal spin rotation axis) is shown in figure 7. The value of $a\gamma$ is 1.7. The ring design and energy are

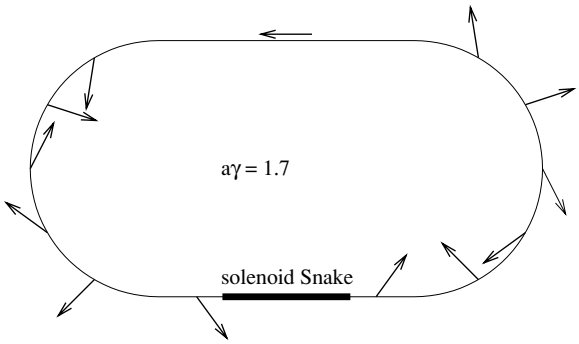


**Figure 7.** Orientation of the stable polarization direction around the circumference of a planar ring with a solenoidal Siberian Snake.

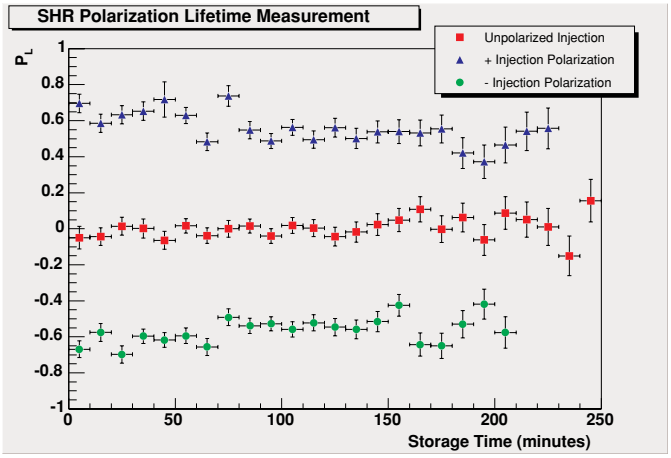


**Figure 8.** Longitudinal stored polarization at the SHR, for positive, negative and zero polarization at injection. Courtesy of W A Franklin (private communication) and MIT-Bates Linear Accelerator Center.

roughly typical for SHR. Unlike the case for a planar ring, the polarization direction lies in the horizontal plane.

Hence the use of a single Siberian Snake in a ring serves both to avoid depolarizing resonances *and* to automatically provide horizontal polarization in a storage ring. At both AmPS and SHR, the Snakes are solenoids, so the polarization direction is longitudinal (at any energy) in the straight section opposite the Snake. Not surprisingly, the experimental detectors at both rings are therefore located in the straight sections opposite to the Snake. At AmPS the beam was injected in the same straight section as the Snake (see figure 2), hence the direction of the incoming polarization varied with energy at AmPS. At SHR the beam is injected at the opposing straight section (see figure 3), hence the direction of the injected polarization is always longitudinal at SHR. The longitudinal polarization level at SHR, as a function of storage time, for three scenarios (positive, negative and zero polarization at injection), is shown in figure 8. One sees that the polarization is stable, although there is increasing scatter with time. The increased scatter in the data as a function of time may be correlated with loss of beam current and reduced statistics in the polarization measurements, and should not be taken seriously until more extensive data are available. We are grateful to W A Franklin

for originally providing us with this data ahead of publication (the data are now published in Franklin (2004)).

The first demonstration that a polarized beam depolarizes when $G\gamma \simeq k$, which is a resonance in a planar ring, but does *not* depolarize when a full-strength Snake is present in the ring, was carried out at the IUCF Cooler (Goodwin *et al* 1990). The resonance was $G\gamma = 2$. The Snake was a superconducting solenoid. Since the polarimeter could only measure the transverse polarization component, the vertical polarization was measured with the Snake off and the radial polarization with the Snake on. Depolarization was observed for $G\gamma \simeq 2$ with the Snake off, but there was no measureable depolarization with the Snake on. Goodwin *et al* (1990) also demonstrated that there was no depolarization, with a Snake on, in the vicinity of $G\gamma \simeq Q_y - 3$, which is an intrinsic betatron spin resonance in a planar ring, but not a resonance when a Snake is present.

### *4.7. Ring with two Siberian Snakes*

As appealing as the above ideas are, they are limited to low-energy rings. Despite the experimental success of the SHR (and earlier at AmPS), the use of a single Snake is not terribly good at very high energies because the spins precess in the horizontal plane all around the ring. The rate of precession increases with the energy. This makes the individual spins more susceptible to perturbations, increasing the risk of decoherence, i.e. loss of polarization. At RHIC, where $G\gamma \simeq 450$ at the design top energy of 250 GeV, small perturbations to the spin motion will likely cause serious problems. It is preferable if the polarization direction is vertical in the arcs of the ring *and* the spin tune is independent of the beam energy.

Consider a planar ring equipped with *two* Siberian Snakes. The Snakes are placed at diametrically opposite points of the ring, say at $\theta = 0$ and $\theta = \pi$. The Snake spin rotation axes are also orthogonal: say at $\xi$ and $\xi + \pi/2$. The Snake spin rotation matrices are

$$M_{s1} = \mathrm{e}^{-\mathrm{i}\xi\sigma_3}(-\mathrm{i}\sigma_1), \qquad M_{s2} = \mathrm{e}^{-\mathrm{i}\xi\sigma_3}(-\mathrm{i}\sigma_2). \tag{26}$$

We place the origin just *after* the exit of the first Snake. The one-turn spin rotation matrix is

$$M_{2\mathrm{Snakes}} = \mathrm{e}^{-\mathrm{i}\xi\sigma_3}(-\mathrm{i}\sigma_1)\,\mathrm{e}^{-\frac{\mathrm{i}}{2}\pi\nu_0\sigma_3}\,\mathrm{e}^{-\mathrm{i}\xi\sigma_3}(-\mathrm{i}\sigma_2)\,\mathrm{e}^{-\frac{\mathrm{i}}{2}\pi\nu_0\sigma_3} = -\mathrm{i}\sigma_3 = \mathrm{e}^{-\mathrm{i}\pi\sigma_3/2}. \tag{27}$$

This is simply a spin rotation of 180° around the vertical axis. Equating this expression to the parametrization $M_{\mathrm{ring}} \equiv \mathrm{e}^{-\mathrm{i}\pi\nu_{\mathrm{c.o.}}\boldsymbol{\sigma}\cdot\boldsymbol{n}_0}$ we again find that the value of the spin tune is $\nu_{\mathrm{c.o.}} = \frac{1}{2}$ independent of the beam energy. Obviously

$$\boldsymbol{n}_0 = \begin{cases} \boldsymbol{e}_3 & \text{for} \quad \theta \in (0, \pi) \\ -\boldsymbol{e}_3 & \text{for} \quad \theta \in (\pi, 2\pi) \end{cases} \tag{28}$$

This is a very satisfying result. The spin tune is one-half, independent of the beam energy, and the polarization direction is vertically up in one arc of the ring and vertically down in the other arc. A sketch of the orientation of $\boldsymbol{n}_0$ around the ring circumference, for a racetrack design with two Snakes, is shown in figure 9.

Another possibility is to make the Snake axes *not* orthogonal. Suppose the spin rotation axis of the second Snake is at an angle $\xi + (\pi/2) + \chi$. Then the spin rotation matrix of the ring is

$$M_{\mathrm{nonorthog}} = (-\mathrm{i}\sigma_1)\,\mathrm{e}^{\mathrm{i}\xi\sigma_3}\,\mathrm{e}^{-\frac{\mathrm{i}}{2}\pi\nu_0\sigma_3}(-\mathrm{i}\sigma_2)\,\mathrm{e}^{\mathrm{i}(\xi+\chi)\sigma_3}\,\mathrm{e}^{-\frac{\mathrm{i}}{2}\pi\nu_0\sigma_3} = \mathrm{e}^{-\mathrm{i}(\pi/2-\chi)\sigma_3}, \tag{29}$$

and so

$$\nu_{\mathrm{c.o.}} = \frac{1}{2} - \frac{\chi}{\pi}. \tag{30}$$

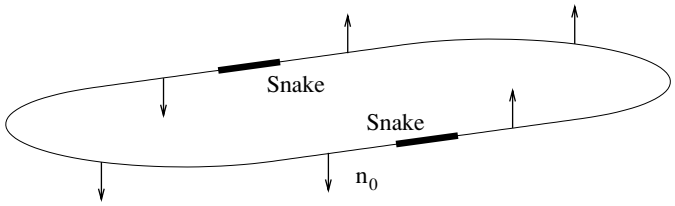


**Figure 9.** Sketch of the $\boldsymbol{n}_0$ axis (stable polarization direction) for a planar ring with two Siberian Snakes at diametrically opposite points in the ring.

The value of the spin tune is still independent of the beam energy. The value of $\nu_{\text{c.o.}}$ is farthest from an integer when $\chi = 0$, which is why attention is generally paid to pairs of Snakes with orthogonal spin rotation axes. The spin rotation axis $\boldsymbol{n}_0$ is still vertical (up or down) in the arcs. There are reasons, pertaining to the orbital motion and not treated in this review, why it may be desirable to operate a storage ring with a value of the vertical betatron tune close to one-half. The reasons have to do with the beam–beam interaction in colliding beam storage rings. In such a case, there may be valid reasons to consider the use of Snakes with nonorthogonal spin rotation axes, to hold the spin tune at a fixed (i.e. energy-independent) value not equal to $\frac{1}{2}$. In RHIC, however, the Snake spin rotation axes are orthogonal and the design value of the spin tune is $\frac{1}{2}$.

Other possibilities are to place the Snakes *not* diametrically opposite each other. However the spin tune then depends on the beam energy. A more important scenario is to employ more pairs of Snakes. An example is based on work by Steffen (1985). One can consider a set of $N$ pairs of Snakes, where the spin rotation axes of each pair are $\xi_1 = \frac{\pi}{2}\left(1 - \frac{1}{2N}\right)$ and $\xi_2 = -\frac{\pi}{2}\left(1 - \frac{1}{2N}\right)$. The overall spin rotation angle will still add up to $\pi$, yielding a closed-orbit spin tune of $\frac{1}{2}$. The closed-orbit spin direction alternates from vertically up to down in successive arcs. For example, for $N = 2$ (total of 4 Snakes), the spin rotation axes would be oriented at $(67.5^\circ, -67.5^\circ, 67.5^\circ, -67.5^\circ)$. We leave it to the reader to verify all of the above statements. The use of more pairs of Snakes is desirable for various reasons, but need not concern us here. A single pair of Snakes may be adequate for each RHIC ring.

Up to 2003, the analysing power of the RHIC polarimeters had been calibrated only at the injection energy of 24.3 GeV, not at the flattop of 100 GeV. The injected polarization at RHIC in 2003 was about 40% (this figure may be higher in the 2004 run). An absolute calibration of the RHIC polarimeters was obtained in the 2004 polarized proton run, but the results will unfortunately not be available in time for this review. A graph of the beam intensity, polarization and luminosity from the RHIC 2004 polarized proton run is shown in figure 10 (Huang *et al* 2004). The polarization is preserved for several hours during the RHIC stores. The spin rotators were also on when the data in figure 10 were taken. Because of the large beam excursions in the spin rotators at low energy, the rotators are actually off at injection (24 GeV) and are adiabatically turned on during flattop at 100 GeV. Huang *et al* (2004) present additional data that the polarization tilts over to the longitudinal direction at the particle detectors, without loss of polarization.

The first measurement of polarized proton collisions at RHIC was reported by Goto (2002) for the PHENIX Collaboration and by Surrow (2002) for the STAR Collaboration. The above measurements were made using transversely polarized beams because the spin rotators were not installed yet. Bültmann *et al* (2004) report the first measurement of pp elastic scattering at RHIC (at $\sqrt{s} = 200$ GeV) using the pp2pp detector. This measurement also used transversely polarized protons because there are no spin rotators around the pp2pp interaction point.

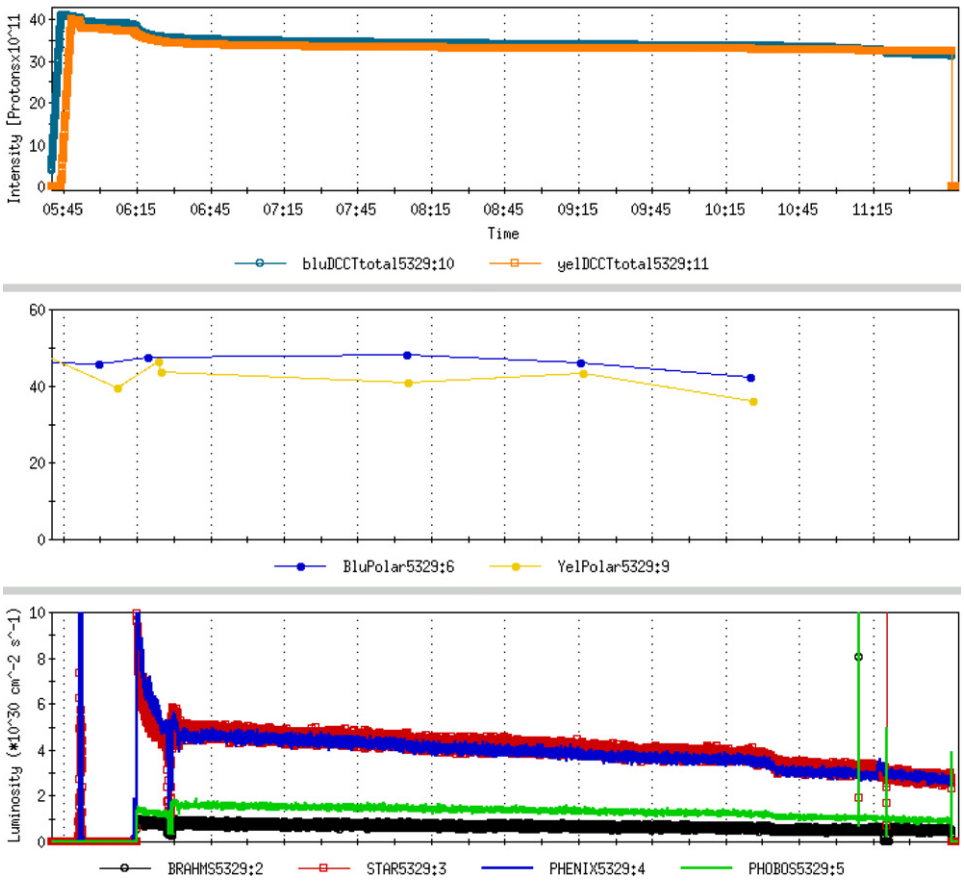


**Figure 10.** Graph of data from the RHIC 2004 polarized proton run. Top plot: beam intensity, centre plot: polarization, bottom plot: luminosity. Data for both the Blue and Yellow rings are shown. Courtesy of H Huang (private communication) and BNL.

An example of physics experiments using longitudinally polarized colliding proton beams is by Adler *et al* (2004).

### *4.8. Snake resonances*

It is not completely true that a ring equipped with one, or a pair, of Siberian Snakes encounters no depolarizing resonances. It is merely the case that the value of the closed-orbit spin tune is $\nu_{\text{c.o.}} = \frac{1}{2}$, or at least independent of the beam energy. Depolarizing resonances in a ring with Siberian Snakes are called 'Snake resonances'. Snake resonances are not a new type of resonance, but are generated by the same mechanism of coherent interference between the orbital and spin motion that characterizes the depolarizing resonances in planar rings. They are, in short, higher-order depolarizing resonances in a nonplanar ring. Experimental and theoretical work on Snake resonances will be reviewed in section 7.

### *4.9. Partial type 3 Snake*

There is an exception to the rule that the spin rotation axis of a (partial) Siberian Snake lies in the horizontal place. The exception is called a 'type 3' Snake, where the spin rotation axis points vertically, i.e. normal to the median plane of the accelerator. The name 'type 3' follows

from an early classification of Snakes as 'type 1' and 'type 2' but that terminology is archaic. We do not use the names 'type 1' and 2 in this review. Type 3 Snakes are a special case, and in this review (and also throughout the literature) the term 'Snake', without qualification, implies that the spin rotation axis lies in the horizontal plane. Nobody has ever deliberately built a partial or full-strength type 3 Snake. However, Anferov (1998) has suggested that the use of full-strength type 3 Snakes might improve the stability of the spin dynamics in high-energy storage rings.

In general type 3 (partial) Snakes are more of a curiosity, or a source of systematic error, depending on one's point of view, than anything else. They are really spin tune shifters rather than rotators of the polarization direction. In fact the concept of a partial type 3 Snake was originally discovered as a systematic error in beam energy calibration measurements at the IUCF Cooler (Pollock 1991). The notion of 'beam energy calibration measurements' and the work at the IUCF Cooler will be reviewed in subsection 5.13.2.

Consider a single point-rotator partial type 3 Snake with a fractional strength $\lambda$, in a planar ring. The Snake spin rotation matrix is $M_3 = \mathrm{e}^{-\mathrm{i}\pi\lambda\sigma_3/2}$. Placing the origin just before the partial type 3 Snake, the one-turn spin rotation matrix is

$$M = \mathrm{e}^{-\mathrm{i}\pi\nu_0\sigma_3}\,\mathrm{e}^{-\mathrm{i}\pi\lambda\sigma_3/2} = \mathrm{e}^{-\mathrm{i}\pi(\nu_0+\lambda/2)\sigma_3}. \tag{31}$$

Equating this to the parametrization $\mathrm{e}^{-\mathrm{i}\pi\nu_{\mathrm{c.o.}}\boldsymbol{\sigma}\cdot\boldsymbol{n}_0}$ yields the obvious answers

$$\boldsymbol{n}_0 = \boldsymbol{e}_3, \qquad \nu_{\mathrm{c.o.}} = \nu_0 + \frac{\lambda}{2}. \tag{32}$$

Hence the spin tune is shifted, but the spin precession axis is not affected. A clean demonstration of this effect was observed in some studies at the IUCF Cooler by Baiod *et al* (1993). The solenoid Snake was switched off in the study. However, the structure of the electron cooling section of the IUCF Cooler (see figure 4) contained a partial type 3 Snake. The imperfection resonance at $G\gamma = 2$, which is normally a single resonance in a planar ring, was observed to split into a doublet $G\gamma = 2 \pm \lambda/2$.

### *4.10. Spin rotators*

The subject of spin rotators is closely related to that of Siberian Snakes. Spin rotators are used to rotate the spin (polarization) direction from the vertical to the horizontal plane, and back again. This is because most particle physics experiments with polarized beams in colliding beam accelerators require longitudinally polarized beams. As with Snakes, spin rotators can exist because the spin and the orbit rotate through different angles when passing through a magnet. As we have also seen, the use of a single solenoidal Siberian Snake can provide the requisite longitudinal polarization, for lower energy rings. Spin rotators are required in high energy rings, such as RHIC, where the polarization is vertical in the arcs.

Obviously, a solenoid can be used as a spin rotator, if the spin rotation angle is set to 90° rather than 180°. If a spin is vertical at entry, then it will point radially upon exit from the solenoid. Hence a further horizontal bend is required, between the solenoid and the interaction point, to rotate the spins to be longitudinal at the particle detector. Another horizontal bend and solenoid are required downstream of the interaction point, to restore the polarization direction to the vertical. As with solenoid Snakes, the magnetic field of a solenoid spin rotator must scale with the beam momentum. Spin rotator designs with transverse fields are therefore required for operation at high energies, because the magnetic fields need only to scale with $\beta$.

At RHIC there is a horizontal bend of $\pm 3.675$ mrad between a spin rotator and the collision point. Since the spin precession angle through a horizontal bend is energy dependent, a RHIC spin rotator must actually rotate the spins from the vertical to an energy-dependent direction in the horizontal plane, to attain longitudinal polarization at the collision point. As with the

RHIC Snakes, the RHIC spin rotators are also built using helical magnetic fields. The design will be reviewed in section 5.

The symmetry of the spin rotator placement around a RHIC interaction point automatically guarantees that the spins are restored to the vertical after passage through both rotators. This fact is not trivial. For example, in the initial commissioning of the RHIC spin rotators (MacKay *et al* 2003), a sign error was made in the spin rotation angles. This caused all the spin rotators to be connected with the leads to the power supplies reversed. At 100 GeV, the spins should be rotated from the vertical to an angle of about 40° to the longitudinal. Instead they were rotated to an angle of −40°, leading to an almost *radial* polarization (about 80° from longitudinal) at the PHENIX detector. The error was quickly identified and rectified. Nevertheless, under all circumstances the spins were restored to the vertical in the arcs. Fortunately, the design of the spin rotators was such that the error could be rectified by simply reversing the leads to the power supplies. In fact, the mistake built confidence in both the PHENIX polarimeter and the overall theoretical model of the spin rotators.

Spin rotators have also been employed at HERA. The HERA spin rotators are built using horizontal and vertical dipole bends. The design is known as the HERA 'minirotator' (Buon and Steffen 1986). HERA is a two-ring lepton-hadron collider. The lepton ring (HERA-e) circulates electrons or positrons of approximately 27.5 GeV beam energy. The hadron ring (HERA-p) circulates protons, originally at 820 GeV, now upgraded to 920 GeV (the so-called HERA2). The electrons or positrons polarize spontaneously by the emission of spin-flip synchrotron radiation (the Sokolov–Ternov effect). The protons are unpolarized. Spin rotators are employed to rotate the lepton spins to provide longitudinal polarization at the interaction points. HERA is the only ring to attain longitudinal radiative polarization (AmPS and SHR inject beams from polarized electron sources). The first pair of spin rotators was installed in the HERA East Hall in 1994 (Barber 1995b). The lepton and proton beams do not collide in the East Hall; instead the HERMES internal gas jet experiment operates there. In 2003, additional spin rotator pairs were installed at the HERA North and South Halls, for the particle physics detectors H1 and ZEUS, respectively. The HERA West Hall is used for beam injection and no experiments are performed there. Since the leptons polarize spontaneously in the ring, the polarization level starts from zero and builds up exponentially to an asymptotic level. A polarization level of about 40–50% is routinely delivered with the rotators switched on.

In its initial design, there were no plans to accelerate and store polarized protons in HERA. Over the years, a number of feasibility studies have been performed for the installation of Siberian Snakes in the HERA proton ring. At such a high energy (920 GeV), one pair of Siberian Snakes in the ring is not enough; most design studies employ four Snakes. A description of the early ideas on the subject of polarized protons in HERA is given by Barber (1995a). Even with four Snakes, the vertical bends in the interaction regions of HERA would interfere with any standard Siberian Snake configuration. Anferov and Phelps (1997) present the notion of four additional 'flattening' Snakes, which are Siberian Snakes with a radial spin rotation axis. One pair of flattening Snakes would be installed in each of the North and South Hall interaction regions. Their purpose is to make the interaction region look effectively flat to the rest of the ring, i.e. to compensate the effect of the whole vertical bending in the interaction region. The idea utilizes the symmetry of the geometry of the horizontal and vertical bends around a HERA interaction point. An idea for helical Snakes and spin rotators, including the flattening Snakes, was proposed by Barber *et al* (1999). More recent studies, after the luminosity and energy upgrade to HERA2, are reported by Barber *et al* (2002). In this review, a four-Snake scheme is employed. The orientations of the Snake spin rotation axes relative to the beam direction are −45°, 0°, 45° and 90°. In the final stages of writing this review, two new papers were published, by Hoffstaetter (2004) on the subject of Siberian Snake designs

for HERA-p and by Hoffstaetter and Vogt (2004) on higher-order spin resonances in rings with Snakes, also with reference to HERA-p.

## 5. Siberian Snakes and spin rotators II

### *5.1. General remarks*

The previous section reviewed the general concept of Siberian Snakes (also spin rotators). It motivated the need for Snakes in high energy storage rings. Here we shall examine various practical designs of Siberian Snakes and spin rotators. This section will focus on the devices themselves, i.e. 'the magnets'. The beam dynamics issues will be treated in the companion review MSY2. We shall discuss the pros and cons of the various schemes. For the record, we also mention here an early study by Skrinsky (1982) of longitudinally polarized colliding beams (radiatively polarized), which we do not have space to review. An elegant design, which there is also insufficient space to review, is by Fieguth (1987). It consists of a sequence of dipole magnets, which can double as both Snakes and spin rotators, by a repowering of the dipole fields.

### *5.2. Solenoid Snake*

The spin rotates around the longitudinal axis through 180°, at least for the reference particle. However, the longitudinal magnetic field of a solenoid will also cause the horizontal and vertical betatron oscillations to couple to each other, via the $\boldsymbol{v} \times \boldsymbol{B}$ Lorentz force in the solenoid. If left uncompensated, this coupling will propagate around the rest of the accelerator, and will upset the ring optics. The problem is especially acute because a large value for the magnetic field integral is required to make a solenoid a Snake. We discuss the orbital compensation of a solenoidal Snake, to match the orbital oscillations in the Snake to that of the ring optics.

In addition to the $x$–$y$ coupling caused by the magnetic field in the main body of the solenoid, the fringe fields at the entrance and exit of a solenoid also lead to focussing of the betatron orbits. A real solenoid is necessarily of finite length, and at the solenoid entrance and exit the magnetic field is not longitudinal but splays outward. This is a necessary consequence of the Maxwell equation $\nabla \cdot \boldsymbol{B} = 0$. Particles entering and exiting a solenoid therefore see a transverse component of magnetic field, as well as longitudinal. This focussing changes the betatron tunes, and must also be dealt with when matching a solenoid to the ring optics.

The AmPS and SHR Siberian Snake designs consist in both cases of a pair of solenoids in series. The same team, from BINP (led by Yuri Shatunov) designed both Snakes and the matching to the ring optics. The material below is mainly taken from Luijckx *et al* (1997) and Zwart *et al* (1995). The AmPS and SHR solenoids are matched to the rest of the ring by using one pair of quadrupoles and two pairs of skew quadrupoles. The schematic design is (not to scale)

$$\text{SQ1} - \text{SQ2} - \text{SOL} - \text{Q} - \text{Q} - \text{SOL} - (-\text{SQ2}) - (-\text{SQ1}).$$

The quadrupoles (focal length $f$) are placed between the solenoids, and the skew quadrupoles (focal lengths $q_1, q_2$ respectively) are placed upstream and downstream of the solenoids. The overall design is mirror symmetric around the midpoint. The entire collection is called a 'Snake system'. The system has four independent parameters, consisting of the three focussing strengths $f, q_1$ and $q_2$, and the lengths of the two solenoids. (To operate as a Snake only the product $BL$ is constrained, hence $L_{\text{sol}}$ is a free parameter.) Skew quadrupoles, by themselves, couple the horizontal and vertical betatron oscillations, and so their coupling can be used to compensate that of the solenoids. The use of skew quadrupoles to compensate the betatron

coupling induced by the solenoids of high-energy colliding beam particle detectors is standard. It is indeed one of the principal reasons to introduce skew quadrupoles in a ring in the first place. The quadrupoles serve to adjust the overall focussing of the system. The upstream skew quadrupoles are rotated through 45° relative to the $x$-axis, and the downstream skew quadrupoles are rotated through −45°. This is indicated symbolically by the notation (–SQ1) and (–SQ2).

It is convenient to describe the transport of the orbital motion through a beamline element via a 'transfer map'. Consider a drift space of length $L$. For definiteness, we treat the horizontal motion. The variables are $x$ and the slope $x' = \mathrm{d}x/\mathrm{d}s$. Then, given input values $(x_i, x_i')$, the output values $(x_o, x_o')$ are

$$\begin{pmatrix} x_o \\ x_o' \end{pmatrix} = \begin{pmatrix} 1 & L \\ 0 & 1 \end{pmatrix} \begin{pmatrix} x_i \\ x_i' \end{pmatrix}. \tag{33}$$

The transfer map is a $2 \times 2$ matrix. Including the vertical motion leads to a $4 \times 4$ matrix. For AmPS and SHR, the $4 \times 4$ orbit map of the Snake system, using $(x, x', y, y')$ variables, is

$$\begin{aligned} M_{\mathrm{AmPS}} &= \begin{pmatrix} -1 & -L & & \\ 0 & -1 & & \\ & & 1 & L \\ & & 0 & 1 \end{pmatrix}, \\ M_{\mathrm{SHR}} &= \begin{pmatrix} 1 & L & & \\ 0 & 1 & & \\ & & -1 & -L \\ & & 0 & -1 \end{pmatrix}, \end{aligned} \tag{34}$$

where blanks denote zeros in the above matrices. The expressions for the above matrices correct a misprint in Luijckx *et al* (1997). Here $L$ is the length of the Snake system, which is 4.7 m at AmPS and 4.5 m at SHR. The matrix is $2 \times 2$ block diagonal, hence the $x - y$ orbital motion is decoupled. Hence at AmPS, for the vertical betatron oscillations the Snake system is equivalent to a drift space of length $L$, whereas for the horizontal betatron oscillations the Snake system behaves as a drift of length $L$, with an extra horizontal betatron tune advance of $\Delta Q_x = \frac{1}{2}$. During operation of the Snake, the AmPS ring was run with a slightly modified lattice to absorb the horizontal betatron tune shift. At SHR, the design of the Snake system is similar, but the phase advance is interchanged between horizontal and vertical. The horizontal mapping is a drift space, while in the vertical plane the map looks like a drift plus an additional vertical betatron phase advance of $\pi$.

The orbital matching for the IUCF Cooler Snake was different, because the Snake consisted of a single solenoid. Hence all of the compensating quadrupoles and skew quadrupoles had to be upstream or downstream of the solenoid. An attempted design (by Mane) was to make the Snake system look like a drift space in one plane and a drift plus a betatron phase advance of $2\pi$ in the other plane (resulting in a tuneshift of $\Delta Q = 1$). Hence the overall orbital map would have looked like a drift space in both planes. Unfortunately, this design decision required very strong focussing by the quadrupoles and skew quadrupoles, which constrained the useful beam aperture and also made the design sensitive to errors (imperfections). In many of the IUCF spin dynamics studies, the above orbit compensation scheme was not used.

### *5.3. Steffen Snakes*

Steffen (1978, 1983, 1985, 1987, 1989a, 1989b) made many seminal contributions to the design of Siberian Snakes. With Buon, he also designed the spin rotator for HERA (Buon and

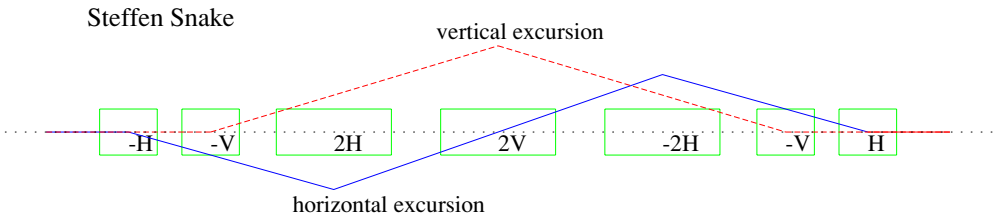


**Figure 11.** Schematic of the horizontal and vertical orbit excursions in a Steffen Snake.

Steffen 1986). Steffen invented a design of a family of Snakes using a sequence of alternating vertical and horizontal dipoles, which he dubbed a 'novel type Snake family'. Their spin rotation axes could be oriented at any angle in the horizontal plane. They are now called 'Steffen Snakes'. A schematic design of a Steffen Snake is shown in figure 11. The treatment below mainly follows Lee (1997). The magnet sequence is (Steffen 1983)

$$S_{\text{Steffen}} = (-H, -V, 2H, 2V, -2H, -V, H),$$

where $H$ denotes a horizontal bend (vertical magnetic field) and $V$ denotes a vertical bend (radial magnetic field). The spacing between adjacent magnets is the same for all the magnets. The particles enter from the left and exit on the right. The key feature of the design is the antisymmetric configuration of the vertical magnetic fields ($H$ bends) and the symmetric configuration of the radial magnetic fields ($V$ bends). The horizontal and vertical bend angles sum separately to zero, and, in addition, the orbit displacement also cancels to zero, in both planes. With this arrangement, the excursion of the design orbit is localized within the Snake, and vanishes outside the Snake. It is essential that there be *no quadrupoles* between the dipoles, else there are complications when matching the betatron oscillations in the Snake to the rest of the ring. This does create a slight problem, in that there is no orbital focussing within the Snake (which can be quite long). We shall not discuss the matching of Steffen Snakes to the optics of the rest of the ring. The interleaving of the vertical and radial magnetic fields in a Steffen Snake yields a set of noncommuting spin rotations. The overall spin rotation matrix is

$$M_{\text{Steffen}} = \mathrm{e}^{-\mathrm{i}\psi_H\sigma_3/2}\,\mathrm{e}^{\mathrm{i}\psi_V\sigma_1/2}\,\mathrm{e}^{\mathrm{i}\psi_H\sigma_3}\,\mathrm{e}^{-\mathrm{i}\psi_V\sigma_1}\,\mathrm{e}^{-\mathrm{i}\psi_H\sigma_3}\,\mathrm{e}^{\mathrm{i}\psi_V\sigma_1/2}\,\mathrm{e}^{\mathrm{i}\psi_H\sigma_3/2}. \tag{35}$$

The field (anti)symmetry guarantees that the spin rotation axis lies in the horizontal plane. However, the overall spin rotation angle does not in general equal 180° unless the values of $\psi_H$ and $\psi_V$ are chosen appropriately. Equating the above matrix product to the parametrization in (20) yields

$$\cos\frac{\lambda_s\pi}{2} = 1 - 2\sin^2\psi_H\sin^2\psi_V \tag{36}$$

and

$$\begin{aligned}\sin\frac{\lambda_s\pi}{2}\cos(\xi-\psi_H) &= -\sin^2\psi_H\sin(2\psi_V)\\ \sin\frac{\lambda_s\pi}{2}\sin(\xi-\psi_H) &= -\sin(2\psi_H)\sin\psi_V.\end{aligned} \tag{37}$$

Alternatively we can express the left-hand sides using only $\sin\xi$ and $\cos\xi$. The answer is

$$\begin{aligned}\sin\frac{\lambda_s\pi}{2}\cos\xi &= 2\sin^2\psi_H\cos\psi_H\sin\psi_V(1-\cos\psi_V)\\ \sin\frac{\lambda_s\pi}{2}\sin\xi &= -2\sin\psi_H\sin\psi_V[\cos^2\psi_H+\sin^2\psi_H\cos\psi_V],\end{aligned} \tag{38}$$

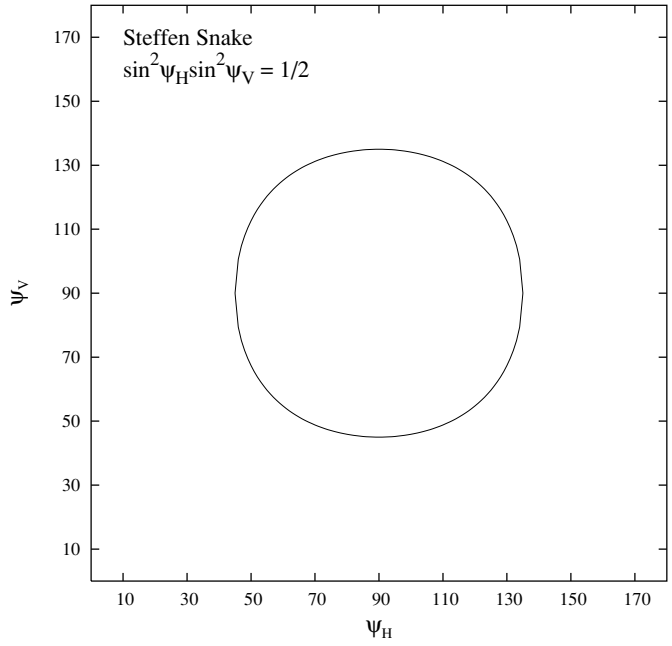


**Figure 12.** Locus of solutions (in the first quadrant) for the horizontal and vertical spin rotation angles for a Steffen Snake.

which is not quite so succint. The Snake spin axis angle is not a simple function of $\psi_{H,V}$. We can read off the following symmetries:

$$\begin{aligned} &\psi_H \to -\psi_H \quad &&\Rightarrow \quad \xi \to -\xi, \\ &\psi_V \to -\psi_V \quad &&\Rightarrow \quad \xi \to \pi + \xi, \\ &\left.\begin{aligned}\psi_H &\to -\psi_H \\ \psi_V &\to -\psi_V\end{aligned}\right\} \quad &&\Rightarrow \quad \xi \to \pi - \xi. \end{aligned} \tag{39}$$

A full Snake is given by setting $\lambda_s = \pm 1$. The resulting constraint on $\psi_H$ and $\psi_V$ is

$$\sin^2 \psi_H \sin^2 \psi_V = \tfrac{1}{2}. \tag{40}$$

This constrains the values of $\psi_H$ and $\psi_V$ to lie in the interval $\psi_{H,V} \in (45^\circ, 135^\circ)$, with 'image' solutions in the other quadrants. A graph of $\psi_V$ against $\psi_H$ in the first quadrant is shown in figure 12. The locus of $(\psi_H, \psi_V)$ values is almost but not quite a circle. A plot of the corresponding values of the Snake axis angle $\xi$, plotted against $\psi_H$, is shown in figure 13. The solution actually consists of two branches, according as $\psi_V \geqslant \pi/2$ or $\psi_V \leqslant \pi/2$. The path of a unit spin vector through a Steffen Snake with $(\psi_H, \psi_V) = (90^\circ, 45^\circ)$ is shown in figure 14. This choice of spin rotation angles leads to simple spin rotations which one can work out by hand. From (37) or (38) one can deduce that the Snake axis angle is $\xi_1 = -90^\circ$, i.e. a longitudinal spin rotation axis.

The maximum excursions of the design orbit in a Steffen Snake in the horizontal and vertical directions are, respectively,

$$x_{\max} = (\ell_x + \ell_y + 2\ell_g)\frac{\psi_H}{G\gamma}, \qquad y_{\max} = (2\ell_x + \ell_y + 2\ell_g)\frac{\psi_V}{G\gamma}, \tag{41}$$

where $\ell_x$ and $\ell_y$ are the effective lengths (i.e. including corrections due to the fringe fields) of the $H$ and $V$ magnets and $\ell_g$ ($g$ for 'gap') is the spacing between the magnets. Hence smaller

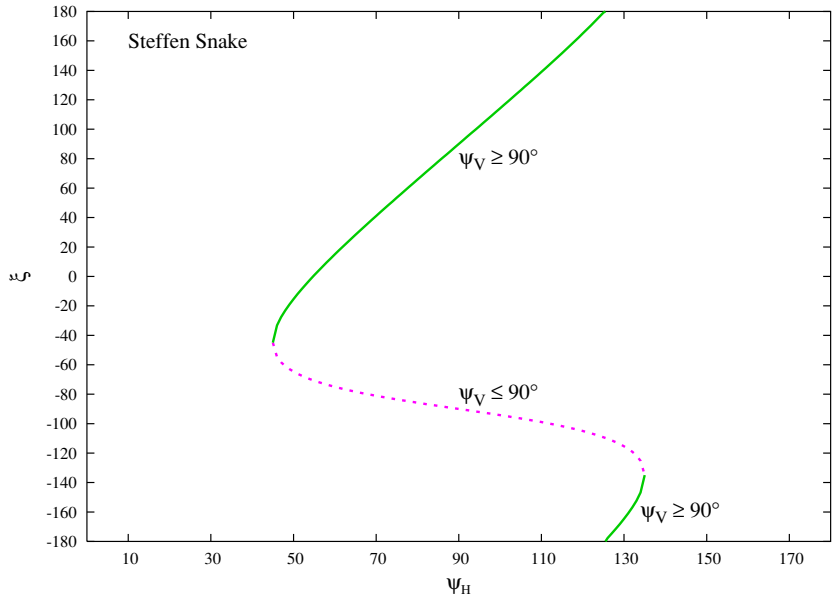


**Figure 13.** Graph of the Snake axis angle for a Steffen Snake.

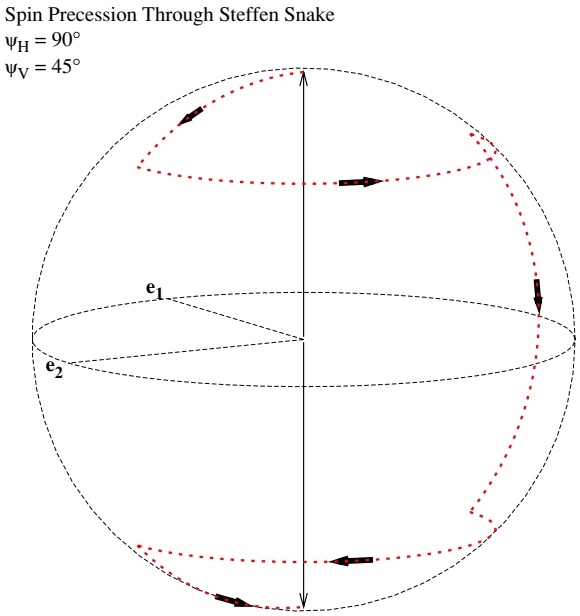


**Figure 14.** Path of a unit spin vector through a Steffen Snake.

values of $\ell_{x,y,g}$ will reduce the values of $x_{\max}$ and $y_{\max}$. Assuming that all the magnets have the same magnetic field strength $B$, then

$$\ell_x \simeq \frac{mc\beta}{G}\frac{\psi_H}{B}, \qquad \ell_y \simeq \frac{mc\beta}{G}\frac{\psi_V}{B}. \tag{42}$$

The value of $\beta$ is approximately unity, and the other parameters are constants. Hence, for a given choice of values for $\psi_H$ and $\psi_V$, we see that $\ell_{x,y} \propto B^{-1}$, so a higher value of the magnetic field yields a smaller orbital excursion.

Steffen Snakes are, essentially, a one-parameter family of Snakes, where the Snake axis angle can be varied through all values. By orienting the spin rotation axes at $\pm 45^\circ$, one can obtain orthogonal spin rotation axes using essentially the same design for both Snakes. Steffen Snakes have been the basis for much additional work on Snake designs.

Steffen Snakes do have the disadvantage that they are not compact devices, and the beam orbit excursions are rather large. A number of ideas have been proposed to overcome these deficiencies, while retaining the good qualities of Steffen's design. Lee (1997) describes a variety of ideas, for example, 'split Snakes' and 'compact Snakes', many of them invented by Lee himself. The basic idea is to work with a design of the form

$$S_m = (-H, -V, mH, V, V, -mH, -V, H), \tag{43}$$

where $m$ is a number determined by the geometry. Note that we write $(V, V)$ instead of $2V$ for the central magnet, because we allow for a gap of length $2d$ between the two $V$ magnets. This gap is not the same as the gap $\ell_g$ between the other magnets. Then the value of $m$ must satisfy a quadratic equation (Lee 1997)

$$\ell_H + \ell_V + 2\ell_g = (m-1)(d + \ell_V + \ell_g) + \tfrac{1}{2}(m-1)^2 \ell_H. \tag{44}$$

Further details of such work will be omitted.

### *5.4. Helical Snakes*

Another important idea is that of helical Snakes. The first published statement that a helical wiggler can act as a Snake appears to be by Kondratenko (1982). The orbit performs a corkscrew around the central axis. They have a shorter length than Steffen Snakes, and with a smaller orbit excursion. We use $s$ to denote the arc-length along the *central axis*: the basis vector $\boldsymbol{e}_1$ points radially outward, $\boldsymbol{e}_2$ points along the central axis and $\boldsymbol{e}_3$ is vertical. The helical magnetic field $\boldsymbol{B} = B_1\boldsymbol{e}_1 + B_2\boldsymbol{e}_2 + B_3\boldsymbol{e}_3$ is given by

$$B_1 = B_h \sin(ks), \qquad B_2 = 0, \qquad B_3 = B_h \cos(ks) \tag{45}$$

for small excursions from the central axis. Here $k$ determines the pitch of the helix and $B_h$ is a constant. To avoid unnecessary clutter we have chosen the field at the entrance of the magnet ($s = 0$) to be vertical. The above field pattern is the same as that of a helical wiggler. The wavelength of a full twist of the helix is $\lambda_h = 2\pi/|k|$. A positive (negative) sign for $k$ denotes a right-handed (left-handed) helix. In more sophisticated designs $k$ is a function of $s$, but we take it to be a constant. The above expression satisfies the Maxwell equation $\boldsymbol{\nabla} \cdot \boldsymbol{B} = 0$, but not Ampère's Law for time-independent fields in a current-free region: $\boldsymbol{\nabla} \times \boldsymbol{B} \neq 0$. Hence the above expression is only approximate. However, the additional terms contribute only small effects. We shall discuss them later.

With the above approximation, the magnetic field is transverse to the axis, and 'twists' along the axis. Helical Snakes were extensively studied by Courant (1989). A practical implementation of the helical magnetic field, using dipole magnets with horizontal and vertical fields, was given by Wienands (1991). In Wienand's design the magnetic field is not truly helical, but is rather a dipole field, whose direction changes in steps along the axis. In the early designs of helical Snakes, the spin rotation axis was close to the longitudinal direction. Steffen (1987) proposed a modification, borrowing from his own work on Steffen Snakes, to enable the spin rotation axis to be oriented at an arbitary angle. The treatment below mainly

follows Courant (1989), but with changes of sign because of our coordinate system. The orbital equations of motion are (using primes to denote differentiation with respect to $s$)

$$x'' = \frac{eB_h}{pc}\cos(ks), \qquad y'' = -\frac{eB_h}{pc}\sin(ks). \tag{46}$$

The general solution of the above equations is

$$\begin{aligned} x(s) &= -r_h(1-\cos(ks)) + x_0 + x_0' s \\ y(s) &= -r_h \sin(ks) + y_0 + (y_0' + kr_h)s, \end{aligned} \tag{47}$$

where

$$r_h = -\frac{1}{k^2}\frac{eB_h}{pc}. \tag{48}$$

The above solution is a straight line plus a helical orbit, whose radius is $r_h$ and whose pitch is the same as that of the magnetic field. For the spin equation of motion, define a parameter $\kappa$ via

$$\kappa = -(G\gamma + 1)\frac{eB_h}{pc} \tag{49}$$

and represent the spin by a spinor $\Psi$. Then

$$\frac{\mathrm{d}\Psi}{\mathrm{d}s} = \frac{\mathrm{i}}{2}\frac{e}{pc}\boldsymbol{\sigma}\cdot[(G\gamma+1)\boldsymbol{B}_\perp + (G+1)\boldsymbol{B}_\parallel]\Psi. \tag{50}$$

Strictly speaking, $\boldsymbol{B}_\perp$ and $\boldsymbol{B}_\parallel$ are defined with respect to the particle velocity, but it is an adequate approximation to reference them to the central axis. Then we can neglect the term in $\boldsymbol{B}_\parallel$, since the major interest in Snakes is for $G\gamma \gg 1$. This yields

$$\frac{\mathrm{d}\Psi}{\mathrm{d}s} \simeq -\frac{\mathrm{i}}{2}\kappa[\sigma_1\sin(ks) + \sigma_3\cos(ks)]\Psi = -\frac{\mathrm{i}}{2}\kappa\sigma_3\,\mathrm{e}^{\mathrm{i}ks\sigma_2}\Psi. \tag{51}$$

We transform to a frame rotating around the axis and define a new spinor $\Psi_h$ via

$$\Psi_h = \mathrm{e}^{\mathrm{i}ks\sigma_2/2}\Psi. \tag{52}$$

The equation of motion for $\Psi_h$ is

$$\frac{\mathrm{d}\Psi_h}{\mathrm{d}s} = -\frac{\mathrm{i}}{2}(\kappa\sigma_3 - k\sigma_2)\Psi_h. \tag{53}$$

This can be solved explicitly, because the spin rotation matrix is a constant. The answer is

$$\Psi_h(s) = \mathrm{e}^{-\mathrm{i}s(\kappa\sigma_3 - k\sigma_2)/2}\Psi_h(0). \tag{54}$$

The transformation of the original spinor is

$$\Psi(s) = M_H\Psi(0), \tag{55}$$

where the spin rotation matrix of the helix is

$$M_H = \mathrm{e}^{-\mathrm{i}ks\sigma_2/2}\,\mathrm{e}^{-\mathrm{i}s(\kappa\sigma_3 - k\sigma_2)/2}. \tag{56}$$

The parameters must be chosen such that the overall spin rotation angle is 180°, in addition to the fact that the design orbit must match the rest of the machine. The most elegant solution to these issues is that by the VEPP-2M design team, which will be reviewed shortly below.

### *5.5. Helical magnetic fields*

The full solution for the transverse magnetic field components, in terms of modified Bessel functions, is given by MacKay *et al* (1999). In practice, a paraxial approximation suffices for most purposes; the higher-order field corrections have only a small effect, which can be dealt with by numerical programs. We previously displayed the simplest approximation to the above fields, which were the terms independent of $r$. At the next-lowest order, one has (using a right-handed coordinate system $(x, y, s)$)

$$\begin{aligned} B_x &\simeq -B_0 \left\{ \left[ 1 + \frac{k^2}{8}(3x^2 + y^2) \right] \sin(ks) - \frac{k^2}{4} xy \cos(ks) \right\}, \\ B_y &\simeq \quad B_0 \left\{ \left[ 1 + \frac{k^2}{8}(x^2 + 3y^2) \right] \cos(ks) - \frac{k^2}{4} xy \sin(ks) \right\}, \\ B_s &\simeq -B_0 k \left\{ 1 + \frac{k^2}{8}(x^2 + y^2) \right\} [x \cos(ks) + y \sin(ks)]. \end{aligned} \tag{57}$$

Hence a helical magnet has an intrinsic sextupole component. However, this is a higher-order effect; all that happens is that the orbit compensation and matching to the rest of the ring is slightly more complicated, but not seriously so. The Snakes and spin rotators still work basically as described in the rest of this review.

### *5.6. Full-twist helical Siberian Snakes and spin rotators*

The design of the helical Snakes and spin rotators that we shall now review was created by the VEPP-2M design team, led by Yuri Shatunov. They developed a design of helical magnets which can serve to construct *both* Siberian Snakes and spin rotators, with automatic compensation of the orbit excursions, i.e. localized entirely within the Snake/rotator (Ptitsyn and Shatunov 1995, 1997b). The above papers are part of a long tradition of work at BINP, both practical and theoretical, with helical magnets. The VEPP-2M team's design has been employed for the RHIC Snakes and spin rotators (Alekseev *et al* 2003). We begin with some observations pertaining to the excursions of the design orbit, and treat the spin later. From now on we follow the formalism of Ptitsyn and Shatunov (1997b).

The first key idea is to consider a helix with a full 360° twist of the magnetic field, i.e. a helix of length $\lambda = 2\pi/|k|$. For convenience we define a parameter $\eta = k/|k|$ which expresses the handedness (the helicity) of the magnet. Then $\eta = +1(-1)$ for a right (left) handed helix. We set $ks = \pm 2\pi$, i.e. $\cos(ks) = 1, \sin(ks) = 0$ in (47) to obtain the solution for the beam excursion at the exit

$$\begin{aligned} x &= x_0 + x_0' \lambda, \qquad & y &= y_0 + y_0' \lambda + 2\pi r_h \eta, \\ x' &= x_0', & y' &= y_0'. \end{aligned} \tag{58}$$

The contribution from the helix vanishes *automatically*. Furthermore, if the entrance values are $x_0 = y_0 = 0$ and $x_0' = y_0' = 0$, then the orbit value at the exit is simply a displacement along the direction of the entrance magnetic field (in this case the vertical). One easily sees that $x = 0, x' = y' = 0$ and $y = 2\pi r_h \eta$, where the sign of $y$ is equal to the sign of the product $r_h \eta$.

If we therefore place two full twist helices in series, with equal and opposite values of $r_h \eta$, then the final orbit displacement at the exit of the two-helix system will *automatically* vanish, for an arbitrary magnitude of $r_h \eta$. The two possible designs are (i) the same handedness $\eta$, and equal but opposite values for $r_h$ (opposite sign of magnetic field at helix entrance), or (ii) opposite handedness for $\eta$ (helices of opposite pitch), and equal values for $r_h$. In either case,

however, this gives only one degree of freedom, namely the value of $|r_h|$, which is not enough to control both the spin rotation angle *and* the direction of the spin rotation axis.

We obtain two independent parameters if we employ a system of *four* helices in series. Before proceeding further, we note the following constraint equations. We define $\alpha$ to be the angle of the magnetic field to the vertical, at the entrance of a helix. In the above examples, $\alpha_1 = \alpha_2 = 0$, but in general we can take the $\alpha_i$ to be adjustable parameters. Then the conditions for automatic compensation of the orbit excursions are

$$\sum_{i=1}^{4} r_{hi}\eta_i \sin\alpha_i = 0, \qquad \sum_{i=1}^{4} r_{hi}\eta_i \cos\alpha_i = 0. \tag{59}$$

We now hark back to the Steffen Snake design and note that the horizontal magnetic fields were symmetrical and the vertical magnetic fields were antisymmetrical with respect to the midpoint of the Snake. This feature guaranteed automatic internal closure of the beam orbit excursions and also that the overall spin rotation axis would lie in the horizontal plane. The next key idea in the BINP design is to seek a configuration of helical fields with similar symmetry. Suitable conditions on the four helices are

- $\eta_1 = \eta_4, \eta_2 = \eta_3$.
- $r_{h1} = -r_{h4}, r_{h2} = -r_{h3}$.
- $N_1 = N_4, N_2 = N_3$, where $N_j$ is the number of periods in the $j$th helix.
- The magnetic field at the entrance of each helix is vertical ($\alpha_i = 0$).

The indices 1–4 obviously correspond to the four helical magnets. Since $\alpha_i = 0$ in all the magnets, the first condition in (59) is trivially satisfied, and the second reduces to

$$\sum_{i=1}^{4} r_{hi}\eta_i = 0. \tag{60}$$

It is immediately obvious that this condition is satisfied by the above solution, because $r_{h1}\eta_1 + r_{h4}\eta_4 = 0$ and similarly $r_{h2}\eta_2 + r_{h3}\eta_3 = 0$. Hence the parameters of the fourth helix are determined by the first, while the parameters of the third helix are determined by the second. Effectively, we have two nested helix pairs. In fact, the above conditions express the same symmetry as Steffen's Snakes, namely, symmetric horizontal fields and antisymmetric vertical fields, about the Snake midpoint.

The two independent parameters are then $r_{h1}\eta_1$ and $r_{h2}\eta_2$. It should be noted that the above configurational symmetry allows two families of solutions, where (i) the first and second magnets have the same helicity $\eta_1 = \eta_2$, and (ii) opposite helicity $\eta_1 = -\eta_2$. There are multiple solutions within each family, including varying the number of periods $N_1, N_2$. Ptitsyn and Shatunov (1997b) state that numerical calculations indicate that increasing the number of periods decreases the magnitude of the orbit excursions only slightly, while increasing the overall field integral and total length. Hence small values for $N_1$ and $N_2$ are preferable. Furthermore, schemes with all magnets having the same helicity $\eta_1 = \eta_2 (= \eta_3 = \eta_4)$ provide, in general, solutions having a smaller value for the field integral. The solution chosen for the RHIC Snakes is the simplest: $\eta_1 = \eta_2 = 1, N_1 = N_2 = 1$. The schematic (field, helicity) configuration of the Snake is

$$S_{\mathrm{RHIC}} = \begin{matrix} + & + & + & + \\ B_1 & B_2 & -B_2 & -B_1 \end{matrix}. \tag{61}$$

This yields two independent parameters $r_{h1}$ and $r_{h2}$, which can be used to set the overall spin rotation angle to 180° and also to set the direction of the spin rotation axis.

Let us now consider the spin rotations. Returning to a single helix, the spin rotation matrix of a full-twist helix is, from (56) with $s = 2\pi\eta/k$,

$$M_H = \mathrm{e}^{-\mathrm{i}\eta\pi\sigma_2}\,\mathrm{e}^{-\mathrm{i}\eta\pi((\kappa/k)\sigma_3-\sigma_2)} \equiv -\mathrm{e}^{-\mathrm{i}\psi_h\boldsymbol{\sigma}\cdot\boldsymbol{n}_h/2}, \tag{62}$$

where the symbols have obvious meanings. We can simply drop the global minus sign because a spinor $-\Psi$ yields the same spin vector as $\Psi$. Defining $\chi = \kappa/k$, the spin rotation angle is

$$\psi_h = 2\pi\sqrt{1+\chi^2} \tag{63}$$

and the direction of the spin rotation axis is

$$\boldsymbol{n}_h = -\frac{\eta}{\sqrt{1+\chi^2}}(\boldsymbol{e}_2 - \chi\boldsymbol{e}_3). \tag{64}$$

Thus far we have followed the published literature. We now depart therefrom, and solve for the spin motion ourselves. We begin with the simpler problem of only two full-twist helices, with equal and opposite values of $r_h\eta$, and derive the overall spin rotation matrix. We assume the entrance magnetic fields are vertical, so the expressions derived in (63) and (64) are applicable. We begin with equal handedness $\eta_1 = \eta_2 = 1$. Then $r_{h1} = -r_{h2}$ which implies $\chi_1 = -\chi_2 = \chi$. Then

$$\psi_1 = \psi_2 = \psi = 2\pi\sqrt{1+\chi^2} \tag{65}$$

and

$$\boldsymbol{n}_{h1} = -\frac{1}{\sqrt{1+\chi^2}}(\boldsymbol{e}_2 - \chi\boldsymbol{e}_3), \qquad \boldsymbol{n}_{h2} = -\frac{1}{\sqrt{1+\chi^2}}(\boldsymbol{e}_2 + \chi\boldsymbol{e}_3). \tag{66}$$

With an obvious notation, the overall spin rotation matrix is

$$\begin{aligned} M_{21} &= \mathrm{e}^{-\mathrm{i}\psi\boldsymbol{\sigma}\cdot\boldsymbol{n}_{h2}/2}\,\mathrm{e}^{-\mathrm{i}\psi\boldsymbol{\sigma}\cdot\boldsymbol{n}_{h1}/2} \\ &= \cos^2\frac{\psi}{2} + \mathrm{i}2\cos\frac{\psi}{2}\sin\frac{\psi}{2}\frac{\sigma_2}{\sqrt{1+\chi^2}} - (\boldsymbol{n}_{h1}\cdot\boldsymbol{n}_{h2} + \mathrm{i}\boldsymbol{\sigma}\cdot(\boldsymbol{n}_{h1}\times\boldsymbol{n}_{h2}))\sin^2\frac{\psi}{2}. \end{aligned} \tag{67}$$

Using

$$\boldsymbol{n}_{h1}\cdot\boldsymbol{n}_{h2} = \frac{1-\chi^2}{1+\chi^2}, \qquad \boldsymbol{n}_{h1}\times\boldsymbol{n}_{h2} = -\frac{2\chi}{1+\chi^2}\boldsymbol{e}_1, \tag{68}$$

we deduce

$$M_{21} = \cos^2\frac{\psi}{2} - \frac{1-\chi^2}{1+\chi^2}\sin^2\frac{\psi}{2} + \mathrm{i}\frac{2\chi}{1+\chi^2}\sin^2\frac{\psi}{2}\sigma_1 + \mathrm{i}\frac{1}{\sqrt{1+\chi^2}}\sin\psi\sigma_2. \tag{69}$$

Equating this to the parametrization of a rotation matrix $M_{21} = \mathrm{e}^{-\mathrm{i}\psi_{21}\boldsymbol{\sigma}\cdot\boldsymbol{n}_{21}/2}$ yields, for the term independent of the Pauli matrices,

$$\cos\frac{\psi_{21}}{2} = \cos^2\frac{\psi}{2} - \frac{1-\chi^2}{1+\chi^2}\sin^2\frac{\psi}{2} = \frac{\chi^2+\cos\psi}{\chi^2+1}. \tag{70}$$

Equating the terms in the Pauli matrices, it is clear that the overall spin rotation axis $\boldsymbol{n}_{21}$ has components only in the horizontal plane, because there is no term in $M_{21}$ in $\sigma_3$. To make the device a Snake, one must have $\psi_{21} = \pi$, or more accurately $\cos(\psi_{21}/2) = 0$. Hence

$$\chi^2 + \cos\left(2\pi\sqrt{1+\chi^2}\right) = 0. \tag{71}$$

This is a constraint on the value of $\chi$. Given $\chi$, the directions of the spin rotation axes $\boldsymbol{n}_{h1}$, $\boldsymbol{n}_{h2}$ and $\boldsymbol{n}_{21}$ are uniquely determined. There is not enough freedom to vary the directions of the spin rotation axes. Equation (71) can be solved by graphical means. The relevant functions are depicted in figure 15. Clearly one must have $|\chi| < 1$ because the value of the cosine lies

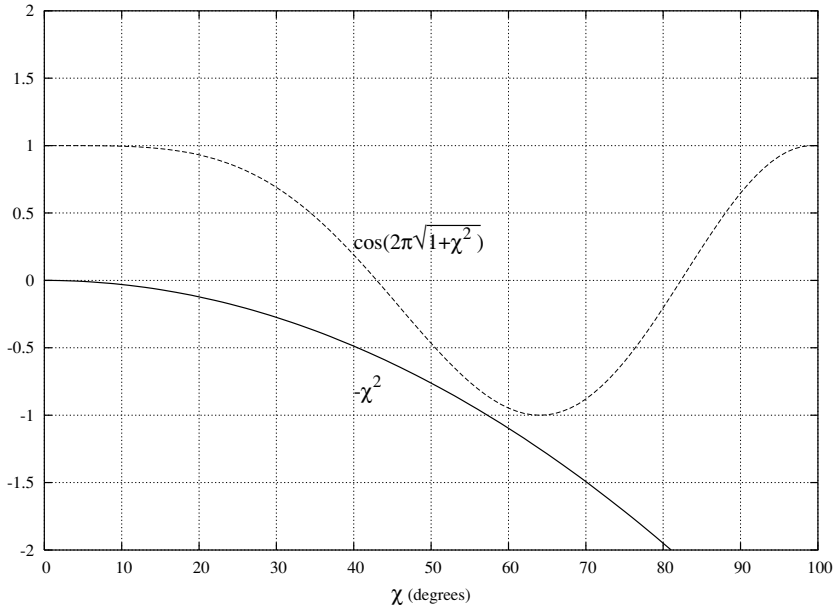


**Figure 15.** Graphical solution for helical Snake with two modules. The curves do not intersect, hence there is no solution.

in this interval. The graphs of the functions *do not intersect*, hence there is no real solution for $\chi$. Hence the above combination of two helices *cannot* yield a full-strength Snake.

We next consider helices of opposite handedness, namely $\eta_1 = 1, \eta_2 = -1$. Once again $\chi$ is of opposite sign in the magnets, $\chi_1 = -\chi_2 = \chi$. Then

$$\psi_1' = \psi_2' = \psi = 2\pi\sqrt{1+\chi^2} \tag{72}$$

and

$$\boldsymbol{n}_{h1}' = -\frac{1}{\sqrt{1+\chi^2}}(\boldsymbol{e}_2 - \chi\boldsymbol{e}_3), \qquad \boldsymbol{n}_{h2}' = \frac{1}{\sqrt{1+\chi^2}}(\boldsymbol{e}_2 + \chi\boldsymbol{e}_3), \tag{73}$$

i.e. $\boldsymbol{n}_{h1}' = \boldsymbol{n}_{h1}$ and $\boldsymbol{n}_{h2}' = -\boldsymbol{n}_{h2}$. Hence the overall spin rotation matrix is now

$$\begin{aligned} M_{21}' &= \mathrm{e}^{\mathrm{i}\psi\boldsymbol{\sigma}\cdot\boldsymbol{n}_{h2}/2}\,\mathrm{e}^{-\mathrm{i}\psi\boldsymbol{\sigma}\cdot\boldsymbol{n}_{h1}/2} \\ &= \frac{1+\chi^2\cos\psi}{1+\chi^2} - \mathrm{i}\frac{2\chi}{1+\chi^2}\sin^2\frac{\psi}{2}\sigma_1 - \mathrm{i}\frac{\chi}{\sqrt{1+\chi^2}}\sin\psi\sigma_3. \end{aligned} \tag{74}$$

The condition for the overall spin rotation angle to equal $\pi$ is

$$1 + \chi^2\cos(2\pi\sqrt{1+\chi^2}) = 0, \tag{75}$$

which *does* have multiple real solutions for $\chi$. However, the spin rotation matrix has a term in $\sigma_3$, hence the spin rotation axis *does not lie in the horizontal plane*. We can trace this fact to the configurational symmetry of the horizontal and vertical magnetic fields. Hence this combination of helices also cannot rotate a spin from vertically up to down. Hence, overall, a combination of two full-twist helices *cannot* in fact function as a full-strength Siberian Snake. We proceed to four full-twist helical modules.

For four full-twist helices, we systematize the calculation to avoid a plethora of terms. We consider only the design with all helicities equal $\eta_1 = \eta_2 = \eta_3 = \eta_4 = 1$. Then $r_{h4} = -r_{h1}$ and $r_{h3} = -r_{h2}$ to compensate the orbital motion. Then $\chi_4 = -\chi_1$ and $\chi_3 = -\chi_2$. Hence

$$\psi_1 = \psi_4 = 2\pi\sqrt{1+\chi_1^2}, \qquad \psi_2 = \psi_3 = 2\pi\sqrt{1+\chi_2^2} \tag{76}$$

and

$$\begin{aligned} \boldsymbol{n}_{h1} &= -\frac{\boldsymbol{e}_2 - \chi_1 \boldsymbol{e}_3}{\sqrt{1+\chi_1^2}}, \qquad & \boldsymbol{n}_{h3} &= -\frac{\boldsymbol{e}_2 + \chi_2 \boldsymbol{e}_3}{\sqrt{1+\chi_2^2}}, \\ \boldsymbol{n}_{h2} &= -\frac{\boldsymbol{e}_2 - \chi_2 \boldsymbol{e}_3}{\sqrt{1+\chi_2^2}}, \qquad & \boldsymbol{n}_{h4} &= -\frac{\boldsymbol{e}_2 + \chi_1 \boldsymbol{e}_3}{\sqrt{1+\chi_1^2}}. \end{aligned} \tag{77}$$

Now note that

$$\boldsymbol{n}_{h1} \cdot \boldsymbol{n}_{h2} = \boldsymbol{n}_{h3} \cdot \boldsymbol{n}_{h4} = \frac{1+\chi_1\chi_2}{\sqrt{(1+\chi_1^2)(1+\chi_2^2)}} \tag{78}$$

and

$$\boldsymbol{n}_{h1} \times \boldsymbol{n}_{h2} = \boldsymbol{n}_{h3} \times \boldsymbol{n}_{h4} = \frac{\chi_1 - \chi_2}{\sqrt{(1+\chi_1^2)(1+\chi_2^2)}} \boldsymbol{e}_1. \tag{79}$$

The spin rotation matrix through the first two helices is, using the notation $S_{21}$ for 'Snake',

$$\begin{aligned} S_{21} = \mathrm{e}^{-\mathrm{i}\psi_2 \boldsymbol{\sigma}\cdot\boldsymbol{n}_{h2}/2}\,\mathrm{e}^{-\mathrm{i}\psi_1 \boldsymbol{\sigma}\cdot\boldsymbol{n}_{h1}/2} &= \cos\frac{\psi_1}{2}\cos\frac{\psi_2}{2} - \boldsymbol{n}_{h1}\cdot\boldsymbol{n}_{h2}\sin\frac{\psi_1}{2}\sin\frac{\psi_2}{2} \\ &\quad - \mathrm{i}\boldsymbol{\sigma}\cdot\boldsymbol{n}_{h1}\cos\frac{\psi_2}{2}\sin\frac{\psi_1}{2} - \mathrm{i}\boldsymbol{\sigma}\cdot\boldsymbol{n}_{h2}\cos\frac{\psi_1}{2}\sin\frac{\psi_2}{2} \\ &\quad + \mathrm{i}\boldsymbol{\sigma}\cdot(\boldsymbol{n}_{h1}\times\boldsymbol{n}_{h2})\sin\frac{\psi_1}{2}\sin\frac{\psi_2}{2}, \end{aligned} \tag{80}$$

which we can express in the form $S_{21} = a + b\sigma_1 + c\sigma_2 + d\sigma_3$. The values of the coefficients are

$$\begin{aligned} a &= \cos\frac{\psi_1}{2}\cos\frac{\psi_2}{2} - \frac{1+\chi_1\chi_2}{\sqrt{(1+\chi_1^2)(1+\chi_2^2)}}\sin\frac{\psi_1}{2}\sin\frac{\psi_2}{2}, \\ b &= \mathrm{i}\frac{\chi_1-\chi_2}{\sqrt{(1+\chi_1^2)(1+\chi_2^2)}}\sin\frac{\psi_1}{2}\sin\frac{\psi_2}{2}, \\ c &= \mathrm{i}\left[\frac{1}{\sqrt{1+\chi_1^2}}\cos\frac{\psi_2}{2}\sin\frac{\psi_1}{2} + \frac{1}{\sqrt{1+\chi_2^2}}\cos\frac{\psi_1}{2}\sin\frac{\psi_2}{2}\right], \\ d &= -\mathrm{i}\left[\frac{\chi_1}{\sqrt{1+\chi_1^2}}\cos\frac{\psi_2}{2}\sin\frac{\psi_1}{2} + \frac{\chi_2}{\sqrt{1+\chi_2^2}}\cos\frac{\psi_1}{2}\sin\frac{\psi_2}{2}\right]. \end{aligned} \tag{81}$$

The values of the coefficients are not particularly important. What matters is the *pattern*. Given the expressions for $\boldsymbol{n}_{h3}$ and $\boldsymbol{n}_{h4}$, and the values of $\boldsymbol{n}_{h3}\cdot\boldsymbol{n}_{h3}$ and $\boldsymbol{n}_{h3}\times\boldsymbol{n}_{h3}$, one sees that the spin rotation matrix through the third and fourth helices is $S_{43} = a + b\sigma_1 + c\sigma_2 - d\sigma_3$. It is the same matrix, with reversal of the sign of $d$. The overall spin rotation matrix is then

$$S_{4321} = S_{43}S_{21} = (a + b\sigma_1 + c\sigma_2 - d\sigma_3)(a + b\sigma_1 + c\sigma_2 + d\sigma_3). \tag{82}$$

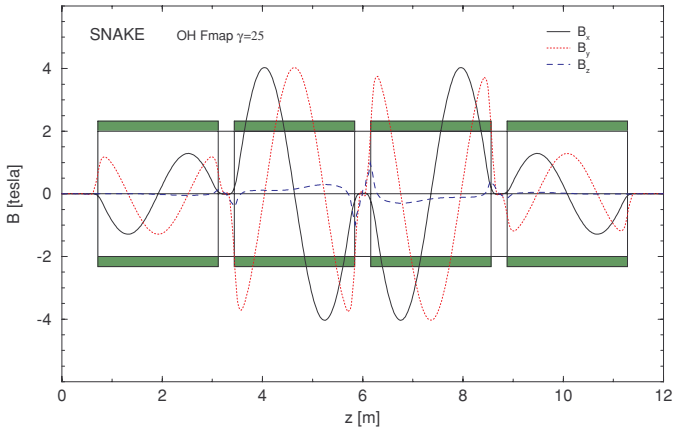


**Figure 16.** Helical field components through a RHIC Snake at injection ($\gamma = 25$). Courtesy W W MacKay (private communication) and BNL.

One can work with this parametrization directly, *without* knowing the detailed forms for $a$, $b$, $c$ and $d$. Expanding the matrix product,

$$\begin{aligned} M_{4321} &= a^2 + b^2 + c^2 - d^2 + 2ab\sigma_1 + 2ac\sigma_2 \\ &\quad + bc(\sigma_1\sigma_2 + \sigma_2\sigma_1) + bd(\sigma_1\sigma_3 - \sigma_3\sigma_1) + cd(\sigma_2\sigma_3 - \sigma_3\sigma_2) \\ &= a^2 + b^2 + c^2 - d^2 + 2(ab + \mathrm{i}cd)\sigma_1 + 2(ac - \mathrm{i}bd)\sigma_2. \end{aligned} \tag{83}$$

By the symmetry of the fields, the terms in $\sigma_3$ cancel automatically. The spin rotation axis is therefore guaranteed to lie in the horizontal plane, as reported by Ptitsyn and Shatunov (1997b). The criterion to make this a full-strength Siberian Snake is

$$a^2 + b^2 + c^2 - d^2 = 0. \tag{84}$$

The actual solutions for $\chi_1$ and $\chi_2$ are best found numerically. At RHIC the Snake spin rotation axes are oriented at $\pm 45^\circ$ to the beam direction. If a solution set $(a_*, b_*, c_*, d_*)$ is found with the spin rotation axis at $45^\circ$ to the longitudinal direction, then $(-a_*, b_*, -c_*, d_*)$ and $(a_*, -b_*, c_*, -d_*)$ are two solutions with orthogonal spin rotation axes.

Graphs of the (a) field components, (b) orbit excursions and (c) spin precession (at injection) in a (i) RHIC Snake and (ii) spin rotator are shown in figures 16, 17, 18, 19, 20 and 21, respectively.

### *5.7. Full-twist helical-field spin rotators*

This is really a continuation of the above analysis of helical magnets, but we now turn our attention to spin rotators instead of Siberian Snakes. The same basic design of multiple full-twist helices can also be used to construct a spin rotator. Multiple solutions are presented by Ptitsyn and Shatunov (1997b), including the notion that *three* full-twist helices will suffice to construct a spin rotator. In the design selected for RHIC, the spin rotator consists of four full-twist helical magnets. The criterion for automatic compensation of the orbit excursions is still (59).

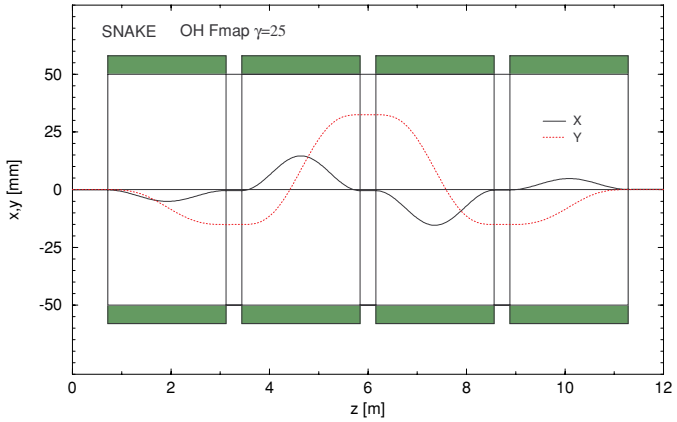


**Figure 17.** Design orbit through a RHIC Snake at injection ($\gamma = 25$). Courtesy W W MacKay (private communication) and BNL.

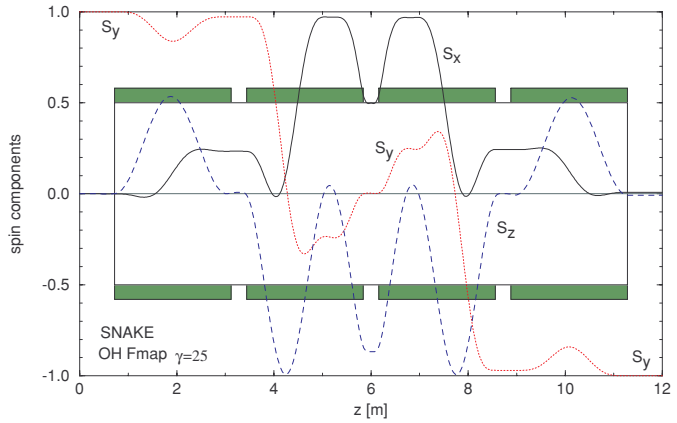


**Figure 18.** Spin precession through a RHIC Snake at injection ($\gamma = 25$). Courtesy W W MacKay (private communication) and BNL.

In the RHIC spin rotator, the entrance magnetic fields point in the *horizontal* direction, i.e. $\alpha_i = \pi/2$. Now it is the second equation in (59) which is trivially satisfied, but the remaining orbit compensation condition is still

$$\sum_{i=1}^{4} r_{hi}\eta_i = 0. \tag{85}$$

For the design of the spin rotator chosen for RHIC, the first and fourth magnets have opposite helicity $\eta_1 = -\eta_4$, and $r_{h1} = r_{h4}$. Similarly, for the second and third magnets $\eta_2 = -\eta_3$ and $r_{h2} = r_{h3}$. In addition, the first and second magnets have opposite helicity: $\eta_1 = -\eta_2$. The overall helicities are therefore $(+, -, +, -)$. The schematic (field, helicity) configuration of the rotator is

$$R_{\mathrm{RHIC}} = \begin{matrix} + & - & + & - \\ B_1 & B_2 & B_2 & B_1 \end{matrix}.$$

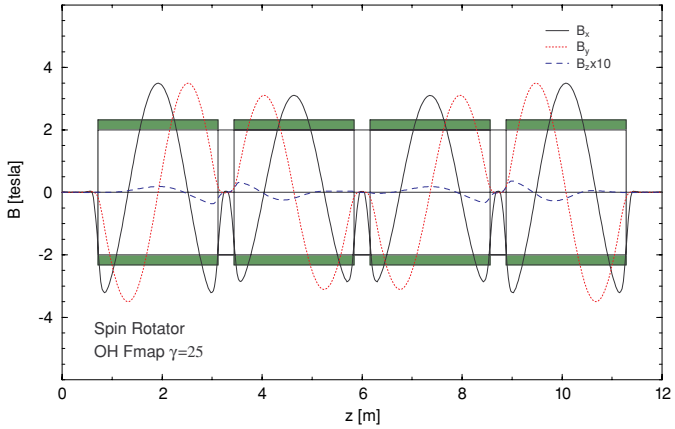


**Figure 19.** Helical field components through a RHIC spin rotator at injection ($\gamma = 25$). Courtesy W W MacKay (private communication) and BNL.

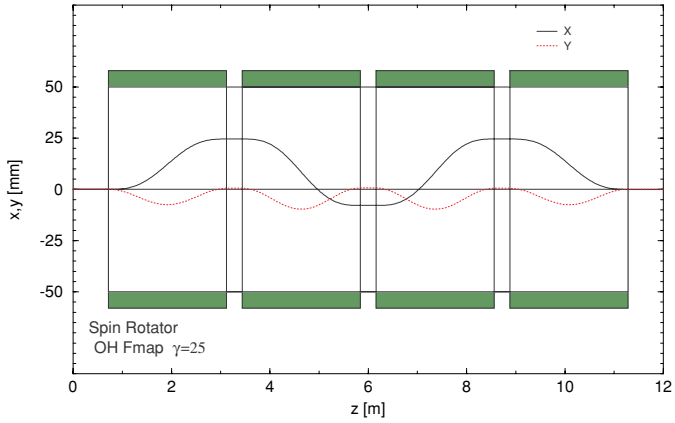


**Figure 20.** Design orbit through a RHIC spin rotator at injection ($\gamma = 25$). Courtesy W W MacKay (private communication) and BNL.

Note that the entrance fields point in the horizontal direction. Hence in the RHIC spin rotator, the configuration of *both* the horizontal and the vertical magnetic fields is symmetric about the rotator midpoint. The successful commissioning of the RHIC spin rotators was announced by MacKay *et al* (2003).

We again solve for the spin motion through the spin rotator by ourselves. The magnetic field is now

$$\boldsymbol{B} = B_h[\boldsymbol{e}_1 \cos(ks) - \boldsymbol{e}_3 \sin(ks)], \tag{86}$$

i.e. horizontal at the entrance. The solution of the spinor equation of motion is

$$\Psi(s) = \mathrm{e}^{-\mathrm{i}ks\sigma_2/2}\,\mathrm{e}^{-\mathrm{i}s(\kappa\sigma_1 - k\sigma_2)/2}\Psi(0). \tag{87}$$

The spin rotation angle through the helix is

$$\psi = 2\pi\sqrt{1+\chi^2} \tag{88}$$

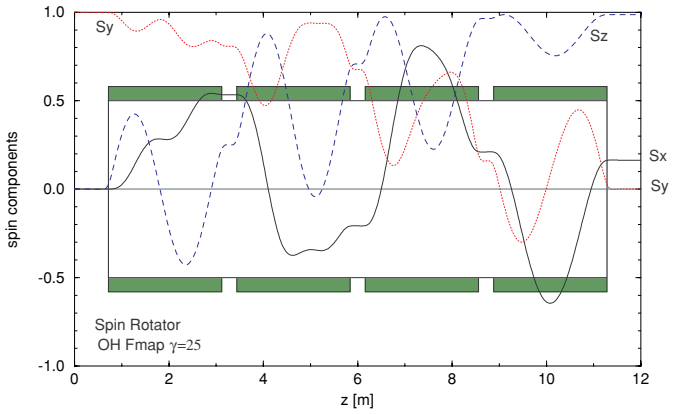


**Figure 21.** Spin precession through a RHIC spin rotator at injection ($\gamma = 25$). Courtesy W W MacKay (private communication) and BNL.

and the spin rotation axis is

$$\boldsymbol{n}_h = \frac{\eta}{\sqrt{1+\chi^2}}(\chi \boldsymbol{e}_1 - \boldsymbol{e}_2). \tag{89}$$

This is just the solution for the Snake, rotated through a right angle around the longitudinal axis, because the magnetic field in (86) is rotated through a right angle around the longitudinal axis relative to (45). For the RHIC spin rotator design, we have $\eta_1 = 1$, $\eta_2 = -1$, $\eta_3 = 1$ and $\eta_4 = -1$. Then $\chi_4 = -\chi_1$ and $\chi_3 = -\chi_2$ and

$$\psi_1 = \psi_4 = 2\pi\sqrt{1+\chi_1^2}, \qquad \psi_2 = \psi_3 = 2\pi\sqrt{1+\chi_2^2} \tag{90}$$

and

$$\begin{aligned} \boldsymbol{n}_{h1} &= -\frac{\chi_1 \boldsymbol{e}_1 - \boldsymbol{e}_2}{\sqrt{1+\chi_1^2}}, & \boldsymbol{n}_{h3} &= \frac{\chi_2 \boldsymbol{e}_1 + \boldsymbol{e}_2}{\sqrt{1+\chi_2^2}}, \\ \boldsymbol{n}_{h2} &= \frac{\chi_2 \boldsymbol{e}_1 - \boldsymbol{e}_2}{\sqrt{1+\chi_2^2}}, & \boldsymbol{n}_{h4} &= -\frac{\chi_1 \boldsymbol{e}_1 + \boldsymbol{e}_2}{\sqrt{1+\chi_1^2}}. \end{aligned} \tag{91}$$

Then

$$\boldsymbol{n}_{h1} \cdot \boldsymbol{n}_{h2} = \boldsymbol{n}_{h3} \cdot \boldsymbol{n}_{h4} = -\frac{1+\chi_1\chi_2}{\sqrt{(1+\chi_1^2)(1+\chi_2^2)}} \tag{92}$$

and

$$\boldsymbol{n}_{h1} \times \boldsymbol{n}_{h2} = \boldsymbol{n}_{h3} \times \boldsymbol{n}_{h4} = \frac{\chi_1 - \chi_2}{\sqrt{(1+\chi_1^2)(1+\chi_2^2)}} \boldsymbol{e}_3. \tag{93}$$

Without spelling out all the details, it should be evident that the spin rotation matrices have the forms ($R$ for 'rotator')

$$R_{21} = \bar{a} + \bar{b}\sigma_1 + \bar{c}\sigma_2 + \bar{d}\sigma_3, \qquad R_{43} = \bar{a} + \bar{b}\sigma_1 - \bar{c}\sigma_2 + \bar{d}\sigma_3, \tag{94}$$

where it is not necessary to write out the detailed expressions for $\bar{a}$, etc. Then the overall spin rotator matrix is

$$\begin{aligned} R_{4321} &= (\bar{a} + \bar{b}\sigma_1 - \bar{c}\sigma_2 + \bar{d}\sigma_3)(\bar{a} + \bar{b}\sigma_1 + \bar{c}\sigma_2 + \bar{d}\sigma_3) \\ &= \bar{a}^2 + \bar{b}^2 - \bar{c}^2 + \bar{d}^2 + 2(\bar{a}\bar{b} - \mathrm{i}\bar{c}\bar{d})\sigma_1 + 2(\bar{a}\bar{d} + \mathrm{i}\bar{b}\bar{c})\sigma_3 \\ &\equiv \mathrm{e}^{-\mathrm{i}\psi_R \boldsymbol{\sigma}\cdot\boldsymbol{n}_R/2}, \end{aligned} \tag{95}$$

where the notation in the last line is self-explanatory. Note that the spin rotation axis of a RHIC spin rotator has *no* longitudinal component. It always lies in the transverse plane, defined by $(\boldsymbol{e}_1, \boldsymbol{e}_3)$. Hence the spin rotation axis cannot, in general, be 90°. It is important to realize that a spin rotator simply rotates a spin from the vertical direction into the horizontal plane, and vice versa. Nothing in the definition states that the overall spin rotation angle must be 90°.

The constraint for this device to rotate a spin from the vertical direction into the horizontal plane is derived as follows. An initial spinor $\Psi_i = (1\ 0)^T$ is transformed into a final spinor $\Psi_f = (\Psi_+ \Psi_-)^T$. The vertical component of the exit spin is

$$s_3 = \langle \Psi_f | \sigma_3 | \Psi_f \rangle = |\Psi_+|^2 - |\Psi_-|^2, \tag{96}$$

which is required to vanish. Now

$$\Psi_+ = \bar{a}^2 + \bar{b}^2 - \bar{c}^2 + \bar{d}^2 + 2(\bar{a}\bar{d} + \mathrm{i}\bar{b}\bar{c}), \qquad \Psi_- = 2(\bar{a}\bar{b} - \mathrm{i}\bar{c}\bar{d}). \tag{97}$$

Hence the constraint condition to function as a spin rotator is

$$|\bar{a}^2 + \bar{b}^2 - \bar{c}^2 + \bar{d}^2 + 2(\bar{a}\bar{d} + \mathrm{i}\bar{b}\bar{c})|^2 = 4|\bar{a}\bar{b} - \mathrm{i}\bar{c}\bar{d}|^2. \tag{98}$$

The helical field pattern, design orbit excursions and spin precession (at injection) in a RHIC spin rotator were shown in figures 19, 20 and 21, respectively.

Curiously, it is difficult to find an explicit statement in the literature that the spin rotation axis of a RHIC spin rotator always lies in the transverse plane. It is clearly stated in several places that the spin rotation axis of a four-helix *Snake* lies in the horizontal plane, but the only statement about the orientation of the spin rotation axis of a RHIC *spin rotator* is by MacKay *et al* (2003), in the the caption of figure 2 of that paper. Even more curiously, that same figure 2 is *not* cited in the text of MacKay *et al* (2003). It is, however, recognized in several places that the spin rotation angle of a RHIC spin rotator is not always 90°.

### *5.8. HERA mini-rotator*

The only other design of spin rotator which has been installed in a storage ring is the 'Buon–Steffen minirotator', used at HERA (Buon and Steffen 1986). Initially, Steffen (1978) found a Snake design using dipoles (not one of the Steffen Snakes described earlier). The design in this case consists of *two* sets of six magnets. Each group of six magnets consisted of an interleaved vertical and horizontal orbit beam bump: define $S = S_1 S_2$, where

$$S_1 = (-V, -H, 2V, 2H, -V, -H), \qquad S_2 = (-H, V, 2H, -2V, -H, V).$$

There is no need for $S_1$ and $S_2$ to be contiguous; there can be an arbitrary gap between them (provided the gap contains no spin rotations). In Steffen's original design, the spin rotation angles were $\psi_H = \psi_V = 45°$. A spin enters $S_1$ pointing vertically upwards. After exit from $S_1$, the spin points horizontally, in the radial direction. It then enters $S_2$ and after exit from $S_2$, the spin points downwards. Overall, the orbital excursion cancels out, and so the design orbit exits the system pointing the same as its initial (longitudinal) direction.

Steffen subsequently realized that if the sign of the last horizontal bend in $S_1$ were reversed, and so also the first horizontal bend in $S_2$, the spin would point *longitudinally* after exit from $S_1$, and would rotate back to vertically *up* after exit from $S_2$. This is therefore a vertical to longitudinal and back to vertical (up) pair of spin rotators. Since $S_1$ and $S_2$ do not need to be contiguous, they can be placed on opposite sides of the interaction point of a colliding-beam storage ring. (Any spin rotations due to a particle detector solenoid must be compensated.) The spin rotator design is therefore

$$R_1 = (-V, -H, 2V, 2H, -V, H), \qquad R_2 = (H, V, 2H, -2V, -H, V).$$

The 'mini-rotator', as it is called, produces an overall horizontal bend in the particle orbit, because the overall horizontal spin rotation of one member of the pair nets to $-H + 2H + H = 2H$, or $4H$ for the total, so the total orbital bend angle is $4\psi_H/(a\gamma)$. Hence the bend of the mini-rotator must be added into that of the arcs of the accelerator, to add up to 360° overall. Since the bend angle is energy-dependent, the geometry of the ring changes with the operating energy, hence the magnets must be repositioned. Furthermore, the mini-rotator was designed for use in the electron ring of HERA, i.e. a ring with radiative polarization. The presence of horizontal magnetic fields and vertical beam excursions raised the possibility of generating unwanted resonance driving terms, which would depolarize the beam. The optimization of the mini-rotator design is described by Buon and Steffen (1986), to match the orbital optics to the rest of the accelerator and to minimize any contribution to the magnitude of the spin resonance driving terms. Most of their paper is devoted to these optimizations, which are important but tedious, and need not concern us.

The mini-rotators also offer the flexibility of a choice of positive or negative helicity at the interaction point. For this, the signs of the vertical bends must be reversed. The orbital excursions are sufficiently large that the magnets must be repositioned vertically. Once again, this cannot be done in real-time. The helicity for a particular run of the machine must be chosen ahead of time, and the magnets locked in position appropriately. The joints between the magnets contain flexible bellows. Note that the choice of helicity at any one interaction point is *independent* of that at the others—the various mini-rotators do not all have to be configured the same way.

As should be obvious, the actual spin rotation angles in the mini-rotator are not always $\psi_H = \psi_V = 45°$. The above was just a simple illustrative example which Steffen noted. The actual angles are computed numerically at each beam operating energy, to satisfy the orbit and spin matching conditions. Note that in general the spin rotators also shift the value of the spin tune, so one cannot equate the value of the spin tune to $a\gamma$.

We did not comment on this fact above, but RHIC is a superconducting ring, and the spin rotator and Snake magnets in RHIC do not move. One changes the currents in the magnets, to alter the direction of the spin rotation axis, or to reverse the helicity of the longitudinal polarization at the interaction point. The beam excursions are sufficiently small that they are contained with the bores of the Snake and spin rotator magnets. The construction of helical magnetic fields is more complicated than the construction of dipole fields, but there are advantages in both the mechanical operation and beam excursions.

### *5.9. HERA solenoid spin rotator*

Perhaps the greatest tribute to Buon and Steffen's achievement is that the problem of designing a spin rotator with transverse dipole fields was so great that an alternative design, using a solenoid to rotate the spins, was seriously proposed (Barber *et al* 1985) (but not built). This was despite the disadvantage of the factor of $a+1$ versus $a\gamma+1$ faced by the use of longitudinal magnetic fields. The required solenoid integrated field strength is $23.1 \times a\gamma/(1+a)$ kG m. Because a solenoid couples the horizontal and vertical betatron oscillations, quadrupoles are required to compensate the coupling. The eventual design was to split the solenoid into six sections with normal quadrupoles interleaved. For use at HERA at energies of 27.5–35 GeV, the total length of the rotator was 41.6 m, with solenoid fields of 72 kG. This meant the solenoids must be superconducting.

Since a solenoid can only rotate a spin from the vertical to the radial direction in the horizontal plane, a further dipole bend is required between the spin rotator and the interaction point, to achieve longitudinal polarization at the collision point. The dipole orbital bend angle

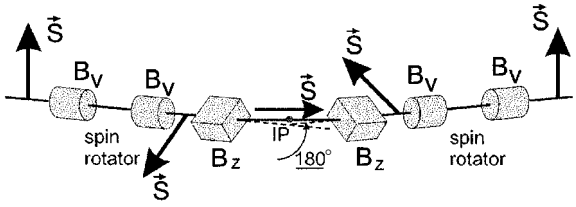


**Figure 22.** Schematic design of a proposed solenoid spin rotator for $e^+e^-$ colliding beams at VEPP-4, for a beam energy of 4.7 GeV. The spin direction is also shown.

must be $\pi/(2a\gamma)$, i.e. an energy-dependent angle. The ring geometry therefore (i) depends on the energy, as with the mini-rotator, or (ii) the polarization is not exactly longitudinal at the interaction point, except at one 'reference' energy.

### *5.10. VEPP-4 solenoid spin rotator*

A solenoid spin rotator was also proposed at VEPP-4 (Derbenev *et al* 1977a). The design schematic is shown in figure 22. The spin direction is also indicated. The VEPP-4 spin rotator would have operated with *colliding* $e^+e^-$ *beams*. The rotator was not built; HERA remains the only high-energy storage ring to attain longitudinal radiative polarization. As with the HERA minirotator, there is an overall orbital bend in this design. In the original rotator design, the horizontal spin rotation between the solenoids was generated in the MD particle detector, which had a vertical dipole field giving an orbital bend angle of about 16°. The rotator was intended for use at a beam energy of 4.7 GeV ($= \frac{1}{2}M_\Upsilon c^2$, to operate at the $\Upsilon$ resonance). At this energy the horizontal spin rotation is about 180°, resulting in longitudinal polarization at the IP. The new KEDR detector at VEPP-4 is equipped with a solenoid (and compensating antisolenoids such that the total field integral is zero). To preserve the ring geometry, horizontal bends are placed on either side of the detector, to enable a possible future installation of the spin rotator. The theoretical asymptotic radiative polarization is approximately 80% for this ring geometry and energy. The spin rotation matrix through the rotator pair is easily worked out to be a 90° around the vertical:

$$M_{v4} = e^{-i\pi\sigma_2/4}\, e^{-i\pi\sigma_3/4}\, e^{-i\pi\sigma_3/4}\, e^{-i\pi\sigma_2/4} = e^{-i\pi\sigma_3/2}. \tag{99}$$

As with the HERA minirotator, the arc contributes a spin rotation angle of $2\pi a\gamma - \pi$, because of the overall bend of the rotator pair, so the total spin precession angle per turn is still $a\gamma$. There is no induced spin tuneshift.

### *5.11. Radial field spin rotator*

We remark briefly on a very early design of spin rotator using radial dipole fields only. The Skrinsky (1982) study mentioned above used radial field rotators. (The first mathematical demonstration that a set of radial fields can act as a spin rotator was given by Derbenev *et al* (1970).) A schematic side view is shown in figure 23. Basically, the orbit is deflected vertically such that the overall spin rotation is 90°. Hence the polarization is longitudinal at the interaction point (IP) (although the beams pass through the IP at an angle to the accelerator design axis). Note that there must be no horizontal bends between the rotator and the IP (as there is at RHIC). Since the orbit excursions are not localized within the rotator, the matching of the rotator to the ring optics can be complicated. The beam passes off-axis through any quadrupoles near the IP, e.g. the 'low-beta' quadrupoles, which will generate unwanted spin rotations (or the quadrupoles must be moved to track the orbit displacement). The proposed

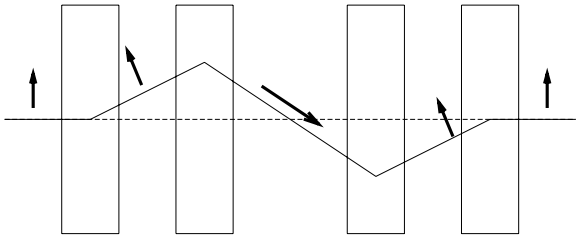

**Figure 23.** Schematic side view of a radial field spin rotator. The orbit displacements are not to scale. The arrows indicate the spin direction.

LEP spin rotator (Grote 1995), which was not built, was a radial field spin rotator. See also Schwitters and Richter (1974) for ideas for a radial field rotator at PEP.

### *5.12. FNAL Snakes and spin rotators*

Several years before spin rotators with horizontal and vertical dipoles were installed in HERA, or helical-field spin rotators were installed in RHIC, a high-energy transverse (dipole) field spin rotator operated successfully at Fermilab, in the MP (Meson Polarized) fixed-target external beam facility. The alert reader will note that this system is not an accelerator but an external target beamline. Nevertheless, the design is so elegant that we include it in this review.

Let us broaden the definition of a Snake to that of a device which rotates a spin through 180° while leaving the orbit unchanged, and *not* insist that this device be in an accelerator. The idea of implementing spin rotators in a Fermilab beamline, for delivery of arbitrary orientations of the polarization (radial, vertical, longitudinal) to fixed-target experiments arose from early work at the ZGS (Colton *et al* 1978) at Argonne National Laboratory. Underwood later designed Snakes and spin rotators with continuously variable spin rotation axes, using eight dipole magnets (Underwood 1980). The actual design implemented at Fermilab contained 12 dipole magnets. We call it a Snake, to avoid unnecessary special terminology for every scenario of its operation. Primary protons of 800 GeV/$c$ momentum were extracted from the Tevatron to strike a Be target, creating $\Lambda$ hyperons in the MP beamline (Grosnick *et al* 1990). The $\Lambda$'s are unpolarized, but they decay via the parity-violating weak interaction reaction $\Lambda \rightarrow \mathrm{p} + \pi^-$. In the $\Lambda$ rest frame, the decay is isotropic and the decay proton polarization is 64% with the spin direction along the proton momentum. The primary beam also created $\bar{\Lambda}$ hyperons, which decay via $\bar{\Lambda} \rightarrow \bar{\mathrm{p}} + \pi^+$. One can select either $\Lambda$'s or $\bar{\Lambda}$'s by reversing the polarity of the secondary beamline magnets, hence it will suffice below to discuss $\Lambda$'s and polarized protons only. Note that no existing accelerator has ever circulated polarized antiprotons; there are no polarized $\bar{\mathrm{p}}$ sources analogous to polarized proton sources. RHIC collides polarized pp beams.

Using the enlarged definition of a Snake, Underwood (1980) performed a search of suitable parameter values for the spin rotation angles, for Snake designs composed of eight dipole bending magnets. Note that for transverse magnetic fields, a 90° spin rotation in one magnet implies a field integral of about 2.74 Tm (for protons), independent of momentum (for high energies). No cases where an individual magnet had a spin rotation greater than 90° were considered in Underwood's study. No cases were considered which produced a net change to the beam direction. All of the interesting solutions found had complete momentum recombination and no net transverse displacement of the beam. Underwood found some elegant designs of Snakes (also spin rotators), indicated symbolically as follows:

$$(-\mathrm{H}) - \mathrm{V} - \mathrm{H} - (-\mathrm{V}) - \mathrm{H} - (-\mathrm{V}) - (-\mathrm{H}) - \mathrm{V}.$$

If the spin rotation angles are $\psi_H$ and $\psi_V$, to borrow the notation of the Steffen Snakes, then it is easily verified that if $\psi_H = \psi_V = \pi/2$ then the spin map is

$$(\boldsymbol{e}_1, \boldsymbol{e}_2, \boldsymbol{e}_3) \mapsto (-\boldsymbol{e}_3, -\boldsymbol{e}_1, \boldsymbol{e}_2), \tag{100}$$

which is a 120° spin rotation around the axis

$$\boldsymbol{e}_r = \tfrac{1}{\sqrt{3}}(-\boldsymbol{e}_1 + \boldsymbol{e}_2 + \boldsymbol{e}_3). \tag{101}$$

It is possible to find designs which act as Snakes, with a continuously variable choice of spin rotation axis.

Underwood (1989) and Grosnick *et al* (1990) are the sources of most of the information below. The Fermilab device was Snake-like in that there was no overall deflection of the orbit upon exit from the rotator; only the spin direction was rotated. Because the Snake consisted only of dipoles with no quadrupoles, it appeared equivalent to a drift space of the same length, to a very good approximation. Hence the beamline could be operated with little perturbation whether the Snake was on or off.

The Snake was required for several reasons. First, it is necessary to reverse the polarization direction in each element of phase space periodically to control systematic errors in physics experiments with polarized beams. Second, the polarized proton beam was transversely horizontally polarized; some experiments required vertical or longitudinal polarization. By different configurations of the dipole fields, it was possible to use the same rotator/Snake to attain either vertical or longitudinal polarization. Hence the design was quite flexible. This is in contrast to the helical Snakes, or the Steffen Snakes, which cannot switch from being Snakes to spin rotators etc, by a simple repowering of the magnets.

The overall Snake consisted of 12 dipoles with spin rotations of 45° in each magnet. However not all 12 magnets were always required. To rotate a spin from horizontal transverse to vertical, only 8 of the 12 were required; these were magnets 3, 5, 6, 7, 8, 9, 10 and 12. To rotate a spin from horizontal transverse to the longitudinal direction, all 12 dipoles were required, but some of the magnets were powered in pairs, to generate 90° spin rotations, hence there were still only 8 independent spin rotations. The spin rotator had some interesting symmetry properties. To reverse the overall sense of the spin rotation, when the rotator was configured to rotate from transverse to vertical, the polarities of only 4 of the 8 magnets needed to be reversed. Reversing the fields in all 8 magnets had no effect on the spin direction. Also, the final spin rotation direction was the *same* for protons and antiprotons, counterintuitively to what one would expect (and opposite to the behaviour of a solenoid spin rotator). When the rotator was configured to rotate the spins from transverse to longitudinal, the polarity of all 12 magnets had to be reversed, to reverse the overall spin rotation. In this case the spin rotation was opposite for protons and antiprotons. The momentum of the polarized protons was so high (about 200 GeV/$c$), that there was no need to reposition the dipoles when reversing the magnet polarities, in contrast to the HERA mini-rotator, which also employed transverse dipole fields. The orbital deflections of the protons were too small at the high energy of the Fermilab beams. We conclude the description of the Fermilab Snake here. It is a truly elegant design.

### *5.13. Type 3 Snakes*

*5.13.1. Uncompensated detector solenoid.* A type 3 (partial) Snake is one whose spin rotation axis is vertical. Consider a spin rotator which rotates a spin through $-\pi/2$ from the vertical to the longitudinal. The spin then passes through a solenoid, and another spin rotator rotates the spin through $\pi/2$ bringing the spin to the vertical. This is, in short, an

uncompensated detector solenoid. Let the spin rotation angle in the solenoid be $\psi_{\rm sol}$. The overall spin rotation matrix of this combination is

$$M = \mathrm{e}^{-\mathrm{i}\pi\sigma_1/4}\,\mathrm{e}^{-\mathrm{i}\psi_{\rm sol}\sigma_2/2}\,\mathrm{e}^{\mathrm{i}\pi\sigma_1/4} = \mathrm{e}^{-\mathrm{i}\psi_{\rm sol}\sigma_3/2}, \tag{102}$$

which is a spin rotation around a vertical axis, i.e. a partial type 3 Snake. The overall one-turn spin rotation matrix of the ring (assumed planar) is

$$M_{\rm ring} = \mathrm{e}^{-\mathrm{i}\pi\nu_0\sigma_3}\,\mathrm{e}^{-\mathrm{i}\psi_{\rm sol}\sigma_3/2} = \mathrm{e}^{-\mathrm{i}(2\pi\nu_0+\psi_{\rm sol})\sigma_3/2}, \tag{103}$$

where $\nu_0 = a\gamma$. The spin tune on the design orbit is then

$$\nu = \nu_0 + \frac{\psi_{\rm sol}}{2\pi}. \tag{104}$$

The solenoid fields in the main RHIC detectors are not compensated, so there are effectively two partial type 3 Snakes in RHIC. However the integrated solenoid fields are small (less than 1 Tm), and because of the high RHIC beam energy the induced spin rotations are very small (Ptitsyn 2005).

*5.13.2. IUCF cooler ring.* The IUCF Cooler had a solenoid Snake which was used in several beam dynamics studies for proof-of-principle demonstrations of the Siberian Snake concept. However, our concern here is with the spin dynamics in the IUCF Cooler with the Snake switched *off*.

Note that since $\nu_{\rm spin} = G\gamma$ in a planar ring and the value of $G$ is known to high precision, a measurement of the location of the imperfection resonance $G\gamma = 2$ should furnish an accurate calibration of the beam energy. However, it was found that the resulting measurements differed systematically from other results which were known to be accurate. The $G\gamma = 2$ imperfection resonance, which should occur at a proton kinetic energy of 108.4 MeV, was instead found to occur at 106.5 MeV, a downward shift of 1.9 MeV. Since the relative accuracy of the energy calibration of the Cooler was better than $10^{-3}$, the discrepancy was a real effect. See Pollock (1991) for details of the energy calibration. It was discovered that the combined effect of the toroidal magnetic field and the vertical steering magnets in the electron cooling section of the ring (see figure 4) were in fact contributing a set of small, noncommuting rotations, whose overall effect was a net spin rotation around the vertical axis (Pollock 1991), effectively shifting the value of the spin tune. A positive spin tuneshift $\Delta\nu$ leads to a downward shift in the observed energy of the resonance. Starting from

$$2 = G\gamma + \Delta\nu \tag{105}$$

and setting $\gamma = \gamma_0 + \Delta\gamma$, where $G\gamma_0 = 2$, and writing $\Delta E = mc^2\Delta\gamma$, we obtain

$$\Delta\nu = -G\frac{\Delta E}{mc^2}. \tag{106}$$

For a proton $mc^2 \simeq 938.272$ MeV and $G \simeq 1.792\,847$, and so an energy shift of $\Delta E = -1.9$ MeV implies a spin tuneshift of

$$\Delta\nu_{\rm exp} \simeq 0.0036. \tag{107}$$

It is from the IUCF Cooler experiments that the name 'type 3' Siberian Snake originates.

The arrangement of magnets in the Cooler's electron cooling section is shown in figure 24. The reference orbit for the protons is a *straight* line through the magnets. The magnetic fields all lie in the horizontal plane, but some are radial and others are longitudinal. Pollock's analysis contained some misspecifications of the spin rotation angles. The analysis below follows Mane (1991). The coordinate basis in this review is $\{\boldsymbol{e}_1, \boldsymbol{e}_2, \boldsymbol{e}_3\}$ with $\boldsymbol{e}_1$ radially outward, $\boldsymbol{e}_2$ longitudinal and $\boldsymbol{e}_3$ vertical. However, the basis employed by Mane (1991)

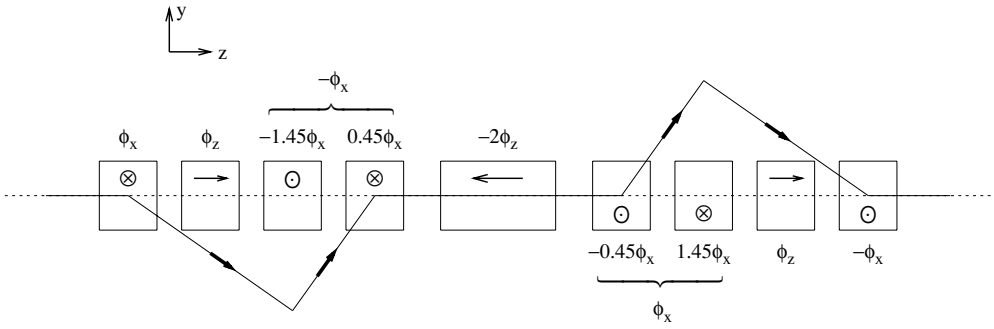


**Figure 24.** Schematic magnet layout and rotations in the electron cooling section of the IUCF Cooler.

(and shown in figure 24) is $(x, y, z)$ with $x$ radially *in*ward, $y$ vertical and $z$ longitudinal and counterclockwise. This implies some differences of sign for the rotations. The magnetic fields impart small vertical deflections to the closed orbit, shown as the dashed line in the figure. The spin rotation angles are also indicated, with arrows indicating the radial or longitudinal sense of rotation. The orbital deflection in the first magnet is $\phi_v = 13$ mrad (Pollock 1991). The spin rotation angle is $\phi_x = (G\gamma + 1)\phi_v = 39$ mrad (Mane 1991). More accurate later measurements indicated $\phi_x = 34$ mrad (Minty and Lee 1993), which is the value we shall use below. See Minty *et al* (1991) and Minty and Lee (1993) for the analysis of spin tuneshift measurements at other beam energies. The spin rotations of $1.45\phi_x$ and $-0.45\phi_x$ in figure 24 net to a single rotation of $\phi_x$. There are three magnets where the spin rotation axis points along $\boldsymbol{e}_2$, a central solenoid and two outer magnets, which inject and later deflect the electrons to/from the protons. The (longitudinal) spin rotation angle in the outer solenoids is $\phi_z$, while that in the central main solenoid of the cooling section is $-2\phi_z$. Nominally, all of these spin rotations should cancel out. Algebraically, they sum to zero, but because of the noncommutation of the $\phi_z$ and $\phi_x$ rotations, the overall spin rotation angle is not zero. The proton velocity $\boldsymbol{v}$ is actually not parallel to $\boldsymbol{e}_3$ in the outer two magnets (again, see figure 4) so they do not contribute purely $\boldsymbol{B}_\parallel$ spin rotations. The spin precession vector is (Mane 1991)

$$\begin{aligned}\boldsymbol{W}_{\text{outer}} &= \phi_z \cos\phi_v \sin\phi_v \left(\frac{G\gamma+1}{G+1} - 1\right)\boldsymbol{e}_3 + \phi_z\left(\cos^2\phi_v + \frac{G\gamma+1}{G+1}\sin^2\phi_v\right)\boldsymbol{e}_2 \\ &\simeq \phi_z \boldsymbol{e}_2 + O(\phi_x)\boldsymbol{e}_3. \end{aligned} \tag{108}$$

The overall spin rotation matrix, using small angle approximations, is

$$\begin{aligned} M_{\text{cool}} &\simeq \mathrm{e}^{\mathrm{i}\phi_x\sigma_1/2}\,\mathrm{e}^{-\mathrm{i}\phi_z\sigma_2/2}\,\mathrm{e}^{-\mathrm{i}\phi_x\sigma_1/2}\,\mathrm{e}^{\mathrm{i}\phi_z\sigma_2}\,\mathrm{e}^{\mathrm{i}\phi_x\sigma_1/2}\,\mathrm{e}^{-\mathrm{i}\phi_z\sigma_2/2}\,\mathrm{e}^{-\mathrm{i}\phi_x\sigma_1/2} \\ &= 1 - \mathrm{i}\phi_x \sin\phi_z\sigma_3 + O\left(\phi_x^2\right) \\ &\simeq \mathrm{e}^{-\mathrm{i}\phi_x \sin\phi_z\sigma_3}, \end{aligned} \tag{109}$$

i.e. a rotation through an angle $2\phi_x \sin\phi_z$ around $\boldsymbol{e}_3$. An initially vertical spin therefore exits vertically, but there is an additional contribution to the spin rotation angle of $2\phi_x \sin\phi_z$, or a shift of the spin tune by

$$\Delta\nu = \frac{\phi_x \sin\phi_z}{\pi}. \tag{110}$$

Using $\phi_x = 34$ mrad and $\phi_z = 21.5^\circ$ yields a spin tuneshift

$$\Delta\nu_{\text{th}} \simeq 0.003\,76. \tag{111}$$

The experimental value in (107) is 0.0036. The difference is explained by Minty and Lee (1993) by the additional contribution of a $k = 2$ Fourier harmonic of an imperfection resonance driving term (driving the resonance at $G\gamma = 2$). Minty and Lee used the above data to imply a magnitude for the resonance driving term of $|\epsilon| \simeq 0.0008$, and then used this number to fit the polarization measurements at other beam energies, on the assumption that the value of $\epsilon$ is energy-independent. This is a reasonable assumption over an energy range of a few MeV.

This explains the spin tuneshift, and the analyses of Pollock (1991), Minty *et al* (1991) and Minty and Lee (1993) stop there. Mane (1991), however, goes further. The tuneshift is more than an exercise in Pauli matrix multiplications. The spin tuneshift has a significance beyond that of a nuisance systematic error. It is a Berry phase (more accurately, an Aharanov–Anandan phase). For self-containedness, and also to avoid disrupting the discussion of Siberian Snakes, we discuss geometric quantum phases in a separate section, in section 6. We shall revisit the partial type 3 Snake in the IUCF Cooler there.

In the subsequent spin dynamics studies at the IUCF Cooler, the presence of the partial type 3 Snake had to be taken into account. Since there was no simple way to calculate the partial Snake strength *a priori*, in many cases a preliminary run had to be performed to calibrate the partial Snake, before proceeding with the main experiment. In some cases, previously published results were reanalysed to refit the data with an additional parameter (the partial Snake strength). See for example the work by Lee and Berglund (1996).

## 6. Geometric quantum phases

### *6.1. General remarks*

Consider a quantum system with a Hamiltonian $H$ and a set of basis states $|\psi_n\rangle$, where $n$ generically denotes a set of quantum numbers. The states evolve according to the Schrödinger equation

$$\mathrm{i}\hbar\frac{\partial}{\partial t}|\psi_n(t)\rangle = H|\psi_n(t)\rangle. \tag{112}$$

We drop the subscript $n$ below. The formal solution is

$$|\psi(t)\rangle = \mathrm{e}^{-(\mathrm{i}/\hbar)\int_0^t H(t')\mathrm{d}t'}|\psi(0)\rangle \equiv \mathrm{e}^{\mathrm{i}\gamma_d(t)}|\psi(0)\rangle. \tag{113}$$

Here $\gamma_d$ is the 'dynamical phase'. Its value can be calculated from

$$\gamma_d(t) = -\frac{1}{\hbar}\int_0^t \langle\psi(t')|H|\psi(t')\rangle\,\mathrm{d}t'. \tag{114}$$

Assume further that the Hamiltonian, and therefore the basis states, also depend on some external parameter $q$. In practice $q$ could be a multi-dimensional set of parameters, but we shall employ a scalar notation for simplicity. Suppose now that the value of the parameter(s) $q$ is not fixed, but is instead varied adiabatically around some closed path $\mathscr{C}$ in a suitably defined parameter space. Then the Hamiltonian varies around the path, returning to its original value after a time period $\tau$, say. The evolution of the state $|\psi(t)\rangle$ is more interesting. In addition to the dynamical phase, it also picks up a geometric phase $\beta = \beta(\mathscr{C})$ which depends only on the geometry of the path, namely

$$|\psi(\tau)\rangle = \mathrm{e}^{\mathrm{i}\phi_{\mathrm{tot}}}|\psi(0)\rangle, \tag{115}$$

where the total phase $\phi_{\mathrm{tot}}$ is the sum of the dynamical phase and the geometric phase:

$$\phi_{\mathrm{tot}} = \gamma_d(\tau) + \beta(\mathscr{C}). \tag{116}$$

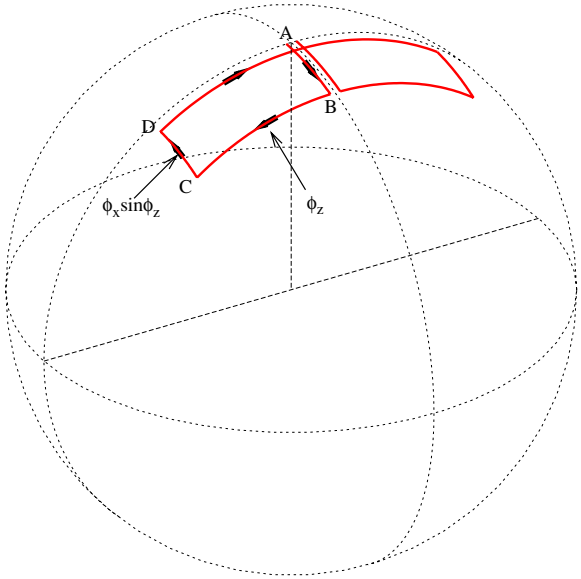


**Figure 25.** Circuit of a classical spin vector through the electron cooling section of the IUCF Cooler.

The phase $\beta(\mathscr{C})$ is called variously a geometric phase, topological quantum phase or a 'Berry phase'. Although specific examples had been known long before, it was Berry's (1984) seminal work which systematized the subject of topological quantum phases. The Aharanov–Bohm effect, known long before Berry's work, is an example of a Berry phase (Aharanov and Bohm 1959).

Many, if not most, demonstrations of geometric phases involve fermionic spin systems. For a particle with a spin projection eigenvalue $m_z$ (for us $m_z = \frac{1}{2}$), the geometric phase is equal to $-m_z$ times the solid angle swept out by the spin, if the tip of the classical spin vector traces out a closed curve $\mathscr{C}$ on the surface of a unit sphere. Aharanov and Anandan (1987) later relaxed the condition of adiabatic variations along the path. It is important for us that the adiabatic condition be removed, because the magnetic fields change abruptly from radial to longitudinal and back again, etc, during passage from one magnet to the next in an accelerator, and so the Hamiltonian does not vary adiabatically along the accelerator circumference. For our purposes the topological quantum phase $\beta(\mathscr{C})$ is more properly called an 'Aharanov–Anandan phase', and was so termed by Mane (1991), who recognized that the noncommmuting rotations and spin tuneshift in the partial type 3 Snake in the IUCF Cooler are evidence of a topological quantum phase. We shall use the terms geometric quantum phase or topological quantum phase below.

We present two examples below, one of actual data (from the IUCF Cooler), and one from the proposed VEPP-4 spin rotator. Further details of geometric phases in accelerators are given by Mane (2005a).

### *6.2. IUCF cooler*

We follow Mane (1991) below. The details of the IUCF Cooler electron cooling section have been described in section 5. We trace out the path followed by the tip of a classical spin vector on the surface of a unit sphere, upon passing through the electron cooling section of the IUCF Cooler, in figure 25. The spin points upwards in the non-cooling sections of the accelerator,

and its tip is at the North Pole of the sphere (point A). Starting from the North Pole at A, the spin rotates through a polar angle $-\phi_x \cos\phi_z$ around $\boldsymbol{e}_1$ to the point B. It then rotates around $\boldsymbol{e}_2$ through an angle $\phi_z$ to reach the point C. It then rotates through $\phi_x \cos\phi_z$ around $\boldsymbol{e}_1$ to reach the point D. The rest of the rotations complete a mirror image of the trajectory, as shown in the figure. Since the curve $\mathscr{C}$ encloses the area in a clockwise sense, the solid angle $\Omega(\mathscr{C})$ is the negative of the enclosed area, and is

$$\Omega(\mathscr{C}) = -(-\phi_x \cos\phi_z) \times 2\phi_z = 2\phi_x\phi_z \cos\phi_z. \tag{117}$$

The geometric phase is minus one-half of the above, or

$$\beta(\mathscr{C}) = -\phi_x\phi_z \cos\phi_z. \tag{118}$$

It was shown in (109) that the total phase advance in the cooling section is

$$\phi_{\text{tot}} = -\phi_x \sin\phi_z. \tag{119}$$

Hence the geometric phase will dominate the contribution to the total phase advance as long as $\sin\phi_z \simeq \phi_z \cos\phi_z$, or $\tan\phi_z \simeq \phi_z$. In the IUCF Cooler, $\phi_z = 21.5^\circ$, so $(\tan\phi_z - \phi_z)/\phi_z \simeq 0.05$. Hence the geometric phase accounts for about 95% of the spin tuneshift observed in the IUCF Cooler.

Note that the geometric phase did not account for *all* of the spin tuneshift. In general, there is no guarantee that the dynamical phase will sum to zero over the closed path $\mathscr{C}$. In experiments designed to demonstrate topological quantum phases, special precautions have to be taken to ensure that the dynamical phase vanishes, usually by arranging the geometry to have a special symmetry. Obviously, no such precautions were taken at the IUCF Cooler because nobody suspected the existence of the partial type 3 Snake in the ring in the first place. There is also not really sufficient freedom with the accelerator parameters to adjust the value of the dynamical phase to a desired value such as zero.

### *6.3. VEPP-4 spin rotator*

It is simpler to track a spin through the proposed VEPP-4 solenoid spin rotator (see figure 22). The circuit of a spin through the spin rotator is shown in figure 26. Since the spin precession vector is everywhere orthogonal to the spin direction in this rotator design, the dynamical phase vanishes identically. Hence the spin rotation angle of this rotator design is a pure geometric phase. The solid angle enclosed is one-quarter of a sphere (a quadrant), i.e. $\pi$. The geometric phase is minus one-half this, or $\Omega = -\pi/2$. The contribution to the spin rotation angle is the negative of this, or $\pi/2$, as we found in section 4.

## 7. Snake resonances

### *7.1. Single resonance model*

In general, the theoretical analysis of the spin dynamics in accelerators can take one of two paths. One is to develop sophisticated numerical formalisms, and computer programs, to solve the spin precession equation. Several numerical algorithms will be reviewed in MSY2. Such programs are essential to design modern high-energy accelerators with complicated structures. Nevertheless, the programs *are* complicated. The alternative path is to develop (very) simple models of accelerators, which are analytically tractable. The behaviour of the spin and the polarization in such models can be calculated exactly. Frequently such models can provide useful estimates even for complicated machines.

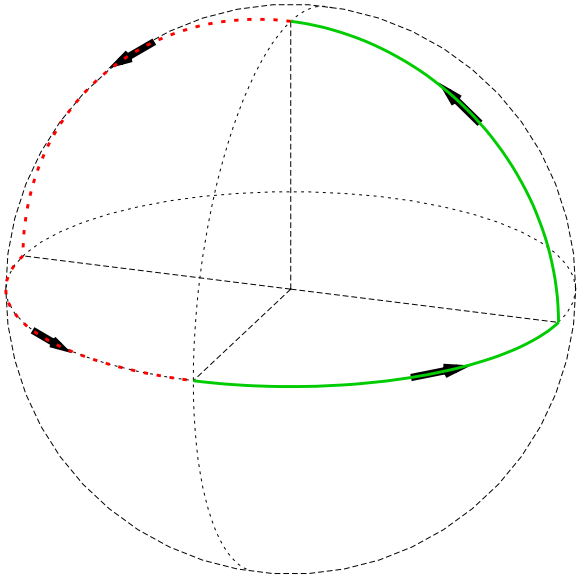

**Figure 26.** Topological circuit of a unit spin vector through the VEPP-4 spin rotator.

Up to now we have solved for the spin rotation axis on the design orbit, namely the vector $\boldsymbol{n}_0$. We now solve for the generalization, denoted by $\boldsymbol{n}$, for the off-axis trajectories. The vector $\boldsymbol{n}$ gives the quantization axis of the spin eigenstates for the accelerator. The simplest nontrivial model for the off-axis spin precessions is the *single resonance model* (SRM). We follow Mane (1988) but with many additional details. Since the spin precession on the design orbit of a planar ring is vertical, additional vertical perturbing fields have a negligible effect. The principal nontrivial perturbation is horizontal. The spin precession vector of the single resonance model is

$$\boldsymbol{W}_{\rm SRM} = \nu_0 \boldsymbol{e}_3 + \epsilon(\boldsymbol{e}_1 \cos\phi + \boldsymbol{e}_2 \sin\phi). \tag{120}$$

Recall $\nu_0 = a\gamma$ or $\nu_0 = G\gamma$. The perturbing term, proportional to $\epsilon$, is horizontal. The tacit assumption is that $\epsilon = 0$ on the design orbit. Also, $\phi$ is a phase, which evolves acording to

$$\frac{\mathrm{d}\phi}{\mathrm{d}\theta} = Q, \tag{121}$$

where $Q$ is a constant. We can write $\phi = Q\theta + \phi_0$. A simple way to solve for the spin motion is to transform to a frame rotating around $\boldsymbol{e}_3$ at tune $Q$. The basic vectors in the lab frame and the rotating frame are shown in figure 27. In the rotating frame the spin precession vector is

$$\boldsymbol{W}'_{\rm SRM} = (\nu_0 - Q)\boldsymbol{e}_3 + \epsilon(\boldsymbol{e}'_1 \cos(\phi - Q\theta) + \boldsymbol{e}'_2 \sin(\phi - Q\theta)), \tag{122}$$

where primes are used to denote quantities in the rotating frame. Here

$$\begin{aligned} \boldsymbol{e}'_1 &= \quad \boldsymbol{e}_1 \cos(Q\theta) + \boldsymbol{e}_2 \sin(Q\theta) \\ \boldsymbol{e}'_2 &= -\boldsymbol{e}_1 \sin(Q\theta) + \boldsymbol{e}_2 \cos(Q\theta). \end{aligned} \tag{123}$$

Note that $\boldsymbol{W}'_{\rm SRM}$ is a *fixed* vector because $\mathrm{d}\boldsymbol{W}'_{\rm SRM}/\mathrm{d}\theta = 0$. Then the spin $\boldsymbol{s}'$ rotates around $\boldsymbol{W}'_{\rm SRM}$

$$\frac{\mathrm{d}\boldsymbol{s}'}{\mathrm{d}\theta} = \boldsymbol{W}'_{\rm SRM} \times \boldsymbol{s}'. \tag{124}$$

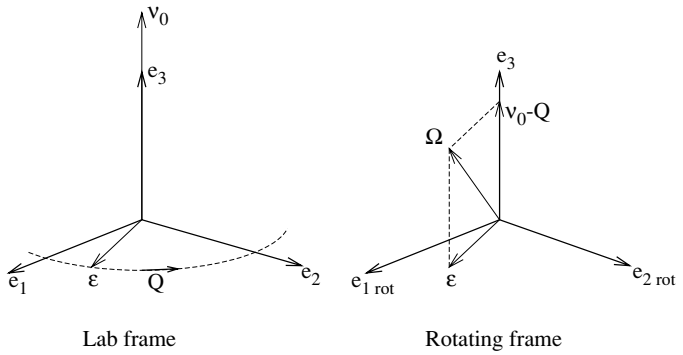


**Figure 27.** Schematic of spin precession vector for the single resonance model in the lab and rotating frames.

Since $\boldsymbol{W}'_{\rm SRM}$ is a fixed vector, the solution for $\boldsymbol{n}'$ is a unit vector in the direction of $\boldsymbol{W}'_{\rm SRM}$, i.e. $\boldsymbol{n}' = \boldsymbol{W}'_{\rm SRM}/|\boldsymbol{W}'_{\rm SRM}|$, while the spin tune is just the magnitude of $\boldsymbol{W}'_{\rm SRM}$, i.e. $\nu' = |\boldsymbol{W}'_{\rm SRM}|$.

We now introduce some important notation. Define the vector $\boldsymbol{\Omega}$ and its magnitude $\Omega$:

$$\boldsymbol{\Omega} = (\nu_0 - Q)\boldsymbol{e}_3 + \epsilon(\boldsymbol{e}_1 \cos\phi + \boldsymbol{e}_2 \sin\phi), \qquad \Omega = \sqrt{(\nu_0 - Q)^2 + \epsilon^2}, \tag{125}$$

where we take the positive root for $\Omega$. Note that $\boldsymbol{\Omega}$ as defined in (125) should not be confused with the previous usage of $\boldsymbol{\Omega}$ to denote the spin precession vector using the time $t$ as the independent variable, in (2).

In the original reference frame, the solution which reduces to $\boldsymbol{n} \to \boldsymbol{n}_0 = \boldsymbol{e}_3$ as $\epsilon \to 0$ is

$$\boldsymbol{n}_{\rm SRM} = {\rm s}_{\nu_0 - Q}\frac{\boldsymbol{\Omega}}{\Omega}, \qquad \nu_{\rm SRM} = Q + {\rm s}_{\nu_0 - Q}\sqrt{(\nu_0 - Q)^2 + \epsilon^2}. \tag{126}$$

Here $\mathrm{s}_x$ is the sign function, and equals $\pm 1$ according as $x > 0$ or $x < 0$, respectively. Exactly at $\nu_0 = Q$, we can accept either sign in (126). Hence $\boldsymbol{n}$ is vertical on the design orbit ($\epsilon = 0$) and tilts towards the horizontal as the magnitude of the driving term increases. However, exactly at $\nu_0 = Q$, $\boldsymbol{n}$ is *horizontal* for all $\epsilon \neq 0$. The spin tilts into the horizontal plane as soon as $\epsilon$ is even infinitesimally nonzero. This is a resonance: an extreme variation of the direction of the spin eigenstates for small changes in the model parameters.

### *7.2. Single resonance model with Siberian Snakes*

For many years, the single resonance model was the only accelerator model which had been solved analytically for the off-axis trajectories. Of course, important results can be derived just by analysing the spin motion on the closed orbit, as for example the discovery of the concept of Siberian Snakes. To study the effects of resonance driving terms in a ring equipped with Siberian Snakes, it is natural to extend the single resonance model to include one or more Snakes. The Snakes are modelled as $\delta$-function point-like objects, as in section 4. The model has no special name; it is simply the 'SRM with Snakes'. It is nevertheless the classic model in the field, for rings with Siberian Snakes. Since, as we have seen, the closed-orbit solution $\boldsymbol{n}_0$ is vertical in the arcs if a ring is equipped with a pair of Snakes, most early theoretical studies treated the SRM with a pair of diametrically opposite Snakes, with orthogonal spin rotation axes. The SRM with a pair of orthogonal Snakes has been widely studied in the literature since at least 1985, e.g. see the work of Buon (1986) and especially Tepikian (1986) at the 1985 Ann Arbor workshop, and also the summary at the workshop by Ruth (1986). Ptitsyn

and Shatunov (1997a) derived approximate analytical expressions, via perturbation theory, for the $\boldsymbol{n}$-axis for the single resonance model with two orthogonal Snakes.

Recently, Mane (2002a, 2002b, 2003a and 2003b) derived the exact analytical solutions for the $\boldsymbol{n}$ axis and the spin tune $\nu$ for a number of storage ring models in a set of four papers. The solutions include the generalization of the single resonance model to include a single Siberian Snake, or a pair of diametrically opposed orthogonal Snakes (Mane 2002b, 2003a). In particular, it was shown for the SRM with one Snake, or two orthogonal Snakes, that the value of the spin tune $\nu$ is $\frac{1}{2}$ on *all* orbits with irrational orbital tunes (Mane 2002a). This was independently confirmed by Mane (2003a) for the one-Snake model, by solving Yokoya's SODOM2 algorithm (Yokoya 1999) analytically. The claim that $\nu = \frac{1}{2}$ off-axis had previously been conjectured by Yokoya (1988), by solving up to second order in perturbation theory.

Mane's solution also confirmed the spectrum of the so-called Snake resonances which had earlier been found by Lee and Tepikian (1986) for the two-Snake model, and by Lee (1997) for the one-Snake model. Even theoretically ideal Snakes do not eliminate all the depolarizing resonances in a storage ring. The Snakes render the spin tune independent of energy, and this is certainly a big help, but it is not the last word. Depolarizing resonances in a ring equipped with Snakes are called 'Snake resonances', although they are in fact due to the same mechanisms of spin–orbit coupling which drive any other type of spin resonance (e.g. imperfection and intrinsic resonances in planar rings). Nevertheless, the term 'Snake resonances' has stuck.

Snake resonances were predicted theoretically by Lee and Tepikian (1986), for a model ring with a pair of Snakes. They used a mixture of perturbation theory and particle tracking to analyse the single resonance model with a pair of diametrically opposed orthogonal Siberian Snakes. See also additional work by Lee (1993) on 'even-order Snake resonances' and also the text by Lee (1997). Snake resonances were first observed by Phelps *et al* (1997) in studies at the IUCF Cooler, and more recently at RHIC (Ptitsyn *et al* 2003, Ranjbar *et al* 2003).

The material below follows the above papers by Mane. The solution for $\boldsymbol{n}$ is expressed as a Fourier sum of so-called sine-Bessel functions. Mane (2002b, 2003a) claimed that the sine-Bessel functions were new mathematical functions which have not previously been published in the literature, but it is now known that they are, in fact, special cases of '$q$-modified hypergeometric functions', after a transformation of variables. Nevertheless, for continuity with previously published work we employ the nomenclature 'sine-Bessel' in this review.

### *7.3. Sine-Bessel functions*

First recall the power series expansion of Bessel functions of the first kind, for integer $m \geqslant 0$ and complex $z$:

$$J_m(z) = \sum_{k=0}^{\infty} (-1)^k \frac{1}{k!(m+k)!} \left(\frac{z}{2}\right)^{m+2k}, \tag{127}$$

with $J_{-m}(z) = (-1)^m J_m(z)$. To introduce the sine-Bessel functions, we first introduce and define the sine-factorial and cosine-factorial functions:

$$\begin{aligned} S_n(x) &\equiv \sin x \sin(2x) \cdots \sin(nx), \\ C_n(x) &\equiv \cos x \cos(2x) \cdots \cos(nx), \end{aligned} \tag{128}$$

with the convention $S_0 = C_0 = 1$. As with the sine-Bessels, it is now known that these are not new functions. They are related to the so-called '$q$-modified factorial' function.

Now introduce real $\delta$ and $\eta$ and define, for $m \geqslant 0$,

$$\begin{aligned}\mathscr{A}_m(\eta,\delta) &= \cos\left(\tfrac{1}{2}m\pi\delta\right)\sum_{k=0}^{\infty}(-1)^k\frac{C^2_{m/2+k-1}(\pi\delta)}{S_k(\pi\delta)S_{k+m}(\pi\delta)}\eta^{m+2k},\\ \mathscr{B}_m(\eta,\delta) &= \sum_{k=0}^{\infty}(-1)^k\frac{C^2_{(m-1)/2+k}(\pi\delta)}{S_k(\pi\delta)S_{k+m}(\pi\delta)}(\eta\,\mathrm{e}^{\mathrm{i}\pi\delta/2})^{m+2k}.\end{aligned} \tag{129}$$

For $m < 0$ define $\mathscr{A}_{-m}(\eta,\delta) = (-1)^m\mathscr{A}_m(\eta,\delta)$ and $\mathscr{B}_{-m}(\eta,\delta) = (-1)^m\mathscr{B}_m(\eta,\delta)$. The analogy with the power series expansion of the Bessel functions is obvious. For $|\pi\delta| \ll 1$ (strictly speaking $\delta \to 0$) and finite $\eta/(\pi\delta)$ we have the asymptotic approximations

$$\mathscr{A}_m \approx J_m\Big(\frac{2\eta}{\pi\delta}\Big), \qquad \mathscr{B}_m \approx J_m\Big(\frac{2\eta}{\pi\delta}\,\mathrm{e}^{\mathrm{i}\pi\delta/2}\Big). \tag{130}$$

The definition of the sine-Bessels given above follows that by Mane (2004) but is slightly different from that by Mane (2002b, 2003a). It is now known that those earlier definitions were too restrictive, and do not generalize easily to connect to the pure mathematical literature. The power series expansion of a Bessel function converges absolutely for all values of the argument $z$. The power series expansions of the sine-Bessel functions have a finite radius of convergence $|\eta| < 1$.

Note that there is an ambiguity in the above definition of $\mathscr{A}_m$ when $m = k = 0$, because the numerator contains a term $C^2_{-1}$. The proper definition is to write, for $n \geqslant 0$, $C_{n-1}(x) = C_n(x)/\cos(nx)$. The rhs is well-defined for $n = 0$, and in fact equals unity for $n = 0$. In addition, the astute reader will note that for $\mathscr{A}_m$ with odd $m$, or $\mathscr{B}_m$ with even $m$, the index on the cosine-factorial is *fractional*: e.g. for odd $m$ the value of $m/2+k-1$ is an integer plus one-half. The notation $C_{n-1/2}(x)$ means

$$C_{n-1/2}(x) \equiv \cos\left(\tfrac{1}{2}x\right)\cos\left(\tfrac{3}{2}x\right)\cdots\cos\left(\left(n-\tfrac{1}{2}\right)x\right). \tag{131}$$

### *7.4. Single resonance model with one Siberian Snake*

We model a Snake theoretically as a $\delta$-function point object, which rotates all the spins through exactly 180°. We have already done so on the closed orbit, and now extend the idealization to all orbits. The spin precession vector for a single resonance model with a single Snake is

$$\boldsymbol{W} = \nu_0\boldsymbol{e}_3 + \epsilon(\boldsymbol{e}_1\cos\phi + \boldsymbol{e}_2\sin\phi) + \pi\delta_p(\theta)(\boldsymbol{e}_1\cos\xi + \boldsymbol{e}_2\sin\xi). \tag{132}$$

Here $\delta_p(\theta)$ is the periodic $\delta$-function

$$\delta_p(\theta) \equiv \sum_{j=-\infty}^{\infty}\delta(\theta - 2\pi j). \tag{133}$$

The Snake is placed just after the origin, and its spin rotation axis is oriented at an angle $\xi$ relative to the radial direction $\boldsymbol{e}_1$. We omit the details of the algebra. We define the parameters $\eta = (\epsilon/\Omega)\sin(\pi\Omega)$ and $\delta = Q - \frac{1}{2}$. We also express the components of $\boldsymbol{n}$ in the form

$$\begin{aligned} n_3 &= a,\\ n_+ = n_1 + \mathrm{i}n_2 &= -\mathrm{i}\mathrm{e}^{\mathrm{i}\pi\delta}\,\mathrm{e}^{\mathrm{i}\xi}\left[\cos(\pi\Omega) + \mathrm{i}\frac{\nu_0 - Q}{\Omega}\sin(\pi\Omega)\right]b.\end{aligned} \tag{134}$$

We now expand in Fourier series

$$a = 2\sum_{m=\text{odd}} a_m\sin[m(\phi_* - \xi)], \qquad b = b_0 + 2\sum_{m=\text{even}} b_m\cos[m(\phi_* - \xi)], \tag{135}$$

where $\phi_*$ is the value of $\phi$ at the origin. The solutions for the Fourier coefficients $a_m$ and $b_m$ are sine-Bessel functions with an argument of $2\delta$:

$$\begin{aligned} a_m(\eta,\delta) &= \mathscr{A}_m(\eta,2\delta) \qquad (m=1,3,5,\ldots), \\ b_m(\eta,\delta) &= \mathscr{B}_m(\eta,2\delta) \qquad (m=0,2,4,\ldots). \end{aligned} \tag{136}$$

The Fourier series for the components of $\boldsymbol{n}$ consists of only sines (with odd $m$) for $n_3$ and only cosines (with even $m$) for $n_+$. Note also that the sine-Bessel functions have small divisor problems when $Q$ is rational, so the above solution is valid for irrational $Q$. The spin tune is $\nu = \frac{1}{2}$ for orbits where $Q$ is irrational, for arbitrary $\epsilon$, provided $|\eta| < 1$.

### *7.5. Single resonance model with two orthogonal Siberian Snakes*

Strictly speaking, we should say 'two orthogonal Snakes at diametrically opposite points in the ring' but this is universally understood. The Snake spin rotation axes are oriented at $\xi$ and $\xi + \pi/2$ relative to $\boldsymbol{e}_1$. The origin is placed just before the first Snake, so the Snakes are located at $\theta = 0^+$ and $\theta = \pi$. The spin precession vector is now

$$\begin{aligned} \boldsymbol{W} = {} & \nu_0 \boldsymbol{e}_3 + \epsilon(\boldsymbol{e}_1 \cos\phi + \boldsymbol{e}_2 \sin\phi) + \pi\delta_p(\theta)(\boldsymbol{e}_1 \cos\xi + \boldsymbol{e}_2 \sin\xi) \\ & + \pi\delta_p(\theta-\pi)(-\boldsymbol{e}_1 \sin\xi + \boldsymbol{e}_2 \cos\xi). \end{aligned} \tag{137}$$

Now define $\eta' = (\epsilon/\Omega)\sin(\pi\Omega/2)$. Also define

$$\begin{aligned} n_3 &= a', \\ n_+ &= -\mathrm{i}\mathrm{e}^{\mathrm{i}\pi\delta/2}\,\mathrm{e}^{\mathrm{i}\xi}\left[\cos\frac{\pi\Omega}{2} + \mathrm{i}\frac{\nu_0 - Q}{\Omega}\sin\frac{\pi\Omega}{2}\right] b'. \end{aligned} \tag{138}$$

Then expand $a'$ and $b'$ in Fourier series, but now set

$$\begin{aligned} a' &= a'_0 + 2\sum_{m=\text{even}} a'_m \cos[m(\phi_* - \xi)], \\ b' &= 2\sum_{m=\text{odd}} b'_m \sin[m(\phi_* - \xi)]. \end{aligned} \tag{139}$$

Then the solutions for the Fourier coefficients are sine-Bessel functions (with an argument of $\delta$):

$$\begin{aligned} a'_m(\eta',\delta) &= \mathscr{A}_m(\eta',\delta) \qquad (m=0,2,4,\ldots), \\ b'_m(\eta',\delta) &= \mathscr{B}_m(\eta',\delta) \qquad (m=1,3,5,\ldots). \end{aligned} \tag{140}$$

The above sine-Bessel solution is now used at BNL to benchmark the spin tracking codes for RHIC (Roser 2005).

Note the pattern of the Fourier series is reversed relative to the model with one Snake: the Fourier series for $n_3$ consists of only cosines (with even $m$) and that for $n_+$ contains only sines (with odd $m$). The above solutions also have small divisor problems when $Q$ is rational. The spin tune is also $\nu = \frac{1}{2}$ for orbits where $Q$ is irrational, for arbitrary $\epsilon$, provided $|\eta'| < 1$.

A quantity of interest is $\langle n_3 \rangle$, the average over the betatron phase $\phi_*$. Clearly

$$\langle n_3 \rangle = \mathscr{A}_0(\eta',\delta). \tag{141}$$

Using perturbation theory, Ptitsyn and Shatunov (1997a) calculated approximate analytical expressions for the $\boldsymbol{n}$-axis and Snake resonance widths for the single resonance model with two diametrically opposed orthogonal Snakes. They obtained the expression

$$\langle n_3 \rangle \simeq J_0\left(\frac{2\eta'}{\sin(\pi\delta)}\right). \tag{142}$$

With the further approximation $|\pi\delta| \ll 1$, this is identical to the asymptotic approximation in (130) for the sine-Bessel function $\mathscr{A}_0$. Lee and Tepikian (1986) employed a spin tracking formalism and did not solve for $\boldsymbol{n}$, but their formalism can be adapted to do so (Mane 2005b). The resulting expression for $\langle n_3 \rangle$ is identical to (142).

### *7.6. Snake resonances*

Even though we write the '*Single* Resonance Model with Snakes', there are obviously many resonances. The model is really better described as retaining only a single Fourier harmonic in the resonance driving terms, but the name 'SRM with Snakes' has taken root. The depolarizing spin resonances (Snake resonances) are given by the singularities in the solutions for $\boldsymbol{n}$ above. This occurs at rational values of $Q$. However, there are some rational values of $Q$ where the sine-Bessel power series reduces to $0/0$ terms, and the solution for $\boldsymbol{n}$ is actually not singular. For a model with one Snake, the spectrum of the Snake resonances is given by

$$\tfrac{1}{2} + mQ = k, \tag{143}$$

where $m$ is a nonzero integer and $k$ is an arbitrary integer. The above spectrum was first reported by Lee (1997) and confirmed by Mane (2002b). The Snake resonance observed at the IUCF Cooler by Phelps *et al* (1997) was at a vertical betatron tune value of $Q_y = 4.75$. Preliminary evidence for depolarization at SHR at a Snake resonance, at a fractional vertical betatron tune of $[Q_y] = \frac{1}{6}$, has been reported by van der Laan *et al* (2003).

For a model with two diametrically opposed orthogonal Snakes, the spectrum of the Snake resonances is given by

$$\tfrac{1}{2} + m'Q = k', \tag{144}$$

where $m'$ is an *odd* integer and $k'$ is an arbitrary integer. These are referred to as 'odd-order' Snake resonances. The above spectrum was first reported by Lee and Tepikian (1986) and was also confirmed by Mane (2002b). If a ring with two Snakes contains closed orbit imperfections, then 'even-order' Snake resonances, where $m'$ is even, can also appear (Lee 1993).

Figure 28 shows plots of $P = \langle n_3 \rangle = \mathscr{A}_0$ in the interval $[Q] \in (0, 0.5)$, for values of $\epsilon$ in steps from 0.1 to 0.8. The graphs in the interval $[Q] \in (0.5, 1)$ are just the mirror images. The model has only odd-order Snake resonances (odd $m'$ in (144)), which are visible in the plots. Note that the locations of the Snake resonances are independent of $\eta$ and depend *only on* $[Q]$, although the resonance widths increase with $\eta$. The last plot $\eta = 0.8$ is mostly numerical noise. There are also other points (not at a Snake resonance) where the value of $\mathscr{A}_0$ crosses zero. We can call these 'nonresonant zeros'. Their locations do depend on both $\eta$ and $[Q]$. These points do not correspond to depolarization of the beam, since in a real beam there is a distribution of orbital amplitudes (values of $\eta$). The Snake resonances imply depolarization, since $\mathscr{A}_0$ (and also the other sine-Bessels) vanish for all $\eta$.

Figure 29 shows a more detailed plot of $P = |\langle n_3 \rangle| = |\mathscr{A}_0|$ in the interval $[Q] \in (0, 0.5)$, for the special case $\epsilon = 0.4$. The graph is identical to that of $\mathscr{A}_0$ for the case $\epsilon = 0.4$ in figure 28 (with an absolute value sign). The calculation of $P$ was performed using a numerical technique called stroboscopic averaging (see Heinemann and Hoffstätter (1996) for details of the method). Values of $[Q]$ where the program failed to converge are omitted from the graph. Numerous (odd-order) Snake resonances are visible, and are labelled. The nonresonant zeros of $\mathscr{A}_0$ are also visible, and are labelled 'nonresonant depolarization' in the figure.

A graph of the polarization exhibiting the first observation of Snake resonances at RHIC is shown in figure 30 (Ptitsyn *et al* 2003). The RHIC polarimeter had only been calibrated at 24 GeV (injection), not at 100 GeV at the time of the above measurements, hence the data show the 'polarization preservation efficiency' $P_f/P_i$, i.e. the asymmetry relative to the beginning of

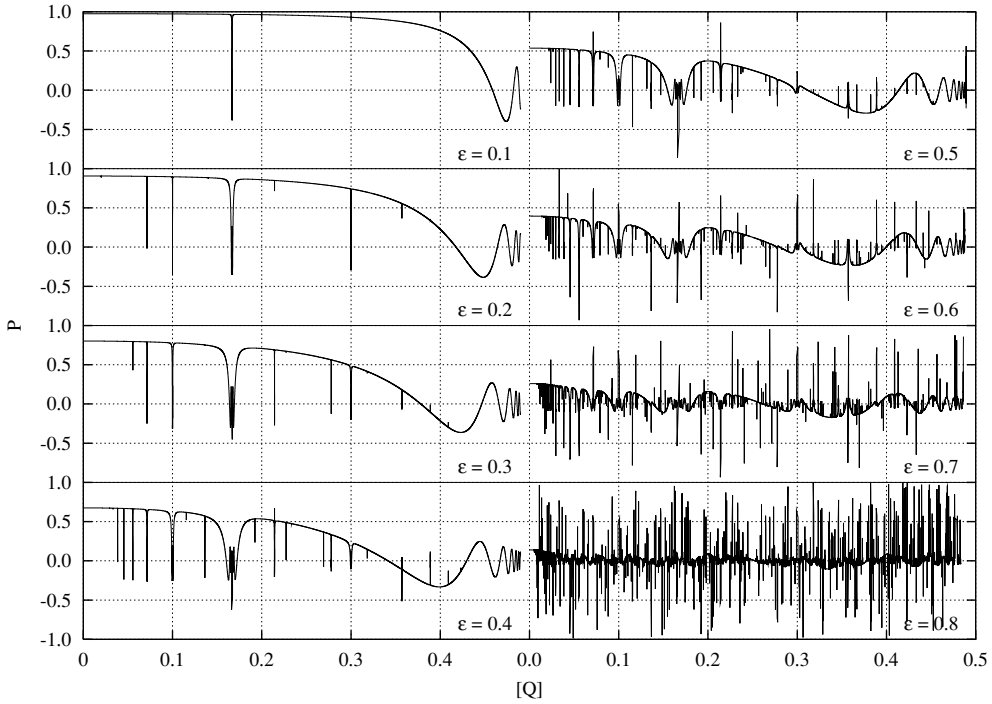


**Figure 28.** Graph of $P$ (defined the average $\langle n_3 \rangle$ over the betatron oscillation phases) in the tune interval $[Q] \in (0, 0.5)$, for values of $\eta$ in steps from 0.1 to 0.8.

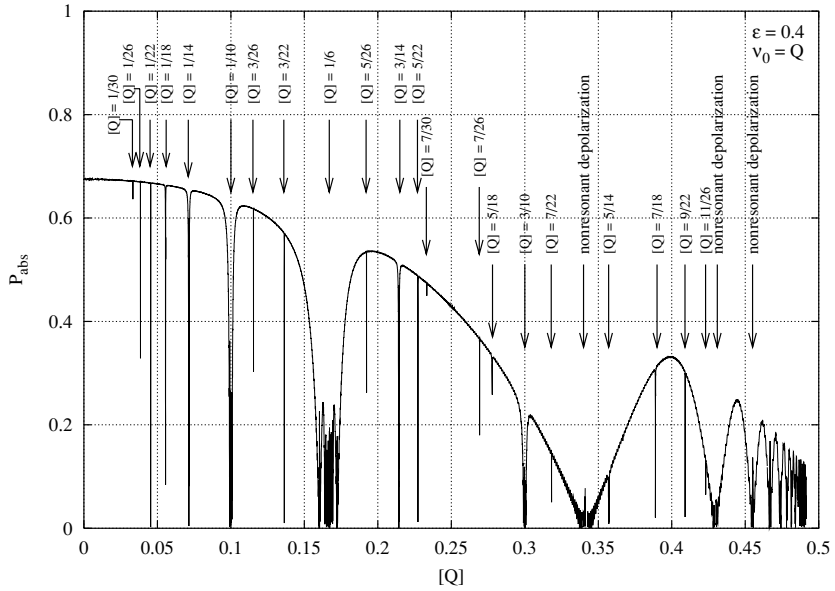


**Figure 29.** Graph of the polarization $P_{\text{abs}} = |\langle \boldsymbol{n} \rangle|$, as a function of the fractional orbital tune $[Q]$. The parameter values used in the plot are shown in the top right corner. Numerous Snake resonances are visible, and are labelled in the figure. Regions of nonresonant depolarization are also visible, e.g. at $[Q] \simeq 0.341$, and are also labelled.

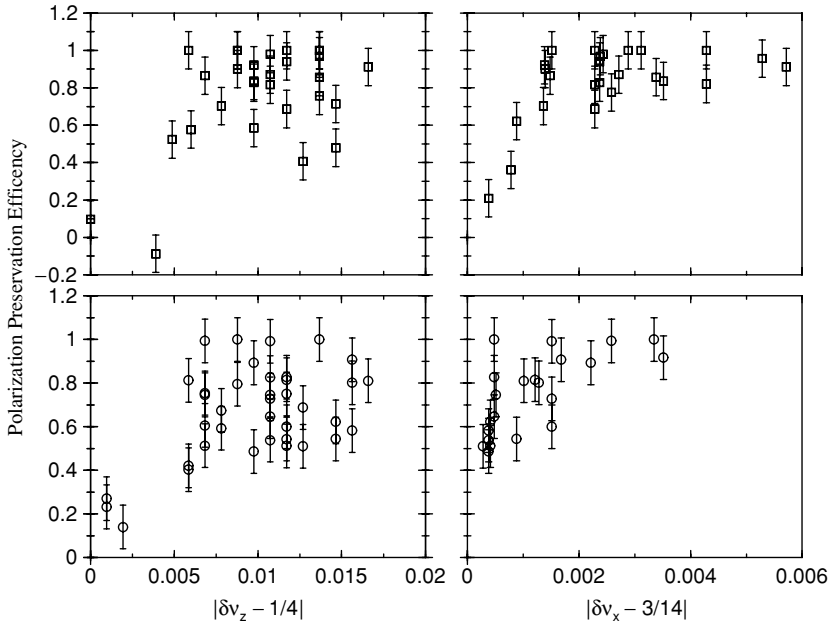


**Figure 30.** Observation of Snake resonances at RHIC. The squares show the data from the yellow ring and the circles show the data from the blue ring. Courtesy of W W MacKay (private communication) and BNL.

the store. The left-hand panel shows the efficiency as a function of the distance of the fractional vertical betatron tune $[Q_y]$ from $\frac{1}{4}$, i.e. $\left|[Q_y] - \frac{1}{4}\right|$. This is an even-order Snake resonance. There are large fluctuations in the data because the values of other machine parameters were not always constant. Nevertheless, there is a loss of polarization as $\left|[Q_y] - \frac{1}{4}\right| \to 0$. The right-hand panel shows the polarization preservation efficiency as a function of the distance of the fractional horizontal betatron tune $[Q_x]$ from $\frac{3}{14}$, i.e. $\left|[Q_x] - \frac{3}{14}\right|$. This is an odd-order Snake resonance, with coupling of the horizontal betatron oscillations into the vertical plane. There is again a clear loss of polarization as $\left|[Q_x] - \frac{3}{14}\right| \to 0$. The data were taken in 2002; more data are given by Ptitsyn *et al* (2004).

### *7.7. Maximum tolerable resonance strength*

Lee and Courant (1990) performed a detailed investigation of the problem of the maximum tolerable resonance strength to avoid sigificant depolarization in a ring with multiple Snakes (say $N_{\text{pair}}$ pairs of Snakes), motivated by design studies for the SSC (Superconducting SuperCollider). Denote that maximum strength by $\epsilon_{\max}$. They found that for a single resonance model with $N_S$ Snakes,

$$\epsilon_{\max} = \frac{\arcsin(|\cos(\pi Q)|^{1/2})}{\pi} N_S \tag{145}$$

where $Q$ is the vertical betatron tune. Since the maximum value of $\cos(\pi Q)$ is unity, we can use the upper bound

$$\epsilon_{\max} \leqslant \frac{\arcsin(1)}{\pi} N_S = \frac{N_S}{2}. \tag{146}$$

Equation (146) had also been deduced in earlier works, e.g., Yokoya (1988) and Lee (1989), based on tracking simulations coupled with perturbation theory. An earlier, more pessimistic, conclusion was that $N_{\rm pair} \propto \epsilon_{\rm max}^2$ (Ruth 1986), but this was based on very approximate estimates.

The analytical solution confirms (146). The controlling parameter determining the strength of the resonances is $\eta_{N_S}$, and we have noted that $|\eta_{N_S}| \leqslant 1$. Hence we set $\eta_{N_S} = 1$ to obtain the maximum tolerable value $\epsilon_{\rm max}$:

$$1 = \eta_{N_S} = \frac{\epsilon_{\rm max}}{\Omega} \sin\left(\frac{\pi\Omega}{N_S}\right). \tag{147}$$

To obtain $\eta_{N_S} = 1$, we require two things: (i) $\epsilon_{\rm max}/\Omega = 1$ and (ii) $\sin(\pi\Omega/N_S) = 1$. The condition $\epsilon_{\rm max}/\Omega = 1$ implies $\nu_0 - Q = 0$, hence $\Omega = \epsilon_{\rm max}$. Then

$$\sin\left(\frac{\pi\epsilon_{\rm max}}{N_S}\right) \leqslant 1. \tag{148}$$

Hence we deduce $\epsilon_{\rm max} \leqslant N_S/2$. This result agrees with the earlier findings by Yokoya (1988), Lee (1989) and Lee and Courant (1990), which were based on perturbation theory and/or numerical analysis. The general rule-of-thumb is that more Snakes are better, since they can handle larger resonance driving terms. However, studies reported by Barber *et al* (2002) for Siberian Snakes in the HERA proton ring indicate that schemes with eight Snakes are *not* as good as those with only four Snakes. However Hofstaetter (2004) presents a milder claim, in studies using four Snakes at HERA-p. Hence the efficacy of the Snakes depends on how and where they can be placed in the lattice of a real machine.

### *7.8. Nonorthogonal Siberian Snakes*

When the Snake axes are *not* orthogonal, the problem becomes much more complicated. Only partial results are known. For example, the spin tune now depends on the orbital amplitude. Define the axes to be oriented at $\xi$ and $\xi + (\pi/2) + \chi$ relative to the radial direction $\boldsymbol{e}_1$. Dropping the prime, redefine $\eta = (\epsilon/\Omega)\sin(\pi\Omega/2)$. Recall also that $\delta = Q - \frac{1}{2}$. When the origin is just after the first Snake, the value of the closed-orbit spin tune is $\nu_{\rm c.o.} = (1/2) - (\chi/\pi)$ (see (30)). Define the spin tuneshift as $\Delta\nu$, so $\nu = \nu_{\rm c.o.} + \Delta\nu$, and write

$$\Delta\nu = \sum_k \Delta\nu_k \eta^{2k}. \tag{149}$$

The leading order tuneshift term is

$$\Delta\nu_1 = -\frac{1}{2\pi}\frac{\sin(2\chi)}{\sin(\chi + \pi\delta)\sin(\chi - \pi\delta)}. \tag{150}$$

A general solution for the tuneshift terms has not yet been worked out. It can be shown, via perturbation theory, that the Snake resonance spectrum is given by

$$\frac{1}{2} \pm \frac{\chi}{\pi} + m''Q = k'', \tag{151}$$

where $m''$ is odd and $k''$ is an arbitrary integer. Equation (151) is also known in the literature, and is used to help calibrate the RHIC Snakes, as we point out below. Compared to the spectrum for orthogonal Snakes ($\chi = 0$), each resonance line splits into a doublet; effectively a lifting of a degeneracy. When imperfections are present, then even values of $m''$ are allowed.

### *7.9. Calibration of RHIC Siberian Snakes*

In fact, the Snake resonances are used to calibrate the RHIC Snakes (Roser 2005). The RHIC Snakes are configured so that if one Snake axis points at an angle $\zeta$ relative to the longitudinal (the beam direction), the axis of the other points at $-\zeta$ to the longitudinal. The goal is to set the currents in the Snake helices so that $\zeta = \pi/4$. To do this the fractional part of the vertical betatron tune is set to 0.24, i.e. close but not exactly equal to the observed Snake resonance at $[Q_y] = 0.25$. The currents in the RHIC Snake helices are varied until depolarization is observed. This corresponds to a Snake resonance with $m'' = 2$ in (151). From this information one can calculate the currents required to attain a spin tune of $\frac{1}{2}$.

## 8. Conclusion

The theoretical idea of Siberian Snakes, originally proposed by Derbenev and Kondratenko (1976) almost 30 years ago, is now bearing fruit. Despite their obvious appeal, Siberian Snakes were not immediately built and operated in accelerators. This was because Snakes/spin rotators are not compact devices, and there was no room to spare in existing machines. Early Snake designs also had limited flexibility in the choice of the orientation of the spin rotation axis, and had large beam excursions. It was not possible to retrofit such Snakes into a synchrotron. It took much research to find Snake designs with a flexible choice for the spin rotation axis, and to minimize the beam orbit excursions and reduce the overall length.

Much of the research on Siberian Snakes and spin rotators therefore focussed on machines of the future, where Snakes could be incorporated into the machine design from the outset, or at least enough space could be left available for later installation in a 'phase II' upgrade. Much of the theory on Siberian Snakes was motivated by the Superconducting SuperCollider (SSC), a 20 TeV $\times$ 20 TeV proton–proton collider. It would otherwise have been necessary to cross approximately 36 000 depolarizing spin resonances to reach the top energy. The SSC was eventually cancelled, and is today a defunct project in Texas. However, the knowledge gleaned in various design studies is now being put to use at other machines.

Siberian Snakes are today operating successfully at RHIC, as well as spin rotators at both RHIC and HERA. The lower energy electron storage rings AmPS and SHR also use (or used) single Siberian Snakes, consisting of solenoids. Beam dynamics studies with a solenoid Snake were performed at the IUCF Cooler, as a proof of principle of the Siberian Snake concept. The studies yielded many valuable insights, including the first observation of a Snake resonance. The concept of type 3 Snakes originates from the work at the IUCF Cooler.

The companion review to this work, MSY2 (Mane, Shatunov and Yokoya 2005), will review excellent work at several facilities (spanning the globe from Japan, across Russia and Europe to the USA West Coast). In addition it will present a more detailed description of the whole BNL polarized proton complex, including not only RHIC but the injector chain shown in figure 1, e.g., 'operational' issues concerning Siberian Snakes will be reviewed.

MSY2 will also review the important idea of 'partial Snakes'. The first operational example of a partial Snake was at VEPP-2M (Derbenev *et al* 1977b). A partial Snake has also been used at the AGS (Huang *et al* 1994). The IUCF currently operates a partial Snake in the Cooler Injection Synchrotron (CIS). The IUCF facilities are described by Friesel *et al* (2000).

Looking to the future, there are new ideas for an electron–ion collider (eRHIC) at RHIC, where an electron storage ring would circulate beams of electrons (or positrons) to collide against the polarized proton beams of RHIC. The electron ring would incorporate Siberian Snakes. New proposals utilizing Siberian Snakes include, for example, the electron-light ion collider (ELIC) at the Thomas Jefferson Lab (de Jager *et al* 2003). The design consists of two

rings, one for the electrons and another for the ions. In both the cases the beams are injected with longitudinal polarization, i.e. the ions are also polarized, and both rings incorporate Siberian Snakes. Derbenev is a member of the ELIC design team.

The material on geometric quantum phases is more exotic. It exhibits the connection of spin dynamics in particle accelerators to other branches of physics. It does not seem to be generally appreciated that the path of a spin around the circumference of a storage ring is a quantum topological circuit.

## Acknowledgments

We are grateful to Vladimir Anferov, Ralph Assmann, William and Beverly Barletta, Mari Berglund, Richard Borcherds, Volker Burkert, John Byrd, Lali Chatterjee, Yaroslav Derbenev, Wilbur Franklin, Dennis Friesel, Frank Frommberger, Joseph Grames, Michael Harrison, Haixin Huang, Peter Karpius, S Y Lee, Simon C Leemann, Alfredo Luccio, Waldo MacKay, Yousef Makdisi, Richard Milner, Igor Passchier, Richard Prepost, Charles Prescott, Vadim Ptitsyn, Rajendran Raja, Thomas Roser, Hikaru Sato, Charles Sinclair, Christoph Steier, Edward Stephenson, Steven Tepikian, David Underwood, Jo van den Brand, Jan van der Laan, Johannes van Zeijts, Wolther von Drachenfels, Fuhua Wang, Jorg Wenninger, Michael Woods and Townsend Zwart.

## References

Adler S S *et al* 2004 *Phys. Rev. Lett.* **93** 202002 (*Preprint* hep-ex/0404027)
Aharanov Y and Anandan J 1987 *Phys. Rev. Lett.* **58** 1593–6
Aharanov Y and Bohm D 1959 *Phys. Rev.* **115** 485–91
Alekseev I *et al* 2003 *Nucl. Instrum. Methods* A **499** 392–414
Anferov V A 1998 *Phys. Rev. ST Accel. Beams* **1** 071001
Anferov V A and Phelps R A 1997 *Nucl. Instrum. Methods* A **398** 423–5
Baiod R *et al* 1993 *Phys. Rev. Lett.* **70** 2557–60
Barber D P 1995a *DESY Report 95-200*
Barber D P 1995b *Proc. 1995 Particle Accelerator Conf. (Dallas)* (Piscataway: IEEE) pp 511–3
Barber D P, Hofstaetter G H and Vogt M 2002 *Proc. 8th European Particle Accelerator Conf. (Paris)* (Geneva: EPAC) pp 302–4
Barber D P, Kewisch J, Ripken G, Rossmanith R and Schmidt R 1985 *Part. Accel.* **17** 243–62
Barber D P, Ptitsyn V and Shatunov Yu M 1999 *Polarized Protons at High Energies: Accelerator Challenges and Physics Opportunities* ed A de Roeck *et al* (Hamburg: DESY) pp 151–62
Bargmann V, Michel L and Telegdi V L 1959 *Phys. Rev. Lett.* **2** 435–6
Berry M V 1984 *Proc. R. Soc.* A **392** 45
Bültmann S L *et al* 2004 *Phys. Lett.* B **579** 245–50
Buon J 1986 *AIP Conf. Proc.* **145** 164–9
Buon J and Steffen K 1986 *Nucl. Instrum. Methods* A **245** 248–61
Colton E, Auer I P, Beretvas A, Hill D, Nield K, Sandler B, Spinka H, Underwood D, Watanabe Y and Yokosawa A 1978 *Nucl. Instrum. Methods* A **151** 85
Courant E D 1989 *AIP Conf. Proc.* **187** 1085–92
Courant E D and Ratner L G 1978 *AIP Conf. Proc.* **42** 41–6
de Jager K, Merminga L and Derbenev Ya 2003 *Nucl. Phys.* A **721** 1067–70
Derbenev Ya S *et al* 1977a *Proc. 5th Russian Conf. on Charged Particle Accelerators (Moscow)* vol 1 (Moscow: Nauka) p 263 (in Russian)
Derbenev Ya S and Kondratenko A M 1976 *Sov. Phys.—Dokl.* **20** 562
Derbenev Ya S, Kondratenko A M, Serednyakov S I, Skrinsky A N, Tumaikin G M and Shatunov Yu M 1978 *Part. Accel.* **8** 115–26
Derbenev Ya S, Kondratenko A M and Skrinsky A N 1970 *Sov. Phys. Dokl.* **15** 583
Derbenev Ya S, Kondratenko A M, Skrinsky A N and Shatunov Yu M 1977b *Proc. 1977 Particle Accelerator Conf. (New York)* vol 2 (Piscataway: IEEE) p 75 (in Russian)

Edwards D A and Syphers M J 1993 *An Introduction to the Physics of Particle Accelerators* (New York: Wiley)
Fieguth T 1987 *Part. Accel.* **22** 183–203
Franklin W A 2004 *Proc. SPIN 2004 (Trieste)* (Singapore: World Scientific) at press
Friesel D L 2005 private communication
Friesel D L, Derenchuk V, Sloan T and Stephenson E J 2000 *Proc. 7th European Particle Accelerator Conf. (Vienna)* (Geneva: EPAC) pp 539–41
Froissart M and Stora R 1960 *Nucl. Instrum. Methods* A **7** 297–305 (in French)
Goodwin J E *et al* 1990 *Phys. Rev. Lett.* **64** 2779–82
Goto Y (PHENIX Collaboration) 2002 *Acta Phys. Pol.* B **33** 3767–71
Grosnick D P *et al* 1990 *Nucl. Instrum. Methods* A **290** 269–92
Grote H 1995 *AIP Conf. Proc.* **343** 307–11
Hasell D K (for the BLAST Collaboration) 2004 *Eur. J. Phys.* A **19** Suppl 1283–7
Heinemann K and Hoffstätter G H 1996 *Phys. Rev.* E **54** 4240–55
Hoffstaetter G 2004 *Phys. Rev. ST Accel. Beams* **7** 121001
Hoffstaetter G and Vogt M 2004 *Phys. Rev.* E **70** 056501
Huang H 2005 private communication
Huang H *et al* 1994 *Phys. Rev. Lett.* **73** 2982–5
Huang H *et al* 2003 *AIP Conf. Proc.* **675** 794–8
Huang H *et al* 2004 *Proc. 9th European Particle Accelerator Conf. (Lucerne)* (Geneva: EPAC) pp 209–11
Jackson J D 1998 *Classical Electrodynamics* 3rd edn (New York: Wiley)
Kondratenko A M 1982 *Institute of Nuclear Physics Novosibirsk Preprint* 82-28
Leader E 2001 *Spin in Particle Physics (Cambridge Monographs on Particle Physics, Nuclear Physics and Cosmology)* (Cambridge: Cambridge University Press)
Lee S Y 1989 *AIP Conf. Proc.* **187** 1105–55
Lee S Y 1993 *Phys. Rev.* E **47** 3631–44
Lee S Y 1997 *Spin Dynamics and Snakes in Synchrotrons* (Singapore: World Scientific)
Lee S Y and Berglund M 1996 *Phys. Rev.* E **54** 806–14
Lee S Y and Courant E D 1990 *Phys. Rev.* D **41** 292–302
Lee S Y and Tepikian S 1986 *Phys. Rev. Lett.* **56** 1635–8
Luijckx G *et al* 1997 *Proc. 1997 Particle Accelerator Conf. (Vancouver)* (Piscataway: IEEE) pp 1063–5
MacKay W W 2005 private communication
MacKay W W *et al* 1999 *Brookhaven National Laboratory Internal Report AGS/RHIC/SN #80*
MacKay W W *et al* 2003 *Proc. 2003 Particle Accelerator Conf. (Portland)* (Piscataway: IEEE) pp 1697–9
Mane S R 1988 *Fermi National Accelerator Laboratory Report* TM-1515
Mane S R 1991 *Phys. Lett.* A **157** 320–4
Mane S R 2002a *Nucl. Instrum. Methods* A **480** 328–38
Mane S R 2002b *Nucl. Instrum. Methods* A **485** 277–97
Mane S R 2003a *Nucl. Instrum. Methods* A **498** 1–15
Mane S R 2003b *Nucl. Instrum. Methods* A **498** 52–89
Mane S R 2004 *Nucl. Instrum. Methods* A **528** 677–706
Mane S R 2005a *Convergent Computing Report* CC05-2
Mane S R 2005b *Convergent Computing Report* CC05-3
Mane S R, Shatunov Yu M and Yokoya K 2005 *Rep. Prog. Phys.* **68** 1998 (issue 9, September 2005)
Minty M G *et al* 1991 *Phys. Rev.* D **44** R1361–5
Minty M and Lee S Y 1993 *Part. Accel.* **41** 71–91
Phelps R A *et al* 1997 *Phys. Rev. Lett.* **78** 2772–4
Pollock R E 1991 *Nucl. Instrum. Methods* A **300** 210–2
Poolman H R *et al* 2000 *Phys. Rev. Lett.* **84** 3855–8
Ptitsyn V 2005 Private communication
Ptitsyn V, Luccio A U and Ranjbar M 2003 *AIP Conf. Proc.* **675** 746–9
Ptitsyn V and Shatunov Yu M 1995 *Proc. 1995 Particle Accelerator Conf. (Dallas)* (Piscataway: IEEE) pp 3331–3
Ptitsyn V and Shatunov Yu M 1997a *Proc. 12th Int. Symp. on High Energy Spin Physics (Amsterdam)* ed C W de Jager *et al* (Singapore: World Scientific) pp 516–8
Ptitsyn V and Shatunov Yu M 1997b *Nucl. Instrum. Methods* A **398** 126–30
Ptitsyn V *et al* 2004 *Proc. SPIN 2004 (Trieste)* (Singapore: World Scientific) at press
Ranjbar V H, Lee S Y, Huang H, Luccio A U, MacKay W W, Ptitsyn V, Roser T and Tepikian S 2003 *Phys. Rev. Lett.* **91** 034801
Roser T 1989 *AIP Conf. Proc.* **187** 1442–6

Roser T 2005 Private communication
Ruth R 1986 *AIP Conf. Proc.* **145** 62–71
Schwitters R and Richter B 1974 *PEP Summer Study* (unpublished)
Shatunov Yu M 1993 *Proc. 10th Int. Symp. on High Energy Spin Physics (Nagoya)* (Japan: Universal Academic Press) pp 445–8
Skrinsky A N 1982 *Institute of Nuclear Physics Novosibirsk Preprint* 82-46
Sokolov A A and Ternov I M 1964 *Sov. Phys.—Dokl.* **8** 1203–5
Steffen K 1978 *DESY-PET Report* 78-11
Steffen K 1983 *DESY-HERA Report* 83-124
Steffen K 1985 *AIP Conf. Proc.* **145** 154–61
Steffen K 1987 *DESY-HERA Report* 87-11
Steffen K 1989a *AIP Conf. Proc.* **187** 1093–104
Steffen K 1989b *Part. Accel.* **24** 45
Surrow B (STAR Collaboration) 2002 *Preprint* hep-ex/0205090
Syphers M *et al* 1997 *Proc. 1997 Particle Accelerator Conf. (Vancouver)* (Piscataway: IEEE) pp 3359–61
Tepikian S 1986 *AIP Conf. Proc.* **145** 199–205
Thomas L H 1927 *Phil. Mag.* **3** 1–22
Underwood D G 1980 *Nucl. Instrum. Methods* A **173** 351–5
Underwood D G 1989 *AIP Conf. Proc.* **187** 1470–3
van der Laan J B *et al* 2003 *Proc. 2003 Particle Accelerator Conf. (Portland)* (Piscataway: IEEE) pp 2324–6
Wienands U 1991 *Part. Accel.* **36** 1–13
Yokoya K 1988 *SSC Report* 189
Yokoya K 1999 *DESY Report* 99-006 (*Preprint* physics/9902068)
Zwart T, Ivanov P, Shatunov Yu, Averill R, Jacobs K, Kowalski S and Turchinetz W 1995 *Proc. 1995 Particle Accelerator Conf. (Dallas)* (Piscataway: IEEE) pp 600–2
Zwart T *et al* 2001 *Proc. 2001 Particle Accelerator Conf. (Chicago)* (Piscataway: IEEE) pp 3597–9